SPi | Journal Code: C M M I | Article ID: 1 6 1 4 | Dispatch: 26.06.14 | CE: | No. of Pages: 32 | ME:

Review

CONTRAST MEDIA & MOLECULAR IMAGING

Received: 25 January 2014, Revised: 22 May 2014, Accepted: 27 May 2014, Published online in Wiley Online Library

(wileyonlinelibrary.com) DOI: 10.1002/cmmi.1614

Superparamagnetic iron oxide nanoparticle for *in vivo* molecular and cellular imaging

Shahriar Sharifi[a†], Hajar Seyednejad[b†], Sophie Laurent[c,d], Fatemeh Atyabi[e] and Morteza Mahmoudi[e,f*]

Over recent years, the biomedical applications of nanoparticles (NPs) (e.g. cell tracking, biosensing, magnetic resonance imaging, targeted drug delivery and tissue engineering) have been increasingly developed. Among the various NP types, superparamagnetic iron oxide NPs (SPIONs) have attracted a considerable amount of attention for early detection of diseases owing to their specific physicochemical properties and their molecular imaging capability. A comprehensive review is presented on the recent *in vitro* and *in vivo* advances in the development of SPION applications for molecular imaging, with their possibilities and limitations. Copyright © 2014 John Wiley & Sons, Ltd.

Keywords: SPIONs; molecular imaging; cellular imaging; MRI; superparamagnetic nanoparticles

1. INTRODUCTION

Molecular/cellular imaging has received considerable attention in the last two decades for its diagnostic and clinical promises (1–3). Molecular imaging (MI) can allow the noninvasive assessment of biological and biochemical processes in living subjects. MI involves several biomedical disciplines including imaging technology, cellular and molecular biology, chemistry, medical physics, biomathematics and bioinformatics. The main aim of MI is to study the biochemical processes of disease without disturbing the integrity of the living subjects. Tracking of the specific biomolecules *in vivo* can highlight the main mechanisms involved in particular diseases. Therefore, the development of new innovative imaging probes with enhanced sensitivity for the molecular recognition of the target molecule looks very promising (4–8). Different kinds of imaging techniques have emerged for molecular imaging (4), which have their inherent advantages and disadvantages. There are many modalities T1 suited to molecular imaging (see Table 1 for details). Nuclear medicine techniques such as positron emission tomography (PET) or single photon emission computed tomography (SPECT) are well suited to MI because of their excellent sensitivity. Receptors can be routinely imaged at nanomolar concentrations with targeting vectors (e.g. antibodies and small molecules) tagged with γ-ray or positron emitting nuclei. The fusion of PET with X-ray computed tomography (CT) allows molecular imaging information (from PET) to be superimposed on anatomical information (from CT). Near-infrared optical agents and targeted ultrasound microbubbles are also being explored.

Among various approaches, magnetic resonance imaging (MRI) has many advantages as a diagnostic imaging modality. It is noninvasive, without radiation, and has excellent (submillimeter) spatial resolution. Soft tissue contrast is good and MRI readily yields anatomical information (8). The overriding challenge with MRI is its relatively low sensitivity (9).

MI depends on the availability of suitable reporter systems that provide a high sensitivity in order to visualize low (submicromolar) concentrations of the molecular target expressed by the tissue or the cell, and a high signal that allows the discrimination of the target interaction from the nonspecific background. Among the different imaging modalities, nuclear and optical imaging display the highest sensitivity, followed by MRI, ultrasound and finally X-rays (10).

In this review, we will concentrate on MRI. If the optimization of the T_1 shortening effect in new paramagnetic Gd complexes is an important goal, superparamagnetic iron oxide nanoparticles (SPIONs) have been extensively used in MR molecular imaging investigations (11). These nanoparticles (NPs) provide several advantages over traditional contrast agents, like relatively low cytotoxicity, high magnetic signal strength and longer contrast

* *Correspondence to: M. Mahmoudi, Nanotechnology Research Center and Department of Nanotechnology, Faculty of Pharmacy, Tehran University of Medical Sciences, Tehran, Iran. E-mail: mahmoudi@stanford.edu*

† *The first two authors contributed equally.*

a *S. Sharifi*
Department of Biomaterials Science and Technology, University of Twente, The Netherlands

b *H. Seyednejad*
Department of Bioengineering, Rice University, Houston, TX, 77005, USA

c *S. Laurent*
Department of General, Organic, and Biomedical Chemistry, NMR and Molecular Imaging Laboratory, University of Mons, Avenue Maistriau, 19, B-7000 Mons, Belgium

d *S. Laurent*
CMMI – Center for Microscopy and Molecular Imaging, Rue Adrienne Bolland, 8, B-6041 Gosselies, Belgium

e *F. Atyabi, M. Mahmoudi*
Nanotechnology Research Center and Department of Nanotechnology, Faculty of Pharmacy, Tehran University of Medical Sciences, Tehran, Iran

f *M. Mahmoudi*
Biomaterials and Advanced Drug Delivery Laboratory, School of Medicine, Stanford University, Stanford, CA, 94305, USA

Biographies

Dr. Shahriar Sharifi was born on 28th May 1977 in Tehran. In 2000, He received his Bachelor of Science degree in Material Engineering and graduated with honors from Amirkabir University of Technology (Poly Technique of Tehran). Following his graduation, he studied Biomedical Engineering at the same University and received his Master of Science in Biomedical Engineering in 2002 and his first Ph.D. degree in 2007 with specialization in the design and development of biodegradable biomaterials and nanocomposites for drug delivery and medical applications. In 2009, He moved to the University of Groningen, and later on to University of Twente, The Netherlands which he earned his second Ph.D in Medical Science. His current research involves development of smart materials including nanomaterials for biomedical and tissue engineering applications.

Dr. Hajar Seyednejad received her PhD in 2012 from Utrecht University (The Netherlands) under supervision of Dr. Hennink and Dr. Dhert. She specialized in development of synthetic, biodegradable, and biocompatible scaffolds based on functionalized polyesters for tissue engineering applications. In May 2012, she joined group of Dr. Mikos at the Department of Bioengineering at Rice University (Houston, USA) as a Postdoctoral Research fellow. During her fellowship, she worked on development of gradient constructs for tissue engineering, using rapid prototyping techniques. Her current research involves development of novel medical devices for biomedical applications.

Dr. Sophie Laurent was born in 1967. Her studies were performed at the University of Mons-Hainaut (Belgium) where she received her PhD in Chemistry in 1993. She joined then Prof R.N. Muller's team and was involved in the development (synthesis and physicochemical characterization) of paramagnetic Gd complexes and super paramagnetic iron oxide nanoparticles as contrast agents for MRI. She is currently working on the vectorization of contrast agents for molecular imaging. She is lecturer and co-author around 90 publications and more than 180 communications in international meetings.

Fatemeh Atyabi is a full professor of pharmaceutics and nanomedicine at Tehran University of medical Sciences. She is the member of Controlled Release Society (USA), Controlled Release Society of Iran. Dr Atyabi received her Ph.D. degree in pharmaceutics from University of Manchester in England. Her research fields are in oral drug delivery systems, nanotechnology based drug delivery systems especially on anticancer drugs and tissue engineering. She is the co-author of 2 book chapters, and 120 papers. She is head of the department of pharmaceutical nanotechnology and biomaterials.

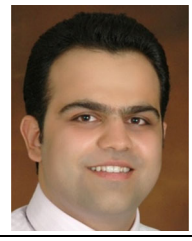

Morteza Mahmoudi received his PhD from Institute for Nanoscience and Nanotechnology at Sharif University of Technology with specialization on the biomedical applications of superparamagnetic iron oxide nanoparticles. He is Director of NanoBio Interaction Laboratory at Tehran University of Medical Sciences (http://www.biospion.com). His current research involves intelligence controlling of the protein corona decoration at the surface of nanoparticles and exploring the hidden parameters at the nanobio interfaces.

enhancement. Therefore, the main focusses of this review are recent advances in the early detection of various diseases using MRI and SPIONs.

Table 1. Imaging modalities employed in molecular imaging and system of detection

Molecular imaging modalities	Means of detection
Computed tomography	X-rays
Single photon emission computed tomography	γ-Rays
Positron emission tomography	Positrons
Magnetic resonance imaging	Radiofrequency waves
Optical imaging	Near-infrared light
Ultrasound	Ultrasound

2. SUPERPARAMAGNETIC IRON OXIDE NANOPARTICLES

There are a number of good reviews covering the different synthesis approaches for preparation of various SPIONs together with their diverse biomedical applications (12–16). Here, we will provide a short overview on the characteristics of SPIONs.

Numerous parameters determine the efficiency of SPIONs, such as the size of the iron oxide crystals, the nature of the coating, the hydrodynamic size of the coated NPs, the polydispersity and the charge. These characteristics have a significant influence on their colloidal stability, biodistribution, protein corona formation, cell uptake, opsonization and pharmacokinetics (17–28).

The fine synthesis of SPIONs is a relatively complex process; the two main challenges are the monodispersity of the magnetic

core and the reproducibility of the synthesis. Various processes have been described to produce SPIONs including classic synthesis by precipitation, high-temperature reactions, reactions in steric environments, sol–gel reactions, decomposition of organometallic precursors and polyol methods (29,30). Each of these methods has its own pros and cons. For instance, the co-precipitation method is an easy, scalable approach but produces SPIONs with a large size distribution (31). In contrast, monodispersed SPIONs can be produced by the thermal decomposition approach; however, the particles have hydrophobic surfaces and need additional stages for changing them to hydrophilic (32).

After the synthesis, a magnetic core coating [with magnetite (Fe_3O_4) or maghemite (γ-Fe_2O_3) as the main structure] is required to prevent agglomeration of the colloidal suspension (33). Many natural and synthetic polymers have been used as coatings, such as dextran and carboxymethylated dextran (34–39), alginate (40–43), starch (44,45), polyethylene glycol (PEG) (46–51), poly(D,L-lactide-co-glycolide) (52–54) and organosilane (33,55–57). Some small charged molecules have also been used as coatings: citrate, aminoacids, hydroxamate and dimercaptosuccinid acid (58–61).

The stable colloidal suspension is, then, fully characterized by different analytical methods (62–64). The size of the crystals is measured by techniques such as transmission electron microscopy or X-ray diffraction and the hydrodynamic size (the global size of the particle with the coating) is obtained by photon correlation spectroscopy. The charge on the surface of the NPs is given by the ζ-potential obtained from measuring the electrophoretic mobility. To characterize MR efficiency, measurements of magnetization and relaxation rate are performed. Magnetometry confirms the superparamagnetic properties of the particle and provides information on the specific magnetization and the mean diameter of the crystals (29,30,65). It is now well known that the surface of NPs is covered by various proteins upon their entrance into biological fluids (66). The type and composition of the associated proteins (so called 'protein corona') at the surface of NPs can define their *in vivo* responses (67,68). There are several methods to evaluate the protein corona at the surface of NPs, including liquid chromatography, mass spectrometry, gel electrophoresis and differential centrifugal sedimentation (69).

The efficiency of a contrast agent is its ability to accelerate the proton relaxation rate, the relaxivity, which is defined as the increase in the relaxation rate of the protons of the solvent (water) induced by 1 mmol l^{-1} of the active ion. In the case of magnetite, the relaxivity is the relaxation rate enhancement observed for an aqueous solution containing 1 mmol of iron per liter:

$$R_{i(\mathrm{obs})} = \frac{1}{T_{i(\mathrm{obs})}} = \frac{1}{T_{i(\mathrm{dia})}} + r_i C; \quad i = 1 \text{ or } 2 \qquad (1)$$

where $R_{i(\mathrm{obs})}$ and $1/T_{i(\mathrm{obs})}$ are the global relaxation rates of the aqueous system (s^{-1}), $T_{i(\mathrm{dia})}$ is the relaxation time of the system before addition of the contrast agent, C is the concentration of the paramagnetic center (mmol L^{-1}) and r_i is the relaxivity (s^{-1} mmol^{-1} L).

The nuclear magnetic relaxation properties of a compound are ideally obtained by the study of its nuclear magnetic resonance dispersion profile, which gives the evolution of the relaxivity with respect to the external magnetic field. The fitting of the nuclear magnetic resonance dispersion curves according to the relevant theories gives the mean crystal size, the specific magnetization and the Néel relaxation time.

SPIONs allow pathological tissues to be distinguished from healthy tissue. Their preferential accumulation in one type of tissue decreases the T_2 MRI signal to provide enhanced image contrast. Some NPs targeting cancerous tissues have been developed. Targeting methods are divided in two categories: passive targeting based on the physiological differences between pathological and normal tissues (70); and active targeting based on ligands grafted onto the NP surface to recognize specific receptors or markers on diseased tissues (71,72). However, recent results showed the extensive effect of protein corona on active targeting (73). More specifically, the protein corona may cover the targeting ligands and considerably reduce the targeting yield (74). In addition, protein corona have the capability to affect the relaxivity and MRI contrast efficiency of SPIONs (75).

Passive targeting methods are generally based on the enhanced permeability and retention (EPR) effect or on the specific uptake of the particles by healthy tissues of the reticulo-endothelial system (RES), such as the liver and the spleen (76–78). SPIONs can be used for detecting diseases in tissues rich in macrophages (79,80). Upon intravenous injection, NPs are easily and rapidly sequestered by macrophages, resulting in hypointensity on T_2-weighted images. Since tumor tissues are devoid of macrophages, in comparison with normal tissue, the tumors are visualized with increased intensity (81).

Active targeting uses NPs grafted with targeting ligands to promote selective binding to receptors on target tissues. The principal aim of active targeting is the acquisition of information regarding the molecular profile of cells, which gives a more accurate diagnosis for tailoring therapeutic treatments for individual patients. This strategy also allows the monitoring of drug efficiency during the treatment. To prepare molecular probes based on SPIONs, two prerequisites must be fulfilled: (a) RES-evading properties of the particles; and (b) the preservation of the bioactivity of targeting molecules through coupling reactions. Many studies have already described the ability of active targeting to identify biomarkers of cancer (72,82–84), apoptosis (85,86), cardiovascular disease (87–93), inflammation (94–97), etc.

3. MOLECULAR IMAGING

Nanoparticles are composed of thousands of iron atoms, which provide a large T_2 effect. After coating, chemical grafting is possible via functional groups. The first strategy used to vectorize NPs was adsorption of antibody (98,99) or protein (100,101) onto the SPIONs' surface. The problem is the difficulty of controlling the reproducibility of this noncovalent grafting. Another strategy based on streptavidin-coated- or biotinylated-SPIONs and streptavidin protein able to bind biotinylated ligands has also been used (102–105).

Several covalent conjugation strategies involving reactions with amino, carboxylic, aldehyde or thiol groups have been developed (106). Glutaraldehyde bioconjugation (107) and amide formation in the presence of 1-ethyl-3-(3-dimethylaminopropyl) carbodiimide (EDCI) on carboxylated SPIONs have been described for peptide (108–110) and protein (111–113) grafting. Another method is based on an oxidative conjugation process, which produces aldehydes on a polysaccharidic coating, such as dextran (114–121). Oxidative processes have also been used by Sonvico *et al.* to graft amino PEG-folic acid onto nanoparticles and by Zhang *et al.* to obtain pegylated SPIONs coated by folic acid (122,123).

The vector molecules (e.g. peptides, antibodies, and proteins) can be covalently linked through a three-step reaction sequence, as described by Josephson *et al*. (124). A peptide or protein was attached to the amino group of cross-linked dextran SPIONs using different classical heterofunctional linkers, such as *N*-succinimidyl 3-(2-pyridyldithio)propionate, named SPDP (125–130) (disulfide bound formation), succinimidyl iodoacetate (124,127,131–137) (carbon–thiol formation), activated suberic acid (138–141) (amide formation), succinic anhydride (142) (amide formation), EDCI (106,128,142,143) (amide formation), thionyl chloride (128) (ether formation) or epoxide (128) (carbon–nitrogen-bound formation). One of the main advantages of utilizing SPDP is that it can be used to determine the number of reactive amines on the particle: as pyridine-2-thione is released upon reaction with dithiothreitol, it can be detected by spectrophotometry and thus quantified. The reaction of ligands with SPDP functionalized particles also liberates pyridine-2-thione, thus allowing the number of conjugated species to be determined. This technology has been successfully applied to develop an NP library that recognizes apoptotic cells thanks to different synthetic small ligands (106,142) grafted on the NPs. Other research groups have used dextran NPs cross-linked by epichlorohydrin and direct substitution by terminal amino groups of a pharmacophore (97,144,145).

The coupling of biovectors on the particles can be performed also with 2,3-dimercaptosuccinic acid (DMSA) and SPDP (146). The particle is coated with DMSA and the vector is linked to SPDP through a peptide bond. These units are joined by an S–S bridge between DMSA and SPDP. This technology has been used to graft antibodies and annexin V to DMSA NPs (59,147–152).

The silane-coupling materials [such as 3-aminopropyltrimethoxysilane (153) or triethoxysilanepropyl succinic anhydride (154)] are able to covalently bind to iron oxide and then to form covalent bonds with biological vectors through organo-functionalities. Magnetite NPs coated with silica have been used to conjugate folic acid (123,155) and bovine serum albumin (33,156). After surface modification with an aminosilane coupling agent, the amino group of the biovector was covalently linked using glutaraldehyde as a cross-linker. Amine-coated NPs are easily modified also by ligands containing NHS-modified carboxylic acids or isothiocyanates. Epoxides and anhydrides also can react easily in sodium bicarbonate buffer at pH 8.6 (106). Alternatively, vectors with carboxylic functions can be directly grafted on the silica-coated particles using EDCI to activate the carboxyl groups. Carboxylic acid-coated particles require activation prior to conjugation. Amine containing ligands are typically conjugated to carboxylic acid-functionalized particles in the presence of EDCI and sulfo-NHS to yield the corresponding amide.

Sun *et al*. (157) have suggested a 'click chemistry' process (azide–alkyne reaction) for vectorization of SPIONs with small molecules. Thorek *et al*. evaluated the efficiency of conjugations between antibodies and SPIONs using click chemistry and showed a better efficiency of labeling compared with other conjugation methods (157). These reactions have several advantages over the above bio-conjugations: (a) click reaction can occur under relatively mild conditions in aqueous solutions; (b) these reactions are also highly specific, occur with high yields and do not produce undesirable side products; and (c) triazoles are biocompatible entities. The Cu(I)-catalyzed reaction between azide and alkyne results in the formation of a stable triazole linker. SPIONs can be functionalized with azide or alkyne moieties by reaction of carboxylic acid-functionalized particles with azido propylamine or propargylamine in the presence of activating reagents, such as EDCI and sulfo-NHS in 2-(*N*-morpholino) ethanesulfonic acid buffer at pH 6.0. Conjugation reactions between the functionalized NPs and ligands occurred in aqueous solution at 37 °C for 5–8 h, resulting in >90% conversion.

In several studies, magnetoliposomes were used as a platform to incorporate antibodies or peptides in the lipidic membrane (158–164). Nitin *et al*. (165) developed a PEG-modified phospholipid micelle coating for functionalization of SPIONs. This PEG-phospholipid coating results in high water solubility, and the functional groups of modified PEG allow for bioconjugation of various moieties, including proteins, oligonucleotides, or peptides. Multifunctional polymeric micelles incorporating NPs and RGD peptides to target cancer cells have been recently described (166).

Numerous examples of molecular imaging applications have been reported in the literature; for more information readers are encouraged to read these comprehensive reviews (4,167–173).

3.1. Inflammation Imaging

Inflammation occurs owing to a reaction of the body to injury (174). The noninvasive diagnosis and monitoring of inflammation processes are very important, since these are involved in numerous pathologies such as infection, ischemia, rheumatoid arthritis, atherosclerosis, graft rejection and formation of tumor metastasis (36,174–179). Molecular markers for imaging are thus needed in diseases where the inflammatory action of misdirected leukocytes can destroy healthy tissues. Inflammatory cells, such as macrophages, can be tagged with SPIONs. Macrophages are indeed able to take up SPIONs by phagocytosis, and to subsequently invade tissues through inflammatory processes. This has been achieved in a model of central nervous system (CNS) inflammation (180,181). Microglial cells can internalize SPIONs and are detected by *in vivo* MRI (182,183). However, this type of cellular MRI requires high doses of SPIONs to saturate the macrophages located in lymph nodes, liver, spleen or bone marrow. Importantly, one should note that the predetermined SPION uptake by macrophages is valid for those SPIONs that have a major contribution of opsonins in their corona compositions (22). Labeling of macrophages with SPIONs in atherosclerotic plaques has also been achieved (184,185).

An alternative approach is to develop specific MR contrast agents that selectively target receptors involved in the inflammatory process (186,187). Cell adhesion molecules (CAM), like E-selectin, are overexpressed on leukocytes and endothelial cells during the inflammatory process (188). The natural ligand of E-selectin is sialyl Lewis X (sLeX), a tetrasaccharide (189). This carbohydrate structure is linked to certain leukocyte surface proteins by specific glycosylation enzymes (190). MRI of E-selectin expression in human endothelial cell cultures was assessed with cross-linked SPIONs functionalized with antihuman E-selectin antibodies (185). Boutry *et al*. (191) described a molecular imaging strategy to target E-selectin with a mimetic of sialyl Lewis X. This mimetic molecule, reported in the literature (192), keeps its E-selectin affinity thanks to the conformation of a 2-(α-D-mannopyranosyloxy)-biphenyl structure (193). This mimetic has previously been coupled with other magnetic reporters, such as gadolinium complexes, and successfully used to detect inflammation (36,194–196). The specific contrast agent, obtained by grafting the synthetic mimetic of sLeX on the dextran coating of SPIONs, was tested *in vitro* on cultured human umbilical vein

endothelial cells (HUVECs) stimulated to express inflammatory adhesion molecules, and *in vivo* on a mouse model of hepatitis induced by injection of concanavalin A. *In vitro* results showed an extensive retention of specific SPIONs on TNF-α stimulated HUVECs. *In vivo*, SPIONs are known to pass through the fenestrae of the liver and to be captured by Kupffer cells, inducing a loss of signal intensity on T_2-weighted MR images. Unexpectedly, when injected to Con A-treated mice, SPIONs-g-sLeX induced a significantly lower attenuation of liver signal intensity than SPIONs, suggesting that the specific contrast media is retained extracellularly by an interaction with E-selectin overexpressed on the vascular endothelium.

Rademacher *et al*. used a multimodal molecular approach, with MRI and EPR to detect inflammation (197,198). The sLeX mimetic was grafted on SPIONs-PEG to prolong the plasma circulation time and minimize the nonspecific accumulation of SPIONs in tissues (198,199). These functionalized particles were evaluated in an *in vivo* model of local inflammation in muscle induced by injection of Freund's complete adjuvant (local stimulation of TNF production). The quantitative detection of iron oxide particles in the tissues was carried out *ex vivo* using EPR spectroscopy and the efficacy of the targeted SPIONs was evaluated using *in vivo* EPR spectroscopy and T_2-weighted imaging.

Funovics *et al*. (200) prepared SPIONs grafted with a fluorescent Cy 5.5 peptide (CDSDSDITWDQLWDLMK), which allows to image E-selectin expression in mouse xenograft models of Lewis lung carcinoma by fluorescence reflectance imaging. Internalization by activated HUVEC was rapid and mediated by E-selectin, indicated by the lack of uptake of NPs bearing similar numbers of a scrambled peptide. To demonstrate the specificity of E-selectin targeting *in vivo*, the authors co-injected peptide-Cy 5.5-SPION and scramble-peptide-Cy3.5-SPION and demonstrated a high Cy5.5/Cy3.5 fluorescence ratio. They concluded that peptide-Cy 5.5-SPION is a useful probe for imaging E-selectin associated with the Lewis lung carcinoma tumor.

3.2. Molecular Tumor Imaging

Many studies have been reported using targeted NPs for *in vitro* and *in vivo* tumor imaging. Antibodies have been grafted owing to their high specificity (201–203). Human epidermal growth factor receptor 2 (Her-2/neu receptor) is a well-known tumor target. Yang *et al*. (204) conjugated about 8 Her-2/neu antibodies per poly(amino acid)-coated NPs. The T_2-weighted MR images confirmed that Her-2/*neu* antibody-conjugated NPs have specific targeting ability for Her2/neu receptors: a significant difference was observed between the NP-Ab-treated and untreated cells overexpressing Her-2. The team of Cheon reported the *in vivo* imaging of breast cancer using the SPIONs–herceptin probe. Herceptin as a specific antibody can target breast cancer cells overexpressing Her-2/neu (148).

Some studies have reported targeted NPs with single chain antibodies (scFv) or peptides with small molecular weight. Compared with intact antibodies, there are many advantages of using scFv as tumor targeting ligands: (a) relatively small size; (b) no loss of antigen binding capacity; (c) no immune response owing to lack of Fc constant domain; and (d) low cost. ScFvEGFR was conjugated to NPs and the results confirmed that the NPs specifically bind to EGFR (epidermal growth factor receptor), as shown by a decrease in MRI signal in the tumor site (Fig. 1) (211,212). These specific NPs accumulated selectively within the pancreatic tumors while nontargeted NPs did not cause MRI signal changes in tumor. Although an antibody is a good

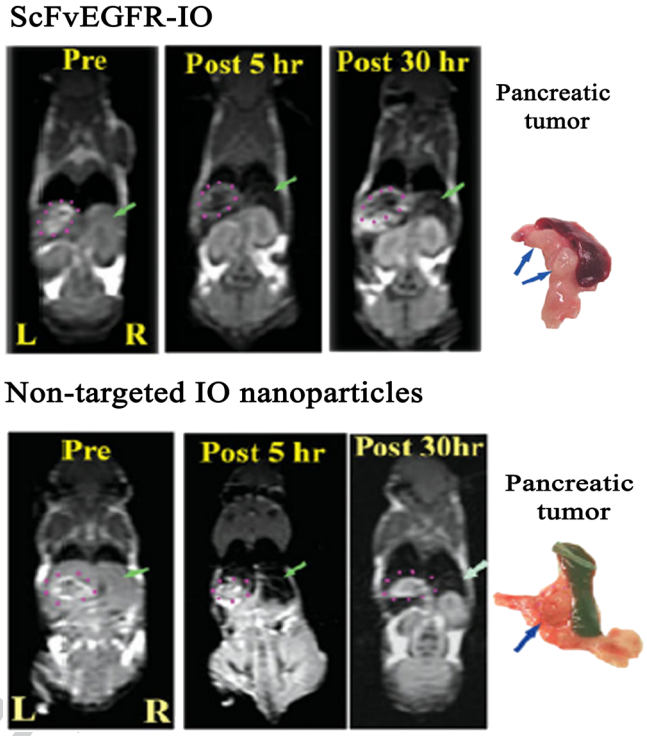

Figure 1. Target specificity of ScFvEGFR nanoparticles (NPs) by MRI using an orthotopic human pancreatic xenograft model; the areas of the pancreatic tumor are marked with a pink dashed circle. On the right is the picture of tumor and spleen tissues, showing sizes and locations of two intra-pancreatic tumor lesions (arrows) that correspond to the MRI tumor images. Reproduced with permission from Yang *et al*. (211).

choice for tumor targeting, the antibody-targeted NPs suffer from their large hydrodynamic size and diffuse poorly through biological barriers, and may also lead to easy uptake by RES (213,214). Small targeting molecules become alternative choices.

The luteinizing hormone releasing hormone (LHRH) (215) is a decapeptide. More than half of human breast cancers express binding sites for receptors for LHRH. Leuschner *et al*. (216) prepared LHRH NPs that were selectively accumulated in primary tumor cells and metastatic cells. These NPs can be used for detecting metastatic breast cancer cells *in vivo*.

Transferrin (Tf) is another example of a targetable protein, since some tumors are known to overexpress transferrin receptors (Tfr). Tf-SPIONs have been used for specific labeling and detection of gliosarcoma (217–219) and breast carcinoma (114). Synaptotagmin I protein-conjugated iron oxide, specific for anionic phospholipids present in apoptotic cells, has been shown to provide specific contrast enhancement of apoptotic tumor cells treated with chemotherapeutics.

The folate receptor (FR) is generally overexpressed in cancerous tissues. Folate molecules (folic acid, FA) have been grafted on several iron oxide NPs coated differently with dextran, PEG, 2-carboxyethyl phosphoric acid, or 2,2′-(ethylenedioxy)bisethylamine. There are many advantages of using FA as a targeting ligand: (a) high binding affinity for its receptor ($K_d = 10^{-10}$ M); (b) low cost; (c) easy conjugation with the imaging probes; and (d) lack of immunogenicity (220). Choi *et al*. (221) showed the first *in vivo* study with FA conjugated to dextran-coated NPs. A specific uptake by tumor cells was observed by a decrease in the tumor signal intensity of 38%.

Sun *et al*. showed that FR-positive HeLa cells could uptake 1.410 pg iron per cell after incubation with specific FA-NPs for

4 h, which was 12-fold higher than the uptake of those cultured with nontargeted NPs (222). Another study showed that FA-targeted NPs could selectively accumulate in human nasopharyngeal epidermoid carcinoma cells both *in vitro* and *in vivo*, as shown by significant MRI signal changes (223).

Peptides that target specific receptors on the tumor cell surface have also been used. The urokinase plasminogen activator receptor is expressed in many different human cancers. The amino-terminal fragment of urokinase plasminogen activator can bind to the urokinase plasminogen activator receptor on the cell surface. Yang *et al*. (211) purified the amino-terminal fragment peptide and conjugated it to amphiphilic polymer-coated NPs. These NPs showed selective accumulation at the tumor mass in a human pancreatic cancer model.

Specific peptides, cholecystokinin-(101) and secretin-linked (224) particles, have been employed for MR visualization of their respective pancreatic receptor and may contribute in the diagnosis of pancreatic cancer. The identification of peptide vectors can be performed by phage screening. Phage display is a technique involving the synthesis of libraries of bacteriophage by standard recombinant DNA technology, each expressing a different peptide sequence on its coat. After identification of the bound phage, it is expanded and sequenced to determine the targeting peptide sequence. Peptide sequences obtained with this method are useful in the development of imaging agents (225).

Angiogenesis is an essential step for the development of tumors. As a marker of angiogenesis, the cell adhesion molecule integrin $\alpha_v\beta_3$ locates on the surface of the tumor vessels and can be directly targeted. Since a specific tripeptide sequence – that is, arginine–glycine–aspartic acid (RGD) – can specifically bind to $\alpha_v\beta_3$, it is often used coupled with SPIONs in detecting tumors, including breast tumors, malignant melanomas and squamous cell carcinomas (226). The RGD peptide has a high binding affinity for the $\alpha_v\beta_3$ integrin receptor and is well known as a tumor vessel-targeted ligand. RGD-NPs could target tumor vessels and resulted in a change in T_2 relaxation detected with a clinical MRI scanner working at 60 MHz, and the signal changes were correlated to the $\alpha_v\beta_3$ integrin expression level (227). In another study, Liu *et al*. (228) showed that RGD-SPIONs can specifically label $\alpha_v\beta_3$ integrin and be taken up by HUVECs. An important decrease in T_2 signal intensity was observed at the periphery of A549 tumor xenografts 30 min after RGD-SPIONs injection. This probe can specifically evaluate the angiogenic profile of lung cancer. Some mimetics of the RGD peptides have been synthesized and grafted onto NPs. The specific nanosystems have shown a good affinity for the $\alpha_v b_3$ integrins (229,230). Xie *et al*. prepared SPIONs coated with 4-methylcatechol and

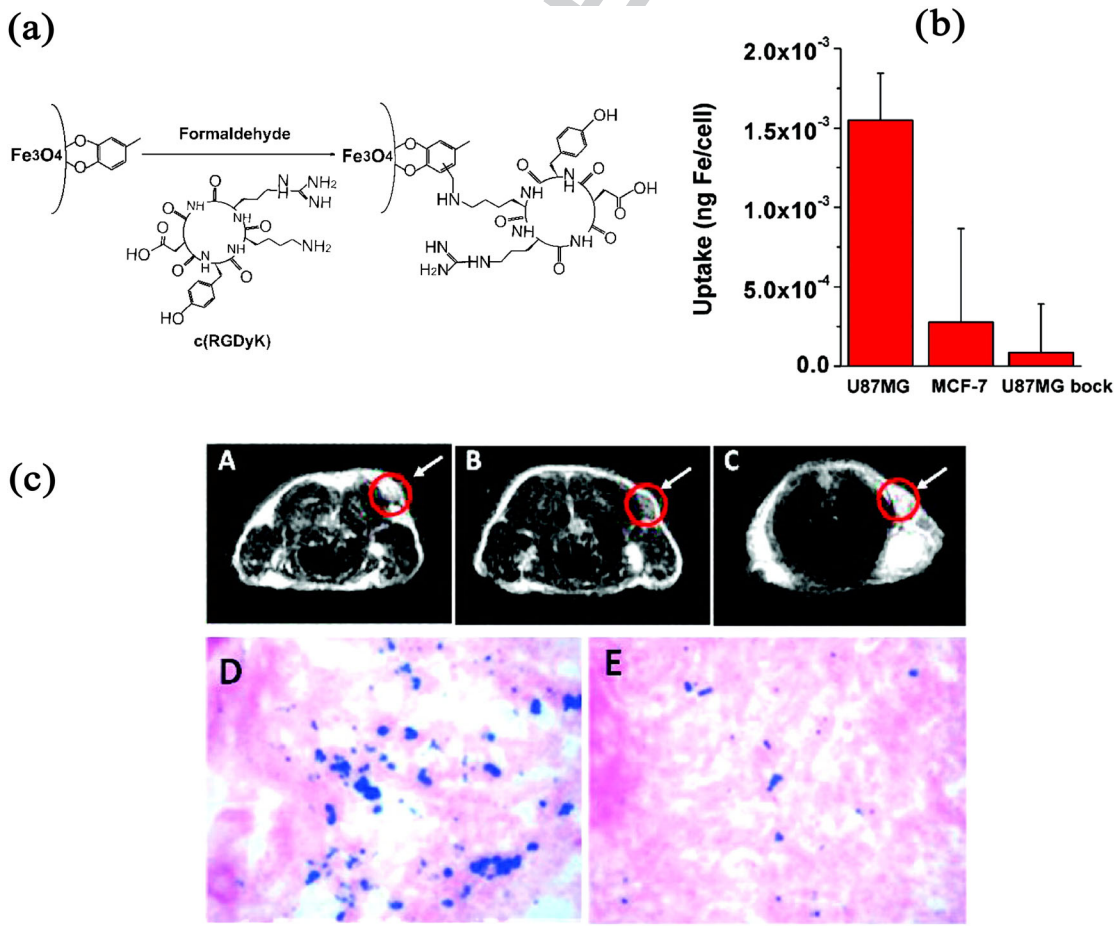

Figure 2. (a) Grafting c(RGDyK) peptide to superparamagnetic iron oxide NPs (SPIONs). (b) Cell uptake of c(RGDyK)-MC-SPIONs by U87MG, MCF-7 and U87MG + c(RGDyK) block. (c) MRI of the cross section of the U87MG tumors implanted in mice: (A) without SPIONs, (B) with the injection of 300 μg of c (RGDyK)-MC-SPIONs, and (C) with the injection of c(RGDyK)-MC-SPIONs and blocking dose of c(RGDyK); Prussian blue staining of U87MG tumors in the presence of (D) c(RGDyK)-MC-SPIONs and (E) c(RGDyK)-MC-SPIONs plus blocking dose of c(RGDyK). Reproduced with permission from Xie *et al*. (231). Copyright (2008) American Chemical Society.

grafted the c(RGDyK) peptide via the Mannich reaction with SPIONs for specific targeting of integrin $\alpha_v\beta_3$-rich human glioblastoma tumor cells (Fig. 2) (231). Thanks to the multivalent binding, these NPs present an increased cellular uptake in comparison with free RGD peptides. Song *et al.* used monoclonal antibody fluorescent magnetic biotargeting multifunctional nano-bioprobes (FMBMNs) to detect and isolate different kinds of tumor cells, such as leukemia cells or prostate cancer cells (Fig. 3) (232).

Aptamers, single-stranded oligonucleotides, can recognize their targets with high specificity and affinity. Aptamers grafted on magnetic NPs have been used for numerous applications, such as magnetic relaxation switches for the detection of molecular interactions (233) or for magnetic extraction of targeted cells in a mixture (234,235). Magnetic relaxation switches allows the detection of molecular interactions with high efficiency and sensitivity using magnetic relaxation measurements (235). Yu *et al.* (236) synthesized a CG-rich duplex containing prostate-specific membrane antigen (PSMA) aptamer conjugated with SPIONs via a hybridization method (*Apt*-hybr-*TCL*-SPION) for prostate cancer-specific theranostic agents. These NPs, loaded with doxorubicin (Dox) through the intercalation into the CG-rich duplex containing PSMA aptamer, showed preferential binding with target prostate cancer cells. The resulting Dox loaded NPs gave a selective drug-delivery efficacy in the targeted prostate cancer cells xenograft mouse model. Wang *et al.* also described the conjugation of aptamers (A10 RNA) to SPIONs via gel electrophoresis (237). Dox was released in a controlled fashion to PSMA expressing PCa cells. Yigit *et al.* prepared new adenosine DNA aptamer functionalized SPIONs (238). The synthesis was performed in two steps: reaction with SPDP and coupling with thiol-modified DNA. T_2-Weighted MR images allowed the quantitative performance analysis with different adenosine concentrations. The brightness of the T_2 image increased with the adenosine concentration. Aptamer-SPIONs also allowed the detection of human α-thrombin protein by MRI (Fig. 4) (239). The nanosystem was specific to thrombin: a detectable change in MRI signal was observed at 25 nM thrombin in human serum. No change was observed in control analytes with streptavidin and bovine serum albumin or with inactive aptamer-SPIONs. These studies demonstrated that aptamer-SPIONs can be used as potential theranostics agents.

4. CELLULAR IMAGING

4.1. Liver Disease Imaging

Liver diseases, mainly categorized as hepatic fibrosis, microbial infections and hepatocellular carcinoma, are a major public health problem worldwide (240). Hepatic liver fibrosis (which originates from chronic liver injury caused by chronic alcohol consumption or viral infection such as hepatitis C or B, or fungal, bacterial or parasite infections) is the scarring process associated with excessive accumulation of extracellular matrix proteins including collagen, proteoglycans and other macromolecules. Advanced liver fibrosis results in cirrhosis, liver failure and portal hypertension and often requires liver transplantation (241). Chronic viral hepatitis (hepatitis B or hepatitis C) with or without cirrhosis most commonly develops into hepatocellular carcinoma (HCC), which is the third most common cause of cancer death worldwide.

Currently, the standard reference for diagnosing and staging liver fibrosis is histological examination of tissue obtained from liver biopsy. However, limitations such as the invasiveness, complications and sampling variability, as well as high expense, make it unsuitable for diagnosis and longitudinal monitoring in the general population (242). Recently, a variety of MR

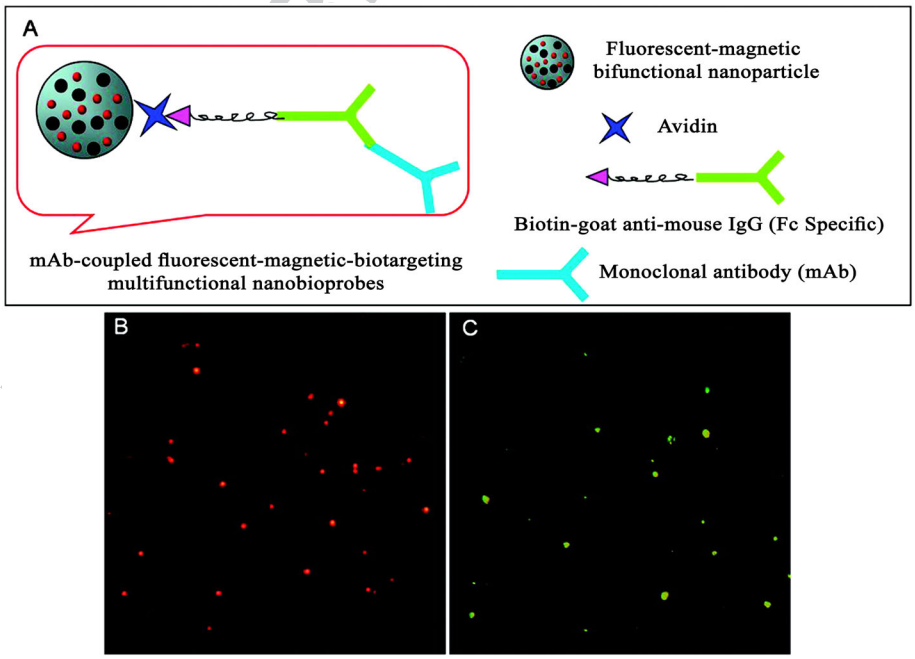

Figure 3. (A) Schematic drawing of a mAb-coupled fluorescent magnetic biotargeting multifunctional nanobioprobes (FMBMN). Fluorescent magnetic bifunctional NPs were covalently coupled with avidin. They were then coated with biotinylated goat antimouse IgG (Fc specific) via the biotin–avidin interaction. Mouse monoclonal antibody (mAb) was then attached to the NPs via the binding to the goat antibody. (B and C) Fluorescent microscopic images of anti-CD3 mAb-coupled red nano-bioprobes (B) and anti-PSMA mAb-coupled yellow nano-bioprobes (C). Each fluorescent dot came from a single mAb-coupled FMBMN containing multiple quantum dots. Reproduced with permission from Song *et al.* (232). Copyright (2011) American Chemical Society.

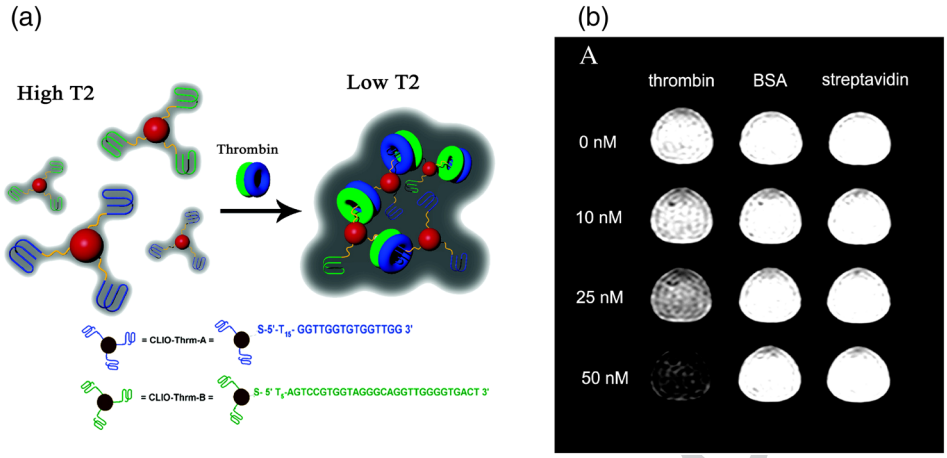

Figure 4. (a) The cross-linked iron oxide (CLIO) NPs (shown as red spheres) were modified with either Thrm-A, a DNA aptamer (shown as blue lines) that binds to fibrinogen-recognition exosite of thrombin, or Thrm-B, a DNA aptamer (shown as green lines) that binds to the heparin-binding exosite of thrombin. Addition of thrombin consisting of both fibrinogen (as blue rings) and heparin (as green rings) exosites resulted in aggregation of CLIO NP assembly, reducing the T_2 relaxation time. The DNA sequences are shown at the bottom. The drawing is not to scale. (b) Contrast change in T_2-weighted MR image in 1:1 CLIO–Thrm–A and CLIO–Thrm–B mixture with 0, 10, 25 and 50 nM thrombin (first column), bovine serum albumin (second column) and streptavidin (third column). Reproduced with permission from Yigit *et al.* (239). Copyright (2008) American Chemical Society.

imaging-based techniques have been used as reproducible and reliable noninvasive diagnostic as well as treatment monitoring methods in patients with chronic liver disease. Although morphological alterations, such as surface nodularity and widening of fissures, are visible in conventional MR imaging, fibrosis itself is not clearly visible in MRI (242). Contrast-enhanced magnetic resonance imaging has retained a significant role in both treatment and follow-up imaging of different types of liver tissue abnormalities, such as fibrosis, particularly at cellular level (240). Since its introduction, SPIO has played a pivotal role especially in hepatic imaging. The superparamagnetic properties of SPIO cause a local magnetic field inhomogeneity around the particles and hence shorten the T_2 and T_2* relaxation times of the neighboring regions, producing a decreased signal intensity in T_2- and T_2*-weighted MR images (243).

Liver cellular imaging using SPIONs is mainly based on passive imaging, which relies on natural and rapid opsonization followed by sequestration of SPIONs by Kupffer cells in the liver upon intravenous injection. Kupffer cells in the liver are specialized macrophages that form part of the RES in liver. They are involved in the normal physiology, homeostasis and innate immune response of the liver. Since they contribute to the pathogenesis of several liver disorders, an imaging method that allows monitoring the activity of Kupffer cells could provide valuable information in diagnosis of liver status in health and disease. SPIONs are typically required to have a large hydrodynamic size and/or a hydrophobic or charged surface to be readily opsonized by plasma proteins and taken up by RES cells, including Kupffer cells (244). After intracellular uptake, SPIOs end up in the lysosomes and then lose their superparamagnetic properties and solubilize to become part of the normal iron pool, such as ferritin or hemoglobin (245). Cellular uptake of SPIOs in healthy liver tissue results in hypointensity on T_2-weighted images of normal parenchyma (246). On the other hand, the fibrotic areas in the liver, which have a much reduced number of Kupffer cells, accumulate less SPIOs. This leads to an enhancement in the contrast-to-noise ratio of the lesion with subsequent improvement of demarcation with increased conspicuousness. In addition to fibrotic tissue, most primary or metastatic liver tumors are deficient in Kupffer cells and do not exhibit SPION accumulation. Similar to fibrotic tissue, liver tumors also appear relatively hyperintense because the background liver darkens preferentially (247). A study reported the use of alginate-coated SPIOs with a hydrodynamic diameter of 193.8 nm to visualize hepatic lesions in a rodent model. After injection, 80% of the SPIOs accumulated in the liver, lowering the signal intensity in healthy liver and revealing previously undetectable HCC in the rats (248). Interestingly, the liver tumors can be detected even in the cirrhotic liver where SPION uptake has been strongly impaired (249). Nevertheless some sorts of hepatic lesions, such as hepatocellular adenoma, focal nodular hyperplasia, dysplastic nodules and well differentiated HCC, sustain phagocytic activity and may demonstrate SPION uptake and become isointense to normal liver tissue (250). For these patients, an MRI finding may not be precisely pathognomonic for the disease. Double contrast imaging using SPIONs and gadolinium-based contrast agents will enhance the clarity of liver lesions, especially for fibrosis. Because of the synergistic effect of signal reduction of background liver tissue by SPIONs and enhancement of the signal of the water component within fibrotic tissue by gadolinium complexes, the visibility of liver fibrosis will be maximized (251). There are some shortcomings when SPIONs are used for cellular imaging of liver (252): (a) inability to assess lesion vascularity; (b) decrease in signal intensity of cirrhotic liver with SPIONs limited compared with that in normal liver; (c) lesion–liver contrast enhancement being weaker for HCCs arising in cirrhotic liver than for hepatic metastases occurring in normal liver; and (d) HCCs possibly containing a number of Kupffer cells, and some well-differentiated HCCs exhibiting signal decrease after SPION administration.

SPION formulations such as Ferumoxides, Endorem® with dextran coating and Ferucarbotran® with carboxyl dextran coating were approved specifically for MR imaging of the liver. These formulations are generally nonspecifically phagocytized by Kupffer cells or endocytosed by RES in the liver, spleen and bone marrow after i.v. injection. Cellular labeling and imaging with these formulations not only show variable engulfment efficacy, but are also limited to phagocytic cells (252).

Since the evaluation of function of nonphagocytic hepatocytes has an important role in clinical conditions such as liver

transplantation or hepatitis, imaging liver with hepatocyte-selective approaches is promising. The selective hepatocellular internalization of SPIONs and targeting can be controlled by modification of NP surfaces with various types of targeting moieties such as antibodies, peptides, nucleic acids and carbohydrates. Since hepatocytes have a high density of asialoglycoprotein receptor (ASGP-R) per cell that readily binds to carbohydrates such as galactose, many SPIONs have been modified on the surface with carbohydrates (253). For example, Lee *et al.* (254) demonstrated the use of SPIONs coupled with galactose as a hepatocyte-targeted MRI and nuclear imaging contrast agent in a mouse model. Using NHS/EDC chemistry, they coupled lactobionic acid, which has high affinity for ASGP-R, onto dopamine-modified SPIONs labeled with ^{99m}Tc. Within a few minutes after tail vein injection, *in vivo* microsingle photon emission computed tomography (SPECT)/CT images and T_2-weighted MR images showed high accumulation of SPIONs in liver, with 38.43 ± 6.45% injected dose per gram. Blocking the ASGP-R with free galactose significantly reduced the liver uptake of SPIONs, indicating ASGP-R-mediated internalization of the NPs into hepatocytes. Transmission electron microscopy images of liver tissues also showed that the lactobionic acid-SPIONs were localized in hepatocytes. Similarly, Yoo *et al.* (255) reported hepatocyte-specific delivery of SPIONs by coating them with galactose-carrying polymer for liver imaging. In their study, modified polystyrene bearing β-galactose side chains (PVLA) were used for coating of SPIONs with an average size of 25 nm. After 1 h post-injection of the PVLA-coated SPIONs in rat tail vein, the relative signal enhancement of the T_2-weighted MR images was observed in the liver with a T_2 signal drop of 75.4% for PVLA-coated SPIONs and 36% for a control, pyrrolidone-coated SPIONs, which clearly indicates the accumulation of NPs in liver. Data obtained from their *in vitro* confocal laser scanning microscopy study using fluorescein isothiocyanate (FITC)-labeled SPIONs also confirmed the presence of SPIONs inside the cell membrane, uniformly distributed in the cytosol. Despite valuable information provided from MRI enhanced with SPIONs contras agent, MRI images are limited to macroscopic information including anatomical data, such as tumor size or location. However, the acquisition of microscopic information such as cellular internalization, intracellular trafficking and specific cell type is not usually easily feasible with MRI enhanced with SPIONs (256). Therefore, SPIONs have been linked to other imaging moieties to bring a multimodal imaging system that can be used to confirm MR visualization of SPIONs monitoring of therapeutic intervention efficacy. Zhu *et al.* (257) reported the synthesis of optically active core–shell SPIONs containing a fluorescent moiety. Since direct contact between iron oxide and fluorescent materials may give rise to fluorescence quenching, SPIONs were first bonded with oleic acid followed by modification with a hydrophobic alkyl segment of polymerizable surfactant sodium undecylenate (NaUA) forming a first and second layer, respectively. Then, styrene and glycerol methacrylate were added to the particles and subsequently polymerized with the active double bond of NaUA to form the primary seeds of SPIONs/poly(St-co-GMA) possessing a uniform core–shell structure. Then, the rare earth complexes [Eu(AA)$_3$Phen] were added to polymerize the remaining styrene and glycerol methacrylate on the preformed seeds to form the core–shell SPIONs with fluorescent properties. Consistent with histological evidence using Prussian blue staining, the appearance of red fluorescence dots confirmed the accumulation of fluorescent SPIONs in the Kupffer cells in the liver after intravenous injection through rat tail vein. Although these particles are mainly phagocytized in liver, the presence of free epoxy groups on the surface of particles can easily allow further modification of fluorescent SPIONs to incorporate a hepatocyte targeting moiety, such as antibodies or carbohydrates, to be able to visualize hepatocyte cells.

In addition to cancer imaging, SPIONs have been used as agents for cell death detection, as an early biomarker of the efficacy of anticancer treatment, and evaluation of tumor progression (258). Radermacher *et al.* injected transplantable liver tumor cells intramuscularly into the right gastrocnemius muscle of mice to induce tumors. As treatment, tumors were irradiated by an X-ray-dose of 10 Gy to induce cell death. Then, pegylated SPIONs were coupled to apoptosis recognizing moieties (PS-targeted E3 hexapeptide, peptide sequence: TLVSSL) and injected in the mice at predetermined intervals. The results obtained *in vivo* demonstrated the selectivity of peptide grafted SPIONs for radiation-induced cell death compared with controls (259).

Despite the fact that SPIONs will naturally accumulate in liver, active targeting of SPIONs to liver macrophages has also been investigated. Vu-Quang *et al.* (260) reported on the use of β-glucan coated SPIONs to target specific receptors, like dectin-1, in immune cells. Using nonopsonic recognition, the specific interactions of these SPIONs with immune cells can be used for the precise detection of metastatic regions deficient in immune cells. Despite the significant drop in MR signal intensity of β-glucan-coated SPIONs compared with dextran and PVA-coated SPIONs in *in vitro* conditions, β-glucan-coated SPIONs had delayed uptake by the liver.

Currently, the only curative treatment for a variety of acute and chronic liver diseases is liver transplantation. Therefore, it is vital to evaluate hepatocyte integration within the liver parenchymal plates after intrasplenic and/or intraportal hepatocyte injection. Different approaches can be applied in order to endow cells with sufficient magnetization to be detectable by MRI. One of the easiest ways is the co-incubation of cells with SPIONs, where the particles are generally internalized through either spontaneous endocytosis pathway or phagocytosis. The uptake of SPIONs by cell can be triggered by linking biological effectors on SPIONs such as antibodies, transferrin or HIV-Tat peptide (261).

The presence of SPIONs in cells allows the detection and location of transplanted cells *in vivo* by MRI (262,263). Nevertheless, robust strategies need to be developed to distinguish single cells from clusters of cells, or contrast agent that leaked from dead cells. For example, donor cell death or any leakage of SPIONs from transplanted hepatocytes can result in particle release followed by endocytosis by Kupffer cells or host hepatocytes in the liver, which make it difficult to distinguish the fate of transplanted cells. Luciani *et al.* visualized the engraftment of intraportally injected mature mouse hepatocytes labeled with anionic SPIONs at 1.5 T. In MRI images, labeled cells were detectable and were mainly found close to portal tracts and along liver sinusoids (264).

4.2. Gastrointestinal Tract Imaging

Chronic inflammatory bowel diseases, that is ulcerative colitis (UC) or Crohn's disease (CD), and gastric or colorectal cancer affect many people worldwide. MRI has great advantages in the diagnosis and monitoring progress of gastrointestinal (GI) diseases, as well as in the noninvasive evaluation of therapeutic outcomes (265). Conventional MRI for the study of GI diseases is usually limited owing to poor luminal contrast resolution. MRI contrast agents are very important for gastrointestinal MR

imaging in the diagnosis of ulcerative colitis and stomach and colorectal cancer, as they overcome this limitation (266). SPIONs as MRI contrast agents for gastrointestinal imaging are usually administrated orally. These SPIONs are required to distinguish bowel from intra-abdominal masses and normal organs in abdominal imaging and allow the luminal surface of the bowel wall to be evaluated accurately (267). Two factors, namely thickness and contrast enhancement of the bowel, are normally used as markers for colitis in MRI studies. There are several preparations of SPIONs as oral MRI contrast agents, including AMI-121 (Lumirem by Guerbet and Gastromark by Advanced Magnetics) and OMP (Abdoscan, Nycomed). These SPIONs are coated with nonbiodegradable and insoluble coatings, such as siloxane and polystyrene, and suspended in viscosity-increasing agents to protect them against digestion in the gastrointestinal tract as well as aggregation (268). In a recent mouse model, D'Arienzo *et al*. (269) showed the high sensitivity of AMI-121 for the assessment of UC, which allowed information to be gained about the colonic luminal surface, as well as the bowel wall in its whole extension and the perivisceral structures. According to their findings, even using gadolinium complexes as double-contrast imaging agent did not provide more information than single oral contrast agents.

UC and CD present uncontrolled inflammation in the small and/or large intestine, associated with increased presence of neutrophils, natural killer cells, mast cells and regulatory T cells. Elevated secretion of inflammatory species, such as tumor necrosis factor alpha (TNF-α), interferon-gamma, interleukin (IL)-17 or matrix metalloproteinase, can induce degradation of the lamina propria or deeper tissue layers such as submucosa, muscularis and serosa in intestine (270). In UC and CD, bowels are infiltrated with inflammatory cells that can take up SPIONs, allowing their accumulation in the inflamed area. SPION-enhanced MRI is a diagnostic imaging modality that can differentiate between unspecific swelling and inflammatory regions in the bowel. Frericks *et al*. reported on cell-specific imaging of UC using SHU 555 C SPIONs. Ninety minutes after intravenous injection of SPIONs into a mouse, the inflamed colon wall showed a significant signal-to-noise ratio reduction in T_1-, T_2- and T_2*-weighted images. Histological evaluations measuring thickening of the bowel wall, transmural infiltrations and ulcerations were in excellent agreement with MRI results (271).

The risk of colon cancer is higher for patients with UC and CD. For these patients, the cumulative exposure to ionizing radiation during diagnosis, treatment and subsequent monitoring can be substantial. Therefore MRI imaging can be a much safer alternative. Development of cell-specific MRI imaging for colon visualization has a major role in clinical oncology. Jalalian *et al*. used SPION-epirubicin for combined colon cancer cell imaging and therapy. They used 5TR1 aptamer as a high-affinity targeting ligand for C26 colon carcinoma in mouse. Aptamer–SPION bioconjugates and free SPIONs as control intravenously injected to C26 colon carcinoma bearing mice were followed by acquiring a T_1 fat suppression MR image of the mice at different times. While there was no reduction in signal intensity after 1 h post-injection of free SPIONs, aptamer–SPIONs exhibited remarkable contrast in the tumor area indicating a large accumulation (272).

When using SPIONs as a colon cellular imaging agent, efficient internalization and transportation by colon cells into deep layers of the tissue is a must, especially when SPIONs are orally administered. These SPIONs need to cross the GI barrier, which is a complex barrier-exchange system composed of the epithelial cells lining the digestive tube and the tight junctions that tie them together (273). Currently, there are few reports on the evaluation of the uptake and transport of SPIONs by human colon cells. In one study, Kenzaoui *et al*. (274) investigated the surface characteristics of SPIONs that allow or prevent their uptake and transport across human colon cells. In their study, they developed a three-dimensional spheroid model system by growing HT-29 or Caco-2 cells under static conditions, which resulted in rounded spheres, and then investigated the uptake of aminoPVA-SPIONs (cationic) and oleic acid-coated SPIONs (anionic). These SPIONs showed different uptake behavior: aminoPVA-SPIONs were observed in deep layers of Caco-2 cell and HT-29 spheroids, while oleic acid-coated SPIONs showed less penetration ability and could only be found in the first cell layers of spheroids of Caco-2 cells. However, neither aminoPVA-coated nor oleic acid-coated SPIONs were transported across gastrointestinal barriers. Colon barrier models, such as the CacoReady or the CacoGoblet, indicate that the penetration ability of SPIONs in tissue does not guarantee their passage through healthy GI barriers. Since in inflammatory bowel disease or colon cancer the barrier may represent a dysfunction, SPION penetration and transportation may be facilitated and provide an opportunity for imaging of colon disease. Corem-Salkmon *et al*. reported SPIONs conjugated with two targeting moieties, peanut agglutinin and anticarcinoembryonic antigen antibodies (αCEA), for *in vivo* colon cancer imaging. These two molecules specifically bind to antigens that are up-regulated on the various colorectal cancer cell lines. After conjugation of cyanine near-infrared fluorescent dye to albumin-modified SPIONs, they were further covalently conjugated with the αCEA and peanut agglutinin. The modified SPIONs were then administered through the anus, using the guidance of mini-colonoscopy, to athymic nude mice bearing 2-week old lumen-facing LS174T tumors. After removing and washing the colon, the tumor area showed a high fluorescence intensity 3–13 times higher than that of the neighboring nonpathological tissue (275).

SPIONs can be used for diagnosis as well as treatment of gastric cancers. This cancer traditionally has a poor prognosis, with 79% of tumors diagnosed at stage IV and 5 year survival $<$5% (276). Therefore, detection of gastric cancer at an early stage is very important. In a recent study, Chen *et al*. (278) Q5 reported combined gene therapy and imaging of gastric cancer. They used polyethylene glycol-grafted polyethylenimine–SPIONs (PEI–PEG–SPION) as a nonviral vector for delivery of small interfering RNA (siRNA) to silence genes involved in the metastatic ability of gastric cancer cells. Two tumor cells, namely SGC-7901 cells with high expression of CD44v6 and A375 cells with no expression for CD44v6, were used. The PEI–PEG–SPIONs containing siCD44v6 were injected to mice to detect the tumor targeting ability. Despite the fact that PEI–PEG–SPION could lead to T_2 hypointense signals in liver, in both SGC-7901 and A375 tumor sites, there was no obvious signal drop. Although the authors related this to a large particle size that promoted their uptake by liver, insufficient stealth characteristics of the particles also aided in their rapid removal from circulation before reaching the cancer site (244).

4.3. Lymph Node Imaging

The lymphatic system is a network of tissues and organs that consists of lymph nodes, lymph vessels and lymph. Spleen, thymus, adenoids and tonsils are all part of the lymphatic system

(277). Diseases and disorders of the lymphatic system include Hodgkin's lymphoma, lymphangiosarcoma, lymphangioma and lymphoma. Nodal diseases, especially metastatic cancers of lymph nodes, are adverse prognostic factors in many types of cancers (278). In some forms of cancers, dissemination of cancerous cells usually follows an orderly progression. Since the flow of lymph has an upwards direction, cancer spread occurs first near lymph nodes close to the tumor site and then the echelons of lymph nodes are engaged. Therefore, the development of a non-invasive, tissue-specific and highly sensitive imaging technique for assessing lymph node status will greatly help to stage cancer, plan neoadjuvant therapy and determine patient outcome (278,279). MR has been considered a particularly attractive platform for lymph node imaging. Despite the fact that measurement of nodal size by imaging is an accepted method for evaluation of nodal incursion by metastatic cells, the size criterion overlooks metastasis, especially if micrometastasis is involved (280,281). An additional criterion, such as morphological change of nodal glands to a more rounded shape after tumor infiltration, can also be used as a supporting factor for better diagnosis, but still cannot reveal microscopic metastasis (282,283). SPIONs that are RES-targeted MR contrast agents have raised great interest. Following intravenous or subcutaneous injection, SPIONs are distributed to the lymph nodes by two distinct pathways: either by way of the high endothelial nodal venules followed by phagocytosis by macrophages, or through transcapillary passage into the interstitium followed by uptake of the NPs by draining lymphatic vessels and lymphatic transport to the lymph nodes via afferent lymphatic channels (283–285). Certain characteristics of SPIONs, such as size, surface charge and coating, are associated with preferential trafficking to lymph nodes (286). For example, while small SPIONs of $<$50 nm can transmigrate the capillary wall and end up in lymph nodes, bone marrow, liver, and spleen, larger SPIONs of around 150 nm can be found only in liver and spleen (277,283).

Ferumoxtran-10 (Combidex, AMAG Pharmaceuticals Inc., Cambridge, MA, USA) is the first and most studied contrast agent for lymphatic imaging. Macrophages in a healthy lymph node with normal function take up a large number of these NPs, leading to shortening of T_2 and T_2* times and resulting in a marked decrease in signal intensity and darkening of the lymph nodes. Lymph nodes with infiltrated malignant tumors are devoid of macrophages and consequently they lack uptake of Ferumoxtran-10 and either remain isointense or display a heterogeneous signal intensity if only partial or micrometastases are involved (282,287). Similarly, if metastases disturb lymphatic flow, SPIONs lose accessibility to the nodes, resulting in a hyperintense nodal image in MR. With a similar mechanism to that described above, SPION-enhanced MR can be used for imaging and differentiating normal, hypercellular and neoplastic tissues in other lymphoid tissues such as bone marrow and spleen (288,289). SPION-enhanced MR has been prospectively used for lymphatic mapping and sentinel node location, as well as to evaluate the stage of different types of cancers through depicting lymph node metastases (290). For example Harisinghani *et al*. (291) reported that, for the patients with prostate cancer in T_1, T_2 or T_3 stage, lymphotropic MR with superparamagnetic NPs correctly identified all patients with nodal metastases, and a node-by-node analysis had a significantly higher sensitivity than conventional MR. Lymphotropic MR with SPIONs has been shown to improve nodal detection and sensitivity, specificity and accuracy in other types of cancer such as bladder (292), testicular (293), penile (294), esophageal (295), rectal (296), endometrial and cervical cancers (297).

Lymph nodes house T cells and B cells, which are immune system cells that originate from bone marrow stem cells. T cells have been involved in a number of diseases, such as multiple sclerosis, and therapeutically in cancer immunotherapy. However, cell-based therapies for cancer are far from being optimal. Therefore, the ability to visualize T cells by MRI and to obtain information on molecular mechanisms that mediate the recruitment of these cells could assist early detection of disease and improve these therapies (298).

Since the earliest cellular MRI experiment, which was endocytosic labeling of rat T cells by dextran-coated SPIONs (AquaMag100 and BMS180549), successful labeling of lymphocytes for MR imaging has continued using different strategies (299,300). As uptake of SPIONs by endocytosis is relatively inefficient, Hu *et al*. reported that citrated anionic SPIONs allow a better labeling of T cells. On T_2-weighted MR images, a heterogeneous decrease in intensity appeared, indicating tumor infiltration of these labeled T cells (301). Functionalization of dextran-coated superparamagnetic iron oxide particles with a peptide sequence from HIV-1 transactivator protein (Tat) has also been shown to dramatically enhance T cell labeling in tumor immunotherapy using a B16-OVA melanoma model. Interestingly, it was shown that the labeled cells showed a heterogeneous spatial and temporal recruitment and therefore multiple administrations are required to provide a more effective therapy for solid tumors (302). Arbab *et al*. also reported that dextran-coated SPIONs (ferumoxides) and protamine sulfate as a cationic cell transfection agent are efficient for T cell labeling (303). Another type of immune cell that has been considered for immune therapy, including cell-based therapy for cancer treatment, is dendritic cells. These cells reside in tissues that are in contact with the external environment, such as the skin or inner lining of the nose, and upon activation migrate to the lymph nodes to interact with T cells and B cells, initiating the adaptive immune response. De Vries *et al*. (304) described immune therapy for patients with melanoma using autologous dendritic cells (DCs). Immature DCs were labeled with ferumoxide administered to patients under ultrasound guidance. Mature labeled DCs kept their phenotype and morphology as their antigen-presentation function and migration ability did not change. In addition they were positive for the dendritic cell markers S100. Eight stage III melanoma patients received an intranodal injection of a 1:1 mixture of ^{111}In- and SPION-labeled DCs and were then imaged by both scintigraphy and MR to both quantify and monitor delivery of the dendritic cells and their subsequent migration to nearby lymph nodes. In MR images (at 3 T), not only the injection site but also remote lymph nodes containing SPION-labeled DCs could be visualized individually. The localization of SPIONs in nodes was further confirmed by immunohistopathology assays. Histological evaluations showed the presence of iron-containing DCs in paracortex and sinuses of the lymph node, indicating the entry of the injected cells via their natural route through the afferent lymph vessels. Most of the labeled cells were collected to T cell areas. The presence of enlarged T cells around SPION-labeled DCs confirmed T cell activation, which is a requirement for effective dendritic cell vaccines. The authors concluded that MRI is significantly better than scintigraphic imaging for tracking dendritic cells. Another study confirmed the possibilities of SPION-enhanced MR imaging for effectively tracking the migration of DCs *in vivo*

(305). While the above-mentioned studies have focused on SPION imaging, Noh *et al.* reported on the fabrication of a one-pot antigen system that delivers antigen to DCs and simultaneously tracked their *in vivo* migration after injection. In their study, PLGA NPs containing bimodal imaging probes, that is, near-infrared fluorophores indocyanine green (ICG) and SPIONs, were used. The particles were loaded with ovalbumin (OVA) as antigen. For *in vivo* imaging, DCs were cultured first with PLGA–SPION–OVA–ICG and then treated with TNF-α (50 mg ml^{-1}) to enhance DC migration to the draining lymph nodes. Particles were injected into the hind leg footpads of mice. Darkened images from the popliteal lymph node of the right hind leg suggested that DCs labeled with SPIONs successfully migrated from the injection site to the adjacent lymph nodes. The induction of OVA-specific CD8 + T lymphocyte response was further checked by cytotoxicity against EG7-OVA tumor model cells. The lymphocytes isolated from mice immunized with DCs treated with PLGA–SPION–OVA–ICG showed high cytotoxicity against EG7-OVA. In contrast, mice injected with DCs treated with controls, including soluble OVA, SPIONs loaded with human albumin serum, or medium, showed moderate and low cytotoxic T lymphocyte responses (306).

4.4. Central Nervous System Disease Imaging

A CNS disease can affect either the spinal cord or brain. Owing to the complexity of the CNS, in particular of the brain, and the complications of cerebrospinal fluid analysis, biopsies and laboratory analyses, and the relative inaccessibility to brain tissue in living models, imaging remains an important tool for a wide range of diagnostic purposes including identification of inflammatory loci, T staging of tumors, visualization of vascular structures and anatomical examination (307,308). The small size of SPIONs, their use as contrast agents and their ability to carry targeting vectors and drugs across anatomical and physiological compartments in the CNS open up new methods for targeted therapy and imaging. Table 2 shows a brief description of CNS diseases and involved pathological mechanisms.

Table 2. Some central nervous system diseases and their pathological mechanisms

Disease	Pathological mechanisms
Multiple sclerosis	Severe alteration of blood brain barrier, loss of tight junctions, degradation of basal lamina, infiltration of T cells and macrophages, autoimmune response against myelin, chronic inflammation, oligodendrocyte cell death, and axonal damage (308).
Stroke	Cerebral ischemia through vascular obstruction initiated by inflammatory processes in the endothelial cells of the vessel wall. Drastic decrease in the supply of oxygen and glucose. Initiation of an ischemic cascade that involves necrotic cell death, apoptotic cell death and an increased infiltration of monocytes and macrophages (309).
Alzheimer's disease	Accumulation of toxic aggregated amyloid fibrils that induce apoptosis. Lesions of Alzheimer's disease are associated with various inflammatory processes that may have a secondary role to tissue damage.
Meningitis	Inflammation of meninges caused by viruses, bacteria and microorganisms.
Epilepsy	Various causes; however, possible prolonged stimulation of pro-inflammatory signals, by seizures or a persistent pro-inflammatory situation in brain, may contribute to the establishment of a pathological substrate (310).
Brain tumors	Gliomas, meningiomas, pituitary adenomas, nerve sheath tumors.

After intravenous administration, the majority of the SPIONs are rapidly sequestered from the blood circulation by cells of the RES. On the other hand, some of them are also captured by circulating phagocytes in the blood, which provides a tool of choice to monitor the involvement of macrophages in CNS diseases such as multiple sclerosis, traumatic nerve injury, cerebral stoke and brain tumors. The common feature of all the above diseases is the involvement of immune system and inflammation (311). Multiple sclerosis (MS) is an inflammatory disease of the CNS characterized by demyelination and axonal loss. MS lesions show patchy infiltrations of autoreactive T cells with T helper 1 cells and macrophages. Phagocytic microglia cells and blood-borne macrophages play central roles in balancing the immune reaction, in myelin attack and removing myelin debris (312). The sensitivity of MR imaging for detecting single cells in brain has been previously demonstrated in the literature (313). The current MRI contrast agent for MS is a non-specific Gd complex that allows visualization of the blood–brain barrier (BBB) leakage, which is the consequence of the inflammatory process, but not inflammation itself (314). In contrast, transcytosis of SPIONs through the endothelium and uptake by local resident microglia or infiltration of activated blood monocytes that have phagocytozed SPIONs allows imaging of cellular infiltration in MS and enhances the cellular visualizing aspects of inflammation (315,316). Amongst these mechanisms, the transcytosis is less probable as recent studies have shown that flux of SPIO lacking any targeting moieties on the surface throughout BBB is very limited under normal conditions (317,318).

In *in vivo* allergic encephalomyelitis studies, MR enhancement from Ferumoxtran-10 is different than that from Gd-complexes. Gd enhancement is associated with BBB leakage, while cellular infiltration in MS lesions is related to macrophage infiltration and not to any alternative path to reach the brain parenchyma. In all of these encephalomyelitis studies, histological examinations corroborated the MRI observation that SPIONs were mainly localized in macrophages in the CNS parenchyma (319–321). Accordingly, Bendszus *et al.* (322) showed that, after peripheral nerve injury in a rat model associated with macrophage infiltration, SPIONs were accumulated in degenerating sciatic nerves. In contrast, after optic nerve crush, which involved microglial activation but lacked macrophage infiltration, there was no SPION accumulation. Similar results have been observed in human studies. Using Ferumoxtran-10 SPIONs (Sinerem, Guerbet Laboratory, France), Dousset *et al.* investigated whether monocyte/macrophage labeled SPIONs infiltrate inflammatory MS brain lesions. Since SPIONs are too large to cross the BBB by passive diffusion, crossing of SPIONs was assumed to be related to SPIONs loaded monocytes, which actively crossed the BBB (312). Vellinga *et al.* (323) conducted a comparative experiment between SPIONs and Gd-complexes in 19 MS patients. In their study, they used SHU555C SPIONs, which are smaller than Ferumoxtran-10, have a shorter blood half-life and enhance

uptake by monocyte owing to their negative charge. Among 14 MS patients, 188 SHU555C positive lesions were detected, 144 of which were Gd negative. On the other hand, there were a total of 59 Gd-positive lesions, 15 of which were SHU555C negative. Owing to the fact that 77% of SHU555C positive lesions were found in areas where the BBB was intact and SHU555C particles were uptaken by monocytes in the bloodstream, the authors suggested that SPION-enhancement is subject to a different, probably cell-specific mechanism. Other studies have also shown that MR imaging with Ferumoxtran-10 exhibits different sizes and locations of lesions in MS than imaging with gadolinium complexes. These differences apparently are due to the difference in size, phagocytic cell specificity and the plasma half-life of the two agents (324).

Another clinical application of SPION cellular imaging is the evaluation of inflammation in cerebral ischemia. Ischemic stroke occurs because of a loss of blood supply to a part of the brain, initiating an intense local inflammatory response that involves microglial cell activation as well as infiltration by monocytes (325). These cells produce a wide spectrum of cytotoxic substances and may thereby aggravate the ischemic tissue damage. The main use of SPIONs in stroke management is the visualization of the affected area, revealing the extent of BBB breakdown and showing the movement and migration of immune cells inside brain (326). Rausch *et al*. (321) studied SPION enhancement in a permanent middle cerebral artery occlusion model in rats. Twenty-four hours after intravenous injection of SPIONs (Sinerem®, Guerbet, France), T_2-weighted MRI revealed accumulation of activated macrophages in the periphery of the lesion area. Subsequent *in vivo* MR studies using a variety of SPIONs, with a similar approach to Rausch *et al*. and Corot *et al*., have shown delayed onset of monocyte infiltration following ischemia in various rodent models (327,328). Histological results have corroborated this, as it has been shown that blood-borne macrophages infiltrate the ischemic area with a minimum delay of 24 h followed by main infiltration between 3 and 6 days (329). Following successful *in vivo* animal studies, Saleh *et al*. pioneered the clinical MRI study of ischemic stroke in 10 patients using Sinerem® at 5–7 days after stroke onset. The cerebral MRI signal was in agreement with the expected distribution of macrophages and confirmed their infiltration from the peripheral blood (330). Nevertheless, for several reasons, there is no consensus yet on whether iron-containing cells in ischemic areas have originated from circulating monocytes. First, owing to the small size and neutral charge of SPIONs, their uptake in monocytes is limited. Furthermore, early MR signal changes are due to transfer through damaged BBB or passive diffusion of free SPIONs by intravascular trapping rather than by macrophage infiltration (331). A comparative study after administration of exogenously SPION-labeled mouse monocytes and free SPIONs revealed a significant difference between temporal and spatial distribution of SPIONs in the ischemic area, demonstrating that SPIONs in brain may not be entirely introduced by monocyte infiltration (332). According to the results of subsequent studies using different labeling techniques and a middle cerebral artery occlusion stroke model, it is suggested that systemically administered SPIONs may be sequestered by RES cells and migrate to inflammation sites in the brain (331,333). SPIONs can be alternatively used for noninvasive *in vivo* imaging of poststroke recovery of brain after cell-based therapies (334). Dunning *et al*. reported on a rodent model of persistent demyelination to demonstrate remyelination and CNS axonal regeneration after transplantation of SPION-labeled Schwann cells and olfactory ensheathing cells into focal areas of demyelination in adult rat spinal cord that can be identified by MR imaging. These cells were shown to readily take up SPIONs by pinocytosis without the need for any other labeling enhancing agents. SPION-labeled Schwann cells and olfactory ensheathing cells retained the ability to myelinate after transplantation into areas of persistent demyelination. In MR images, the transplant site showed a marked reduction in signal intensity on T_2-weighted images in animals receiving SPION-labeled cells that was detectable for 2–3 mm around the point of transplantation (335). In a recent study, Marinescu *et al*. monitored the therapeutic effect of an anti-inflammatory drug, minocycline, by SPION-enhanced MR in a stroke model in mice. Since minocycline inhibited microglia/macrophage activation, enhanced local phagocytic activity in the nontreated group was expected. The area of R_2 appeared significantly decreased in minocycline-treated mice; however, owing to the possible accumulation of SPIONs in noninflammatory tissue and nonphagocytized SPIONs, there was no significant difference upon treatment (336).

Another clinical application of SPIONs is in MR imaging of brain malignancies, which include primary brain tumors that originate within the brain and brain metastases that are initiated from primary tumors outside the CNS. Among primary brain tumors, gliomas are the most common. The tumor's microenvironment contains a mixture of heterogeneous cells including endothelial cells, which support angiogenesis, reactive astrocytes and inflammatory cells such as activated or reactive microglia and macrophages that frequently infiltrate tumors from the blood stream (337,338). Differential phagocytosis by inflammatory cells within and around the tumor vs normal brain tissue may be exploited to label cells with SPIONs for tumor detection, delineation of tumor boundaries, and quantification of tumor volumes (339,340). Zimmer *et al*. reported on intravenous injection of SPIONs in rats containing C6 glioma cells. All tumors became significantly hyperintense relative to brain tissue on T_1-weighted images. Small tumors showed a rather homogeneous hyperintensity, whereas in larger tumors a pattern of concentric rings was observed corresponding to the macrophage infiltration profile (341). In a study comparing ferumoxides to Ferumoxtran-10 in 20 patients with intracranial tumors, Ferumoxtran-10 outperformed ferumoxides in imaging intracranial tumors. Other groups have also shown similar findings (342). For example, Fleigie *et al*. Q6 demonstrated that SPION-labeled microglia can precisely show tumor morphology using *in vivo* MR (343). In addition to tumor diagnosis, SPIONs have been used for treatment monitoring in brain tumors. One of the main ways of suppressing tumor growth in brain malignancy is blockading neoangiogenic signaling pathways. As VEGF (vascular endothelial growth factor) overexpression in cancer cells has been shown to increase angiogenesis in brain tumors (344), neutralization of VEGF by the monoclonal antibody Bevacizumab® has been used as an effective measurement for treatment of gliomas (345). Tumor microvasculature heterogeneity is determined based on the number, diameter and perfusion of functional blood microvessels. Since antiangiogenic treatment of tumor may result in alteration of tumor phenotype, SPION imaging may therefore be an attractive tool for evaluating tumor response to therapy. Claes *et al*. compared conventional T_1-weighted Gd-DTPA-enhanced MRI with T_2*-weighted SPION-enhanced MRI in mice carrying orthotopic U87 glioma; the mice were either treated or not with the antiangiogenic compound

Vandetanib®. Owing to vessel leakage within the tumor and a relatively high tumor blood volume in untreated animals, both Gd-DTPA- and SPION-enhanced MRI resulted in good visibility. However, in groups treated with Vandetanib®, the blood–brain barrier was restored, which resulted in loss of tumor detectability with Gd-DTPA. On the other hand, in spite of decreased blood volume to the tumor, SPION-labeled macrophage continued to infiltrate the tumor, which resulted in its readily detection in SPION-enhanced MRI (345). Depending on the physicochemical properties of SPIONs, they can have a long blood circulation time and can therefore be found in the vascular compartment during the early vascular equilibrium phase before being phagocytized by macrophages (283). These SPIONs can be used as a susceptibility microvascular contrast agent during the vascular equilibrium phase (early post-SPION injection), to monitor therapy and determine blood volume (BV) and microvascular morphology. Hyodo *et al*. reported on the employment of BV as a marker of microvascularity for evaluation of the anti-angiogenic effect of Sunitinib® in squamous cell carcinoma tumor using SPIONs. High-resolution BV images obtained by SPION-enhanced MR showed about 46% reduction in tumor BV 4 days after the start of treatment with Sunitinib® (346).

4.5. Cardiovascular Disease Imaging

Cardiovascular disease is the leading cause of death worldwide. The causes of cardiovascular disease are diverse, but atherosclerosis and hypertension are the most common. In atherosclerosis, oxidized low-density lipoprotein particles in blood plasma invade the endothelium, resulting in its damage and the initiation of an inflammatory response. Circulating monocytes are recruited to the lesion-prone site followed by their migration to the subendothelial space and further activation into monocyte-derived macrophages (347). The presence of macrophages and the resulting phagocytosis of SPIONs are markers of unstable atheromatous plaques, which can be exploited to visualize the lesion prone arterial sites by cellular MR (348,349). Two theories have been proposed regarding the mechanism by which SPIONs enter atheromatous plaques. One is that circulating monocytes are labeled prior to migration to the lesion. The second is that SPIONs enter the plaques through a widened endothelial junction and then are engulfed by macrophages within the plaques (350).

Passive accumulation of SPIONs in inflamed atheromatous plaques and decreased focal signal intensity in the aortic wall has been clearly shown in animal studies (351–354). For example, in hypercholesterolemic rabbit models with double-balloon injury of the infrarenal aorta, Ferumoxtran-10 allowed quantitative MRI assessment of macrophage neointimal infiltration (355). Macrophage accumulation in inflamed artery has been applied to humans for inflammation evaluation and monitoring of stroke risk in patients. Preliminary clinical studies have shown that administartion of Ferumoxtran-10 can induce signal loss in carotid or aorta atheromatous plaques (356,357). Another clinical study confirmed the capture of Ferumoxtran-10 by macrophages in stenotic carotid plaques (358). The potential of MR cellular imaging for detection of inflammation in small-diameter vessels, such as coronary arteries, compared with large vessels may be limited. In small-diameter vessels it may be difficult to distinguish signal loss owing to the SPIONs from the dark vessel lumen (350). In cellular MR, the extent of SPION uptake is dependent on particle characteristics such as size, nature, charge, coating and cell type. For instance, phagocytic cells have been found to internalize large particles more effectively than small ones, whereas nonphagocytic T-cells internalize intermediate sized particles more efficiently than other sizes (359–361).

Nevertheless, SPION uptake and MR enhancement depend on the type of contrast agent and animal model. For example, Herborn *et al*. showed that, despite the larger size of Ferumoxtran-10 than Ferumoxytol, the lumenal enhancement over time with Ferumoxytol was the highest at day 3 and therefore it cleared the blood pool more quickly than Ferumoxtran-10, which had the highest luminal signal intensity on day 5 (362). In a recent study, Tsuchiya *et al*. compared the uptake by four types of SPIONs, that is, SPIONs, mannan-coated SPIONs and ultrasmall SPIONs (USPIONs), and mannan-coated USPIONs, in the rabbit atherosclerotic wall. Histological and imaging analysis showed that mannan-coated SPIONs and USPIONs were taken up more readily by the atherosclerotic rabbit wall than uncoated ones. Iron-positive regions were significantly larger in the mannan-coated particles, while USPIONs showed higher macrophage uptake than SPIONs. Since immune cells, including macrophages and monocyte-derived dendritic cells, express the mannose receptor, coating SPIONs with mannan increased their affinity for active atherosclerotic plaques compared with nonmannan-coated ones (363). The optimum time course for *in vivo* macrophage visualization using SPIONs in symptomatic human carotid disease has been reported to be between 24 and 36 h after SPIONs (Sinerem) infusion (358). SPION may be helpful in imaging aneurysma, especially those at increased risk of growth or rupture. Since abdominal aortic aneurysms have an underlying inflammatory cause, SPION-enhanced MR imaging can potentially be effective in the visualization and assesment of the severity of the aneurysms. In a study by Truijers *et al*., of patients with aneurysms, macrophage infiltration was limited in the aneurysm walls of one patient having aneurysms with a propensity for rupture or growth (364). Use of T_2 and T_2* pulse sequences provides a quantitative method for assessing SPION uptake by the aortic wall (365). Another aspect of the application of SPIONs in cardiovascular disease is imaging inflammatory processes in myocardial infarction. This is especially important for the noninvasive *in vivo* assessment of cellular myocardial inflammation process and healing and regeneration process, and for evaluation of the potential efficacy of therapeutic interventions. Alam *et al*. showed for the first time that Ferumoxytol, (AMAG Pharmaceuticals, Lexington, MA, USA) can be used for *in vivo* labeling of leukocytes in the human infarcted tissue by T_2*-weighted MR. Although they did not perform histology, based on previous evidence that SPIONs are taken up by macrophages, they visualized the cellular inflamation process in the patients with recent myocardial infraction and to a lesser degree in the peri-infarct and remote myocardium (366). For cardiovascular imaging, the proper blood half-life of an imaging agent is extremely relevant, otherwise the residual SPIONs will remain in the intervascural space causing false positive results. The blood half-life of Ferumoxytol in humans is around 15 h, therefore the changes in R_2* seen in the remote zone after the injection of the SPIONs may reflect some contribution from residual Ferumoxytol (367). In another recent study, Richards *et al*. reported the use of ferumoxides with rapid removal from the blood stream for *ex vivo* labeling of human monocytes. After their labeling, their homing to sites of myocardial infarction was visualized. In this study, the authors showed that, while injected

cells retained their viability and migratory function, they were able to migrate to inflammation sites, as confirmed by tuberculin skin testing. Subsequently, SPION-labeled cells could be clearly detected with T_2*-weighted MRI and R_2* maps (368).

In addition to cell myocardial inflammation monitoring, SPIONs have been used for noninvasive monitoring of inflammatory changes associated with cardiac graft rejection. Kanno *et al*. showed the accumulation of dextran-coated SPIONs in rats with heterotopic heart transplantation, revealing the infiltrating macrophages within the rejecting cardiac graft (369).

The ability of MRI to simultaneously image anatomy, physiology and molecular events provides an additional advantage in the study of cardiovascular diseases. Jaffer *et al*. (370) published a good review on molecular imaging strategies in the detection of clinical atheromata. They described some clinically promising applications of molecular imaging for high-risk atherosclerosis. Atherosclerosis, a chronic inflammatory disease of arteries, is characterized by endothelial activation and accumulation of inflammatory cells in the vessel wall. Imaging approaches have been developed to improve inflammatory lesion detection and to evaluate new targeted therapies in patients at risk of clinical events such as myocardial infarction or ischemic stroke.

In vivo molecular imaging in cardiovascular disease has used monoclonal antibodies or peptides covalently grafted to (a) magneto-fluorescent NPs for MRI and fluorescent molecular tomography (371), (b) microbubbles for ultrasound (372,373), (c) radiolabels with fluorine-18 for hybrid positron emission tomography–computed tomography (374), or (d) technetium-99 m radiolabels for single positron emission–computed tomography imaging (375).

McAteer *et al*. used a microsized approach for MRI of vascular endothelial inflammatory responses using microparticles of iron oxide (MPIO) (376,377). Owing to their confinement to the intravascular compartment, MPIO target specifically endothelial cell activation and leukocyte adhesion.

Experimental *in vivo* MRI studies with nano-sized iron oxide agents in hyperlipidemic rabbits (184,378) and in humans (175,379) have shown nontargeted SPION accumulation in macrophage-rich atherosclerotic plaques. In apoE$^{-/-}$mice, administered angiotensin II to accelerate vascular inflammation, SPIONs were localized in macrophage-rich atherosclerotic plaques (380). SPION accumulation in plaques over several days owing to macrophage activity was also observed (184). Applications to atherosclerosis have been reviewed by Mulder *et al*. (381) and then recently by McAteer *et al*. (382). Passive mechanisms were combined with new approaches to inflammation and the investigation of protease activity using activable MRI particles *in vitro* (383).

Cell adhesion molecules such as VCAM-1, ICAM-1, and selectin are attractive candidates for targeted nanosystems to activate endothelium in vascular pathology (384). VCAM-1-targeted cross-linked SPIONs, as diagnostic agents for vascular inflammation, were first described by Tsourkas *et al*. (138). Cy5.5-CLIO agent conjugated to VCAM-1 monoclonal antibodies demonstrated feasibility of *in vivo* imaging of VCAM-1 expression in TNF-α-stimulated mouse ear vasculature.

McAteer *et al*. (385) used 1 μm MPIO targeting to VCAM-1 in mouse models of cerebral inflammation. MRI detected enhanced uptake of anti-VCAM-1 Ab-coated MPIO in a mouse model of acute TNF-induced inflammation in the brain, blocked by pre-injection with anti-VCAM-1 Ab, validating probe specificity (385,386). As an alternative to Ab-targeting, several VCAM-1 targeting peptides have been identified by phage display and coupled to the magneto-optical CLIO particles (141,371).

SPIONs conjugated to a VCAM-1 specific cyclic peptide have recently been prepared for *in vivo* detection of vascular inflammation in early and advanced atherosclerotic plaques at ultra high-field strength MRI (17.6 T) (387).

In mice, a recent study investigated peptide-linked USPIONs with affinity for VCAM-1 and apoptosis, as previously identified by phage display (388). In both cases, these targeted particles displayed co-localization with the plaque, but each were shown to report on distinct biological processes.

4.6. Imaging Infection

During an infection caused by pathogens such as bacteria, phagocytes are activated and migrate to the site of microbial invasion and cytokines are released consequently, resulting in the activation of inflammatory cells. *In vitro*, SPIONs have been shown to be effective on various bacterial strains through a variety of mechanisms (389). However, targeting infectious sites *in vivo* is a bigger challenge. Most of the SPIONs with a size around 150 nm are opsonized and consequently phagocytized by Kupffer cells and the mononuclear phagocyte system of the spleen. A smaller number of SPIONs, which have a longer blood circulation time, are finally entrapped by the mononuclear phagocytic system of the liver and the spleen. The few remaining particles in the bloodstream may then escape into the extravascular spaces owing to the damage to the endothelium and the subsequent increase in vessel permeability in the infected area and may then be engulfed by phagocytes such as macrophages (390). Gellissen *et al*. reported the use of PEG-coated Fe_3O_4 with a mean size of 26 nm for infection monitoring up to a 60 min time delay after SPION administration. Owing to steric hindrance of PEG coating, opsonization was inhibited and these SPIONs had a longer blood circulation time. A model of infection was created by injecting *Staphylococcus aureus* into the right peritibial soft tissue of rats. In their study, the decreased signal intensity observed in inflamed tissue outside the RES was attributed to a net effect of perfusion, extravasation and phagocytosis of SPIONs. Owing to the presence of interstitial iron deposits in proximity to the abscesses, transcapillary iron oxide transport was proved (391). In another study, Kaim *et al*. reported on the visualization of infection in rats with ferumoxtran, by creating an abcess via injection of *S. aureus* suspension into unilateral deep calf muscle. Animals were imaged at different times to monitor acute, early chronic and late chronic infection. A significant decrease in T_2 relative signal intensity was found at 24 h, reflecting intracellular iron accumulation within macrophages (392). Lee *et al*. (393) studied the MR imaging of infectious arthritis of the knee or soft tissue induced by injection of a bacterial suspension. They used SPIONs of 62 nm to avoid entrapment in the RES of the liver and spleen. In their study, a signal intensity on T_2-weighted images characteristic of abscesses in soft tissue was found 4–7 days following SPION injection.

In a recent study, Baraki *et al*. (394) combined the cell tracking idea used in leukocyte scintigraphy for infection with the high anatomical imaging resolution of MRI to detect an acute soft tissue infection. Since neutrophil granulocytes are the first phagocytizing cells that infiltrate infectious tissue, Baraki *et al*. labeled these cells *ex vivo* with FeraTrack™ SPIONs and injected them in rat inoculated with subcutanous *S. aureus* suspension into the left parasternal chest area. MR images confirmed that

granulocytes migrated to the infection site causing signal loss in acute infections. The sensitivity of this technique, however, remains limited to acute infection detection, as chronic infection is associated more with macrophage and lymphocyte rather than granulocyte recruitment. In a recent study, Hoerr *et al.* established a new *in vivo* imaging platform by MR for tracking bacteria in infectious mouse models to study the biology of infection. In their approach, Gram-positive and Gram-negative bacteria were labeled with SPIONs and then injected subcutaneously or systemically to induce the infection model. MR images allowed bacterial tracking and showed that injected labeled bacteria in the foot pad migrate to the popliteal lymph node, resulting in hypointensities in this area (395). Bierry *et al.* evaluated macrophage imaging using SPIONs to differentiate between infectious vertebral osteomyelitis and aseptic inflamation associated with degenerative intervertebral disk endplates in human patients. The authors took advantage of the difference in macrophage distribution between vertebral infection and aseptic disk inflammation. Inflammation is usually associated with an acute, neutrophil-dominated response followed by recruitment of macrophages for cellular debris removal and induction of repair cascade. The population of macrophages then decreases and the major cellular infiltrations are fibroblasts and lymphocytes with macrophages accounting for only 10% of cells. However, there is a constant recruitment of macrophages in bone marrow and their attraction to the site of infection owing to the presence of the infectious agent. Bierry *et al.* in their SPIO-enhanced MR study found similar results. On T_2 MR images in the infection group there was a significant loss in abnormal endplates, while in the degenerative spine group there was no significant signal loss either on T_2 or on T_1 MR images (396).

4.7. Arthritis Imaging

Arthritis is a one of the joint diseases that involves inflammation of one or more joints. The most common form, osteoarthritis, is a degenerative joint disease, which is a result of trauma, infection, overuse or age. Osteoarthritis is associated with mild inflammation as the release of breakdown products from the cartilage into the synovial space mildly recruits inflammatory cells to facillitate debries removal. Another form of arthritis is rheumatoid arthritis, which is a systemic inflamatory disease involving synovial tissues (397). Dardzinski *et al.* used mice for SPION-enhanced visualization of inflammatory cells in arthrits to potentially assess the severity of disease and monitor the response to therapy. SPIONs were injected intravenously or intra-articularly. MR images showed accumulation of SPIONs in the popliteal lymph nodes following intravenous injection. However, the intra-articular injection resulted in signal loss in the joint. Nevertheless, a significant increase in SPION uptake and a decrease in signal intensity were observed in arthritic, as compared with control, mice (398). Apparantly owing to the small size of SPIONs, they extravasate across the discontinuous endothelium of microvessels and are entrapped in lymph nodes. In another study, Simon *et al.* investigated the ability of SHU 555 C, Ferumoxtran-10 and Ferumoxytol to detect and characterize antigen-induced arthritis with MR imaging. Interestingly, despite differences in size, charge and coating, all three SPIONs provided a marked and prolonged positive enhancement on early postcontrast T_1-weighted MR images and a persistent negative enhancement on delayed T_2/T_2*-weighted MR images, reflecting the uptake in activated macrophages in arthritic knees (399).

4.8. Imaging of Cell Migration and Cell Trafficking

Magnetic NPs represent efficient cell labels for cellular imaging. They are biodegradable and can be utilized by the cells in iron metabolism pathways (245,400). A technique has been developed to make ferumoxide transfection agent complexes to facilitate cellular uptake by endocytosis (401–404).

SPIONs like ferumoxtran and ferumoxides were combined with polycationic transfection agents to effectively label cells (401–408). However, most of the commercially available transfection agents are toxic to the cells at relatively low doses (233). By mixing together two agents approved by the US Food and Drug Administration, ferumoxides and protamine sulfate, a complex is generated that efficiently and effectively labels stem cells (401,402,409–411).

Cells are labeled with the ferumoxide–protamine sulfate (FePro) complex via macropinocytosis and can be imaged at clinical MRI fields. The concentration of iron in cells is dependent on the nuclear cytoplasm ratio, iron concentration, incubation times and method of endocytosis of the particles (401,404). These labeled cells have been used in different animal models and tracked by clinical MRI systems (412–414). One of the advantages of labeling cells using agents approved by the US Food and Drug Administration is the possibility of conducting clinical trials without facing major toxicity issues related to contrast and transfection agents. Owing to the susceptibility effect of SPIONs, labeled cells can easily be detected by MRI, compared with the cells labeled with gadolinium or T_1-based MRI contrast agents. Unlabeled stem cells usually contain less that 0.1 pg of iron per cell, whereas the labeled cells grown in suspension (i.e. hematopoietic stem cells, T-cells) contain 1–5 pg iron per cell. Cells that adhere to a culture dish (i.e. mesenchymal stem cells, human cervical cancer cells, macrophages) can take up from 5 to $>$20 pg iron per cell (401,402,412–414).

Different methods were tested to label cells for MRI cellular probes. Some teams have modified the surface charge of the NPs by coating them with cationic materials or modified the surface of the coating by attaching membrane penetrable peptides. Different types of coatings, like dextran or modified cross-linked dextran, dendrimers, starches or citrate, are usually attached through electrostatic interactions to the surface of the iron oxide crystal core (64). NPs are characterized by a positive or negative ζ-potential that determines the contrast agent's ability to interact with the cell/plasma membrane.

Dextran-coated NPs, such as ferumoxides, ferucarbotran or Ferumoxtran-10 (291,415–418) have been used to label cells. The cationic-coated NPs, carboxypropyl trimethyl ammonium (WSIO) and citrate (VSOP C184), were described as nanosystems that could be incorporated into endosomes of macrophages (419).

To facilitate cellular uptake of NPs, Bulte *et al.* prepared magnetodendrimers by coating NPs with PAMAM dendrimer (G = 4.5) (420). The labeled cells were transplanted into the ventricles of neonatal dysmyelinated Long Evans Shaker rats and the migration of labeled cells into the brain parenchyma could be observed by MRI up to 42 days after implantation.

SPION–TAT peptide has shown a very good intracellular magnetic labeling of different target cells such as murine lymphocytes, human natural killer cells and HeLa cells (421). The fluorescent TAT peptide has the sequence Gly–Gly–Cys–Gly–Arg–Lys–Lys–Arg–Arg–Gln–Arg–Arg–Arg–Lys–(FITC)–NH_2. The NPs were cross-linked with N-succinimidyl-3-(2-pyridyldithio) propionate, and TAT–FITC peptides were attached to the sulfhydryl

groups of SPIONs through a disulfide exchange reaction. SPION–TAT-labeled lymphocytes could be visualized in the liver and spleen in normal mice by MRI (422). CLIO–TAT-labeled T-cells have been used in adoptive transfer in an autoimmune diabetes mouse model. The labeled cells have been shown to selectively home to specific antigens in B16 melanoma in a mouse model (302,423,424).

The monoclonal antibody (OX-26) to the rat transferrin receptor was covalently attached to the SPION surface (MION-46 L) (425). Rat progenitor oligodendrocytes (CG-4) were successfully labeled with these NPs and the cells were implanted into the spinal cords of myelin-deficient rats. *Ex vivo* MR images obtained after implantation (10–14 days) showed excellent correlation between the hypointense regions and blooming artifacts caused by the presence of labeled cells and the degree of myelination in the spinal cord detected on immuno-histochemistry. Ahrens *et al*. (426) also labeled dendritic cells by biotinylating anti-CD-11 MoAb in interaction with strepavidin attached to dextran-coated SPIONs.

MRI tracking of stem cells has largely relied upon their *ex vivo* pre-labeling with magnetic NPs that can be internalized by the cells to generate strong MRI contrast (313,427–429). The ability to directly label stem cells with magnetic resonance (MR) contrast agents provides a simple way to accurately monitor cell delivery and track stem cells noninvasively. A variety of NPs can be constructed to obtain MRI contrast (430), and peptide-conjugation approaches can be performed to label cells with multiple-detection NPs (magnetic, fluorescent, isotope) (431,432). SPIONs represent the most widely used contrast agents for the detection of implanted cells *in vivo* because of their contrast effect (433,434). SPIO-labeled stem cells/progenitor cells might contribute to our understanding of cell migration processes in the context of numerous diseases, such as neurological (435) and muscular diseases (436), myocardial infarction (437–439) and cancer (440).

For example, magnetically labeled mouse embryonic stem cells injected into the nonischemic side of the brain of a rat with partial brain ischemia can be tracked during their migration along the corpus callosum (434). Moreover, SPION-labeled human neural stem cells can be visualized in mature rodent brain after their transplantation (435). In this case, MRI demonstrated the migration capacity of labeled stem cells into the cortical region of the brain (435). With the information obtained from cell migration studies, SPION technology might yield important information about the differentiation process of stem cells/progenitor cells. SPION-labeled CD34+ progenitor cells injected into rodents can be isolated by magnetic separation after *in vivo* migration to study the differentiation of these cells exposed to a biological environment (441). A clinical study using stem cells labeled with SPIONs in patients with neurological disease has been described (442). This approach can be adapted to evaluate the therapeutic effects of stem cells in the context of other diseases, including myocardial infarction. The literature also reported the use of MRI to monitor the migration of magnetically labeled cells in early-phase clinical trials (304).

4.9. Stem Cell Labeling

Stem cells are primitive cells found in many multicellular organisms and are known for their differentiation and self-renewal potential (443). Stem cell candidates include embryonic stem cells (ESCs), induced pluripotent stem cells and postnatal adult stem cells (444). ESCs, which are derived from the inner mass of blastocyst, are capable of extensive self-renewal, expansion and differentiation into all mature cell types except extra embryonic tissue (443). Induced pluripotent stem cells are obtained from reprogramming of differentiated human somatic cells into a pluripotent state (445). Adult stem cells comprise undifferentiated cells found in many tissues of an adult organism and have an enormous self-renewal capability and the ability to differentiate into several cell types. Compared with ESCs, adult stem cells are easier to obtain and less controversial; however, the majority of these cells are lineage-restricted, depending on their tissue sources (e.g. mesenchymal stem cells, neural stem cells, etc.) (443).

Adult mesenchymal stem cells (MSCs), which can be obtained from bone marrow, show considerable promise for use in rebuilding damaged or diseased mesenchymal tissues by providing a regenerative microenvironment comprised of a wide spectrum of bioactive molecules (446). Transplanting these cells into defective tissue would ideally result in the differentiation of MSCs along appropriate pathways to restore the tissue morphology and function (447). In order to translate stem cell therapies into clinical approaches for tissue regeneration, one must be able to monitor the cells' migration, homing, survival, differentiation and integration into the newly formed tissue following implantation *in vivo*. Thus, it is highly desirable to develop a multifunctional mechanism to target, track and stimulate stem cells *in vivo* and investigate their migratory pattern following transplantation.

Among several noninvasive techniques to visualize the internal structures and functions of the body, including X-ray, CT, PET, SPECT, ulatrasound and MRI (443), the latter is a safe method to visualize the body with high spatial and temporal resolution. Labeling stem cells with biocompatible and nontoxic markers, such as SPIONs, enables tracking of the cells upon transplantation in the body.

There are two ways to label cells with SPIONs (448): *in situ* labeling or direct intravenous infusing of iron oxide particles (mainly labels phagocytic cells in RES), and *in vitro* labeling, namely, isolating target cells, labeling them in culture and implanting them back. The latter fits all kind of cell types, particularly for these nonphagocytic cells, such as stem cells, that cannot be readily labeled in the RES system *in situ*. This kind of labeling also ensures high cell specificity, high iron internalization in single cells, and thus more sensitivity for MRI detection. Furthermore, *in vitro* labeling can provide straightforward information on labeling efficiency and quantitative iron content in each cell.

Successful detection of magnetically labeled stem cells depends on the number of implanted cells, accumulation of iron in cells, spatial resolution of the image, the field strength of MRI, the signal/noise ratio and the pulse sequence (449). The resolution of MRI (25–100 μm) allows tracking of individual cells while monitoring the surrounding tissues, and this is an important feature for clinicians since they need to study the pathology of the surrounding tissue to assess the level of success in cell transplantation.

Stem cells labeling has been used in three major cellular therapy applications: orthopedic, cardiovascular, and neurodegenerative diseases. Different stem cell types, their labeling strategies, and their application for regenerative purposes are discussed below.

4.9.1. *Stem cell labeling for orthopedic applications*

4.9.1.1. Cartilage regeneration. Cartilage is an avascular and aneural organ that lacks lymphatic drainage, resulting in a poor self-regeneration capacity. Articular cartilage defects normally occur in association with different pathological situations such

as trauma, osteoarthritis and rheumatoid arthritis (450). Cell-based therapies are one of the cartilage repair mechanisms that aim to restore the functional properties of damaged tissue (451). Two major cell types, bone-marrow-derived mesenchymal stem cells and chondrocytes, are currently being used for these approaches; however, the fate of these cells *in vivo* and their degree of survival and integration into the newly formed cartilage remains unclear (452). Jing *et al*. (450) labeled rabbit MSCs using SPIONs (Feridex IV) and a transfection agent (protamine sulfate) and injected those cells into the cartilage defects of a rabbit model. All the rabbits underwent gradient-recalled echo T_2*-weighted MRI up to 12 weeks post-injection. The authors observed that, at 12 weeks post-injection, MSCs migrated to the synovial fluid at the suprapatellar bursa, the popliteal space site and the subchondral bone of the femur, but no MSCs were detected in the defect. They concluded that autologous MSCs do not actively participate in the repair of articular cartilage defect following intra-articular injection. In another study, van Buul *et al*. (451) co-labeled human bone-marrow derived MSCs with SPIONs and green fluorescent protein and used two cell-based cartilage repair techniques, intra-articular cell injection and cell implantation in cartilage defects, to investigate the traceability of labeled cells using a 3.0 T MRI scanner. They found no SPION-related negative effect in the chondrogenic assays with freshly isolated cells. They also observed that the secretion profile of six important factors involved in inflammation and cell growth was not affected by SPIONs. However, they did not investigate the duration up to which SPION-labeled cells could be detected in an intra-articular environment, considering that the label will dilute upon cell divisions. Chen *et al*. (453) studied the feasibility of tracking polyethylenimine-wrapped SPION-labeled bone-marrow derived mesenchymal stem cells (BMSCs) in articular cartilage repair in a minipig model. In order to study the fate of magnetically labeled cells *in vivo*, they co-labeled these cells with green fluorescent protein (GFP). Evaluating the transplanted cells up to 24 weeks after the surgery, using 3.0 T MRI, showed that cell viability, proliferation and differentiation were comparable between labeled and unlabeled cells. Additionally, incubation of BMSCs with more than 8 μg/mL of SPIONs for 24 h was shown to significantly impair cell survival and differentiation, meaning that SPION concentration and incubation time must be taken into account when considering preclinical strategies relying in SPION-based cell tracking techniques.

4.9.1.2. Intervertebral disk regeneration. In the degenerated disk, where existing cells do not respond to any biological stimulus or intrinsic repair capacity has been hampered by inflammatory and catabolic processes, transplantation of healthy or genetically manipulated cells into a degenerated intervertebral disk should partially or fully restore the function of the degenerated disk. However, the intervertebral is isolated from the systemic circulation and, therefore, transport of nutrients and waste removal is limited (454). Hence, the development strategy for monitoring the fate of implanted cell is important. Jiang *et al*. (455) evaluated *in vivo* tracking of SPION-labeled adipose-derived stem cells (ADSCs) and their contribution to the repair of degenerated intervertebral disk in rabbits. They observed that, although SPION-labeled ADSCs showed low signal intensity in T_2 even after 8 weeks post-transplantation, their transplantation is effective in regeneration of degenerated intervertebral disk.

4.9.1.3. Bone tissue engineering. Large bone defects represent a major challenge for orthopedic and reconstructive surgeons. The problems associated with the autologous bone grafts, which are considered a gold standard in bone repair, led to the development of tissue engineering approaches to assist bone regeneration. The concept of bone tissue engineering consists of seeding autologous cells within a three-dimensional scaffold, which upon implantation into the bone defect will be remodeled *in vivo* and generate a new bone, structurally and functionally similar to its surrounding bone (456). To this end, Lalande *et al*. (456) labeled human adipose-derived stem cells with SPIONs and rhodamine, seeded these cells within a 3D porous polysaccharide-based scaffold, and imaged *in vitro* using fluorescence microscopy and MRI. Later, cellularized scaffolds were implanted in nude mice subcutaneously and MRI evaluation (with a 3D T_2*-weighted TrueFISP method) was performed up to 28 days after implantation. They observed that the cells remained detectable in this period and migrated from the scaffold and colonized around it. At day 7, the signal intensity in the center of the scaffold was lost and this was assumed to be due to cell death in the center of the scaffold and release of NPs in the periphery of the implant. Overall, it was shown that MRI is a valuable tool in monitoring the integration of a tissue engineered construct into its surrounding tissue.

4.9.2. Stem cell labeling for cardiovascular diseases

Ischemic heart disease is the most common cause of death in industrialized countries (457). Although treatments such as stabilizing drugs and mechanical revascularization have reduced the mortality rate significantly, mortality is still high within the first year after the diagnosis has been established (458). Human embryonic stem cells are regarded as a potentially new therapeutic approach for treatment of heart diseases. Tracking transplanted cells *in vivo* contributes to our understanding of the mechanism behind the repair and regeneration of damaged tissue in heart. As human ESCs are more fragile and difficult to handle in cell cultures, compared with mouse ESCs and other cell types that might be used for heart regeneration (e.g. myoblasts, neonatal cardiomyocytes, or smooth muscle cells), it is vital to study whether these cells could be tagged magnetically in order to track them upon transplantation (459). Therefore, Tallheden *et al*. (459) labeled human embryonic stem cells with dextran-coated SPIONs, transplanted these cells into an explanted mouse heart (*ex vivo*), and then injected them into the anterior left ventricle of rats (*in vivo*). Although imaging of the heart with MRI is very challenging, since MRI is very sensitive to motion artifacts and the heart is a rapidly moving organ, the authors managed to visualize the magnetically tagged cells *in vivo*. However, they did not evaluate the possible presence of extracellular SPIONs that might interfere with the detection of labeled cells.

The effect of SPION labeling on the cardiac differentiation potential of ESCs has been evaluated by Au *et al*. (460) in an acute myocardial infarction model in mice. The animals were injected with SPION-labeled nondifferentiated ESCs and monitored using a 7.0 T MRI for 10 days post-injection. *In vitro* studies showed that viability and differentiation of ESCs was not affected through SPION labeling. In addition, calcium oscillations in single SPION-labeled ESC-derived cardiomyocytes with spontaneous beating was recorded using confocal microscopy and it was shown that calcium transients from SPION-labeled cells were not different from their nonlabeled counterparts in terms of

amplitude, maximal upstroke velocity and maximal decay velocity. *In vivo* analysis showed that direct intramyocardial injection of ESCs significantly improved the left ventricular ejection fraction and, more importantly, areas of well-defined hypo-intensities were identified at the injection sites in the ESCs groups, while no such hypo-intensities were observed in the control groups. Histological analysis of those hypo-intensities in cell transplantation groups showed discrete clusters of GFP positive cells and troponin-T positive cells, indicating *in vivo* cardiac differentiation of ESCs.

Bone marrow stem cells injected into an animal's heart post-infarction differentiate into cardiomyocytes, smooth muscle cells and endothelial cells; they induce neoangiogenesis and, therefore, restore cardiac function. In one study, bone-marrow-derived stem cells labeled with micron-sized iron oxide particles were grafted in rats *in vivo* and the cardiac function was monitored noninvasively using 11.7 T MRI (461). BMSCs were labeled with chloromethylbenzamidodialkyl carbocyanine (CM-DiI) cell tracker dye and incubated overnight with MPIO ($2\,\mu l\,cm^{-2}$) on the day before transplantation. Labeled cells were injected via either intramuscular or intravenous routes, and tracked using MRI. It was observed that, upon direct injection of cells into the myocardium, the majority of cells remained in the vicinity of the injection site, while in animals that received intravenous infusion the cells were observed throughout the infarcted scar and were not visible in the myocardium. Although the cells remained in the myocardium for up to 10 weeks post-injection, BMSCs did not improve morphology or function of infarcted rat heart and did not increase neovascularization. The authors concluded that BMSCs are not an ideal cell population for treatment of infarcted heart.

The reason behind the inconsistencies between studies with regard to the effect of BMSCs on improvements of infarcted heart is the different methods used to measure cardiac function:

1) Invasive techniques, such as isolated heart perfusion and *in vivo* hemodynamics, allow measurements to be performed only at single time points.
2) Noninvasive methods, such as MRI, allow multiple measurements of heart function and thus monitoring of the progression of post-infarction remodeling.

In another study, Delo *et al*. (462) labeled human amniotic fluid stem cells with micron-sized iron oxide particles and investigated the fate of those cells following injection into mouse heart using a 7.0 T MRI. They found that labeling does not affect the proliferation and differentiation of human amniotic fluid stem cells and these cells were detectable *in vivo* up to 28 days post-injection. In addition, they showed that it would be possible to quantify the amount of stem cells present at various time points according to the hypointensity volumes.

Wang *et al*. (463) also investigated the viability and function of ADSCs labeled with SPIONs (ferumoxides) and evaluated whether the MR signal void resulting from SPIONs in live cells can be distinguished from that caused by dead cells *in vivo*. ADSCs were incubated with SPIONs for 2 days and then injected into infarcted rat heart. Analysis of cells after 4 weeks post-injection *in vivo* showed that T_2* and T_2 relaxation times of labeled ADSCs correlated with the density and passage of cells. It was shown that signal voids in MR images represent the living cells.

Pluripotent stem cells also have been used to regenerate the infarcted heart *in situ*. It has been shown that a cardiopatch based on bone morphogenetic protein-2 and SPION-labeled stem cells embedded into biodegradable fibrin matrices and engrafted into infarcted rat hearts is a promising therapeutic strategy for cell implantation after cardiac infarction (464). The cells were labeled with ferucarbotran via either lipofection or magnetofection and were tracked *in vivo* using 1.5 T MRI. Six weeks after cell transplantation into infarcted rat hearts, both local and global heart functions, as well as left ventricular dilation, were significantly improved. Histological analysis also showed that *de novo* CD31 positive blood vessels were formed in the vicinity of the transplanted cardiopatch and clusters of myocyte enhancer factor-2 positive cardiac committed cells had colonized most of the infarcted myocardium.

In a recent study, imaging-guided cell tracking was used to investigate the feasibility of using a pre-immune fetal sheep model for the assessment of human stem cell fate after direct intra-myocardial mesenchymal stem cell transplantation following acute myocardial infarction (465). Mesenchymal stem cells, of either bone-marrow or adipose-tissue origin, were first labeled with a fluorescent dye (CM-DiI) followed by incubation in the micron-sized superparamagnetic iron oxide particles solution. Magnetically labeled cells were injected through either intra-uterine or intra-myocardial route and were tracked up to 9 days post-injection. Cell retention within the injection site was confirmed using MR imaging and the number of cells within the myocardium could be estimated to approximately 1×10^5 to 5×10^5. The cells appeared viable and integrated, and were found in clusters or in the interstitial spaces. Flow cytometry confirmed intra-myocardial presence and showed further distribution within the spleen, lungs, kidneys and brain. Together, it was shown that, utilizing advanced cell tracking strategies, this model may serve as a unique platform for assessment of human cell fate after intra-myocardial transplantation.

4.9.3. *Stem cells labeling for neurodegenerative diseases*

4.9.3.1. Spinal cord regeneration. Spinal cord injury is a difficult neurological disease with limited therapeutic options; recently, however, the use of stem cell transplantation in animal studies has been shown to improve recovery after spinal cord injury. A wide variety of stem cells, independent of their source, have been used for spinal cord transplantation. In order to translate these therapies to human clinical applications, several questions need to be addressed, such as the best route for cell administration, the sufficient number of cells to be transplanted, and the therapeutic window after injury during which transplantation would be most effective. Tracking magnetically labeled cells upon transplantation is an attractive way to follow the fate and migration pattern of cells *in vivo* and find an answer to these questions. The feasibility of tracking dual-labeled bone-marrow MSCs, using adenovirus-carrying enhanced green fluorescent protein (AD5/F35-eGFP) and SPIONs, in rats has been investigated (9). The labeled cells were injected into rats with spinal cord injury via the subarachnoid space. MRI tracking results demonstrated that BMSCs migrated to the injured spinal cord over time. These results indicate that MRI can be utilized to trace *in vivo* the SPION-labeled BMSCs after grafting. In another approach (466), human CD34+ umbilical cord blood stem cells labeled with SPIONs were injected into the spinal cord of a transgenic amyotrophic lateral sclerosis (ALS) mouse. *In vivo* scanning using 7.0 T MRI showed clear signals of implanted cells. Human umbilical cord mesenchymal stem cells have also been used for spinal cord regeneration (467). Hu *et al*. reported the labeling

of these cells with SPIONs and their injection in rats that underwent spinal cord injury. Rats receiving transplants were scanned using 7.0 T MRI up to 3 weeks post-injection and it was shown that transplanted cells can survive and migrate in the host tissue, promote function recovery and produce a specific hypointense signal on MRI. In another study, Gonzalez-Lara *et al*. (468) tracked the fate of multipotent stromal cells (MSCs) labeled with MPIO after direct transplantation into mice with spinal cord injuries. They also injected mice with dead MPIO-labeled MSCs, unlabeled MSCs, and free MPIO as control. MRI tracking of the implanted cells showed that magnetic resonance imaging might be useful for the *in vivo* visualization of cell transplant in the spinal cord but it might not be very reliable in tracking the fate of those cells *in vivo*. This finding was based on the fact that signal hypointensities observed in all the transplant groups were remarkably similar and independent of the cell source (live vs dead). Histological analysis also showed that there were two different patterns of iron staining in all animals: regions of lightly stained intracellular iron and areas of dense extracellular iron, and it was observed that in all the transplant groups there is some iron that remains extracellularly up to 6 weeks post-transplantation and contributes to the signal loss in the cord. Overall, these studies indicate that the appearance of transplanted cells in MRI scans must be validated by accompanying histological analysis.

4.9.3.2. Brain. It has been shown that neurological disorders (Parkinson disease, stroke, etc.) can be treated using stem cells. Stroke is the leading cause of serious, long-term disability and it has been shown in animal studies that stem cell transplantation is beneficial, but the mechanisms behind the improvements are still unclear. Walczak and his coworkers (469) used intra-arterial cell delivery after transient ischemia and tracked the cells using dual techniques, Doppler flow measurements of cerebral blood flow in conjunction with MRI. They labeled rat MSCs with Feridex and used poly-L-lysine as transfection agent. *In vivo* T_2*-weighted MRI (4.7 T) detected the engraftment of labeled cells within the right internal carotid artery, as presented by strong signal voids and later confirmed by high-resolution *ex vivo* MRI (9.4 T). It was shown that intra-arterial delivery of stem cells offers the advantage of directly targeting the damaged tissue and circumventing the problems associated with cells trapping in other organs, such as liver and kidney.

In another study, the homing potential and fate of epidermal neural crest stem cells as well as BMSCs were determined in a lipopolysaccharide-induced inflammatory lesion model in the rat brain (470). The cells were labeled with dextran-coated SPIONs, which were conjugated with FITC (for histological analysis) and TAT (a peptide for membrane transfection agent), and implanted either directly onto the corpus callosum or injected intravenously into animals with lesions. The labeled cells were visible as hypointense regions on T_2 MR images for the duration of the study (up to 13 weeks). Interestingly, it was observed that, in animals with a focal inflammatory lesion, the transplanted cells migrated toward the lesion, where they ceased migration and remained visible on MRI for months. This migration behavior was assumed to be due to the lipopolysaccharide-induced inflammatory lesion model, which results in an influx of microglia and stimulates the release of cytokines such as IL-1β, TNF and IL-6 that may have provided the chemo-attractant signals for transplanted cells. The authors also mentioned that the signal void is mostly due to live cells, as the dead cells are cleared away from the local area.

Another neurodegenerative disease for which treatment via regenerative medicine has been sought is ALS. ALS affects upper and lower motor neurons and leads to muscular atrophy and paralysis (471). The use of human skeletal muscle-derived stem cells (hKmSCs) for ALS treatment was investigated in the model of spontaneous motor neuron degeneration in the Wobbler (Wr) mouse. In this model, hKmSCs were labeled with SPIONs and Hoechst 33258 dye and injected via the intracerebroventricular route in Wr mice. The transplanted cells were tracked *in vivo* using a 7.0 T MRI up to 18 weeks after injection. A fast and sustained improvement of motor efficacy associated with a relevant protection of functional neuromuscular junctions was observed in the animals treated with hKmSCs. In addition, a remarkable increase in human anti-inflammatory cytokines was observed in the Wr mice, which showed the bystander effect of stem cell transplantation in neurodegenerative disorders.

SPION-labeled MSCs have been used also to evaluate the feasibility of intra-arterial delivery of cells in a canine stroke model (472). It was shown that the cells were visible by 3.0 T MRI just 1 h after transplantation and up to 4 weeks afterwards. The injected cells mainly distributed in the ipsilateral cerebral hemisphere of infarction, while only few MSCs were found in the contralateral side. It was still difficult to extrapolate the exact number owing to heterogeneity in the structure and composition of the brain as well as to differences in MRI sequences and parameters.

Kallur *et al*. (473) investigated the long-term spatio-temporal and functional dynamics of cellular grafts based on human neural stem cells obtained from the human fetal striatum in an *in vivo* model. The cells were labeled with SPIONs (Endorem) and injected unilaterally into the right striatum of neonatal rats. The cells were imaged with MR up to 16 weeks post-injection. A hypointense signal in the striatum was observed at the injection sites, which, when compared with the control groups, proved to be due to SPION-labeled cells. It was shown that the relative graft-to-brain volume ratio decreased by around 50% in 4 months. In addition, a decrease in T_2 values was observed over time. According to post-mortem histological analysis and the fact that almost none of the grafted cells were proliferating after engraftment, this decline in T_2 values is not due to a dilution effect and might be due to cell migration from the graft core. However, since no obvious hypointensities were observed in the other regions of the brain, it was concluded that T_2 decrease over time is due to development-dependent changes during the brain growth.

5. METABOLISM AND EXCRETION OF SPIONS FROM THE BODY

Determination of fate and clearance of SPIONs is important for *in vivo* biomedical applications as it ensures their safe clinical use. As we discussed previously, SPIONs are taken up in the MPS cells via endocytosis Intracellular metabolism of SPIONS is dependent on their composition. For example, depending on the coating of SPIONs, their degradation time and excretion pathway may differ. Breakdown of SPIONs happens through the lysosomal pathway. For instance it was shown that degradation of dextran-coated SPIONSs is initiated by intracellular dextranases followed by degradation of SPIONs in lysosomes.

The degraded iron is finally eliminated from the body or restored in ferritin and/or transferrin or hemoglobin or other forms via normal iron metabolic pathways (474–476).

6. CONCLUSION AND PERSPECTIVES

The field of molecular imaging involves many biomedical disciplines: physics and engineering for detector and instrument design, chemistry for the development of probes, molecular pharmacology for optimized delivery and pharmacokinetics of probes, cell/molecular biology for understanding molecular targets of interest, proteomics for discovery and validation of molecular targets, mathematics for image reconstruction, and, finally, clinical medicine for application of the strategies for medical management.

Recently, a great deal of effort has been aimed at the use of nanoparticles in molecular imaging and therapy; antibody and peptide conjugated nanoparticles are being developed targeting these agents to different disease states. Highly specific molecular and cellular MRI agents represent a noninvasive, nonionizing and powerful tool to visualize physiological and pathological conditions. They have tremendous potential for improving our understanding of molecular processes involved in a variety of important clinical diseases. Functionalized iron oxide nanoparticles, because of the ease of conjugation, have undergone substantial growth in the number of agents and biological applications.

There are several important ignored factors at the nanobiointerfaces [such as temperature (20,477), cell vision (478–480), protein corona (75) and personalized protein corona (481)], which may affect the efficacy of molecular imaging. For instance, it is revealed that protein corona may change the relaxivity of SPIONs (75). Therefore, as slight temperature changes can vary the protein corona composition and consequently cellular uptake of nanoparticles, one should expect changes in the molecular/cellular imaging capability of the nanoparticles at various sites of the human body (the body temperature for healthy humans varies in the range from 35 to 39 °C). These crucial 'hidden' factors should be considered in future research.

The molecular imaging approach offers great potential for earlier detection and characterization of diseases and evaluation of treatment. However, more research is necessary to put these ideas into clinical applications. This approach also has a major impact on the development of new pharmaceuticals and a great potential to make better predictions on the effectiveness and toxicity of drugs.

Acknowledgments

S.L. thanks the Center for Microscopy and Molecular Imaging (CMMI, supported by the European Regional Development Fund and the Walloon Region). This work was supported by Walloon Region (program First spin-off), FNRS (Fond National de la RechercheScientifique), UIAP VII and ARC Programs of the French Community of Belgium.

REFERENCES

1. Weissleder R RB, Rehemtulla A, Gambhir SS. Molecular Imaging: Principles and Practice. People's Medical Publishing House-USAv: Beijing, 2010.
2. Nolting DD, Gore JC, Pham W. Near-Infrared dyes: Probe development and applications in optical molecular imaging. Curr Org Synth 2011; 8(4): 521–534.
3. Modo MMJ BJ. Molecular and Cellular MR Imaging. CRC Press: Boca Raton, FL, 2007.
4. Mahmoudi M, Serpooshan V, Laurent S. Engineered nanoparticles for biomolecular imaging. Nanoscale 2011; 3(8): 3007–3026.
5. Massoud TF, Gambhir SS. Molecular imaging in living subjects: seeing fundamental biological processes in a new light. Genes Dev 2003; 17(5): 545–580.
6. Debbage P, Jaschke W. Molecular imaging with nanoparticles: giant roles for dwarf actors. Histochem Cell Biol 2008; 130(5): 845–875.
7. Kiessling F, Liu Z, Gätjens J. Advanced nanomaterials in multimodal imaging: design, functionalization, and biomedical applications. J Nanomater 2010; 2010. Q10
8. Rinck. Magnetic Resonance in Medicine. Blackwell: Weinheim, 2001. Q11
9. Mahmoudi M, Hosseinkhani H, Hosseinkhani M, Boutry S, Simchi A, Journeay WS, Subramani K, Laurent S. Magnetic resonance imaging tracking of stem cells in vivo using iron oxide nanoparticles as a tool for the advancement of clinical regenerative medicine. Chem Rev 2010; 111(2): 253–280.
10. Vande Velde G, Baekelandt V, Dresselaers T, Himmelreich U. Magnetic resonance imaging and spectroscopy methods for molecular imaging. Q J Nucl Med Mol Imag 2009; 53(6): 565–585.
11. Laurent S, Forge D, Port M, Roch A, Robic C, Vander Elst L, Muller RN. Magnetic iron oxide nanoparticles: synthesis, stabilization, vectorization, physicochemical characterizations and biological applications. Chem Rev 2008; 108(6): 2064–2110.
12. Mahmoudi M, Sant S, Wang B, Laurent S, Sen T. Superparamagnetic iron oxide nanoparticles (SPIONs): development, surface modification and applications in chemotherapy. Adv Drug Deliv Rev 2011; 63(1–2): 24–46.
13. Laurent S, Duts S, Hafeli U, Mahmoudi M. Magnetic fluid hyperthermia: focus on superparamagnetic iron oxide nanoparticles. Adv Colloid Interface Sci 2011; 166: 8–23.
14. Laurent S, Mahmoudi M. Superparamagnetic iron oxide nanoparticles: promises for diagnosis and treatment of cancer. Int J Mol Epidemiol Genet 2011; 2(4): 367.
15. Mahmoudi M, Sahraian MA, Shokrgozar MA, Laurent S. Superparamagnetic iron oxide nanoparticles: promises for diagnosis and treatment of multiple sclerosis. ACS Chem Neurosci 2011; 2(3): 118–140.
16. Hajipour MJ, Fromm KM, AkbarAshkarran A, Jimenez de Aberasturi D, Larramendi IRd, Rojo T, Serpooshan V, Parak WJ, Mahmoudi M. Antibacterial properties of nanoparticles. Trends Biotechnol 2012. Q12
17. Li W, Tutton S, Vu AT, Pierchala L, Li BSY, Lewis JM, Prasad PV, Edelman RR. First-pass contrast-enhanced magnetic resonance angiography in humans using Ferumoxytol, a novel ultrasmall superparamagnetic iron oxide (USPIO)-based blood pool agent. J Magn Reson Imag 2005; 21(1): 46–52.
18. Achiam MP, Løgager VB, Chabanova E, Eegholm B, Thomsen HS, Rosenberg J. Diagnostic accuracy of MR colonography with fecal tagging. Abdominal Imag 2009; 34(4): 483–490.
19. Ghafariyan MH, Malakouti MJ, Dadpour MR, Stroeve P, Mahmoudi M. Effects of magnetite nanoparticles on soybean chlorophyll. Environ Sci Technol 2013; 47(18): 10645–10652.
20. Mahmoudi M, Abdelmonem AM, Behzadi S, Clement JH, Dutz S, Ejtehadi MR, Hartmann R, Kantner K, Linne U, Maffre P, Metzler S, Moghadam MK, Pfeiffer C, Rezaei M, Ruiz-Lozano P, Serpooshan V, Shokrgozar MA, Nienhaus GU, Parak WJ. Temperature: the 'ignored' factor at the nanobio interface. ACS Nano 2013; 7(8): 6555–6562.
21. Mahmoudi M, Azadmanesh K, Shokrgozar MA, Journeay WS, Laurent S. Effect of nanoparticles on the cell life cycle. Chem Rev 2011; 111(5): 3407–3432.
22. Mahmoudi M, Hofmann H, Rothen-Rutishauser B, Petri-Fink A. Assessing the in vitro and in vivo toxicity of superparamagnetic iron oxide nanoparticles. Chem Rev 2011; 112(4): 2323–2338.
23. Mahmoudi M, Laurent S, Shokrgozar MA, Hosseinkhani M. Toxicity evaluations of superparamagnetic iron oxide nanoparticles: cell 'vision' versus physicochemical properties of nanoparticles. ACS Nano 2011; 5(9): 7263–7276.
24. Mahmoudi M, Lynch I, Ejtehadi MR, Monopoli MP, Bombelli FB, Laurent S. Protein-nanoparticle interactions: opportunities and challenges. Chem Rev 2011; 111(9): 5610–5637.
25. Mahmoudi M, Quinlan-Pluck F, Monopoli MP, Sheibani S, Vali H, Dawson KA, Lynch I. Influence of the physiochemical properties of superparamagnetic iron oxide nanoparticles on amyloid β protein fibrillation in solution. ACS Chem Neurosci 2012; 4(3): 475–485.

26. Mahmoudi M, Serpooshan V. Silver-coated engineered magnetic nanoparticles are promising for the success in the fight against antibacterial resistance threat. ACS Nano 2012; 6(3): 2656–2664.
27. Panahifar A, Mahmoudi M, Doschak MR. Synthesis and in vitro evaluation of bone-seeking superparamagnetic iron oxide nanoparticles as contrast agents for imaging bone metabolic activity. ACS Appl Mater Interfaces 2013; 5(11): 5219–5226.
28. Rauch J, Kolch W, Laurent S, Mahmoudi M. Big signals from small particles: regulation of cell signaling pathways by nanoparticles. Chem Rev 2013; 113(5): 3391–3406.
29. Corot C, Robert P, Idée JM, Port M. Recent advances in iron oxide nanocrystal technology for medical imaging. Adv Drug Deliv Rev 2006; 58(14): 1471–1504.
30. Laurent S, Bridot J-L, Elst LV, Muller RN. Magnetic iron oxide nanoparticles for biomedical applications. Fut Med Chem 2010; 2(3): 427–449.
31. Mahmoudi M, Simchi A, Milani A, Stroeve P. Cell toxicity of superparamagnetic iron oxide nanoparticles. J Colloid Interface Sci 2009; 336(2): 510–518.
32. Lee N, Hyeon T. Designed synthesis of uniformly sized iron oxide nanoparticles for efficient magnetic resonance imaging contrast agents. Chem Soc Rev 2012; 41(7): 2575–2589.
33. Mornet S, Vasseur S, Grasset F, Duguet E. Magnetic nanoparticle design for medical diagnosis and therapy. J Mater Chem 2004; 14(14): 2161–2175.
34. Berry CC, Wells S, Charles S, Curtis ASG. Dextran and albumin derivatised iron oxide nanoparticles: influence on fibroblasts in vitro. Biomaterials 2003; 24(25): 4551–4557.
35. Lee K, Kim S-G, Kim W-S, Kim S. Properties of iron oxide particles prepared in the presence of dextran. Korean J Chem Eng 2002; 19(3): 480–485.
36. Barber PA, Foniok T, Kirk D, Buchan AM, Laurent S, Boutry S, Muller RN, Hoyte L, Tomanek B, Tuor UI. MR molecular imaging of early endothelial activation in focal ischemia. Ann Neurol 2004; 56(1): 116–120.
37. Gamarra LF, Brito GES, Pontuschka WM, Amaro E, Parma AHC, Goya GF. Biocompatible superparamagnetic iron oxide nanoparticles used for contrast agents: a structural and magnetic study. J Magn Magn Mater 2005; 289: 439–441.
38. Paul KG, Frigo TB, Groman JY, Groman EV. Synthesis of ultrasmall superparamagnetic iron oxides using reduced polysaccharides. Bioconjug Chem 2004; 15(2): 394–401.
39. Carmen Bautista M, Bomati-Miguel O, Del Puerto Morales M, Serna CJ, Veintemillas-Verdaguer S. Surface characterisation of dextran-coated iron oxide nanoparticles prepared by laser pyrolysis and coprecipitation. J Magn Magn Mater 2005; 293(1): 20–27.
40. Nishio Y, Yamada A, Ezaki K, Miyashita Y, Furukawa H, Horie K. Preparation and magnetometric characterization of iron oxide-containing alginate/poly(vinyl alcohol) networks. Polymer 2004; 45(21): 7129–7136.
41. Finotelli PV, Morales MA, Rocha-Leão MH, Baggio-Saitovitch EM, Rossi AM. Magnetic studies of iron(III) nanoparticles in alginate polymer for drug delivery applications. Mater Sci Eng C 2004; 24(5): 625–629.
42. Ma Hl, Qi Xr, Maitani Y, Nagai T. Preparation and characterization of superparamagnetic iron oxide nanoparticles stabilized by alginate. Int J Pharm 2007; 333(1–2): 177–186.
43. Morales MA, Finotelli PV, Coaquira JAH, Rocha-Leão MHM, Diaz-Aguila C, Baggio-Saitovitch EM, Rossi AM. In situ synthesis and magnetic studies of iron oxide nanoparticles in calcium-alginate matrix for biomedical applications. Mater Sci Eng C 2008; 28(2): 253–257.
44. Roohi F, Lohrke J, Ide A, Schütz G, Dassler K. Studying the effect of particle size and coating type on the blood kinetics of superparamagnetic iron oxide nanoparticles. Int J Nanomed 2012; 7: 4447–4458.
45. Burtea C, Laurent S, Mahieu I, Larbanoix L, Roch A, Port M, Rousseaux O, Ballet S, Murariu O, Toubeau G, Corot C, Vander Elst L, Muller RN. In vitro biomedical applications of functionalized iron oxide nanoparticles, including those not related to magnetic properties. Contrast Media Mol Imag 2011; 6(4): 236–250.
46. Kim DK, Zhang Y, Kehr J, Klason T, Bjelke B, Muhammed M. Characterization and MRI study of surfactant-coated superparamagnetic nanoparticles administered into the rat brain. J Magn Magn Mater 2001; 225(1–2): 256–261.
47. Shultz MD, Calvin S, Fatouros PP, Morrison SA, Carpenter EE. Enhanced ferrite nanoparticles as MRI contrast agents. J Magn Magn Mater 2007; 311(1, spec. iss.): 464–468.
48. Gupta AK, Curtis ASG. Surface modified superparamagnetic nanoparticles for drug delivery: interaction studies with human fibroblasts in culture. J Mater Sci Mater Med 2004; 15(4): 493–496.
49. Kohler N, Fryxell GE, Zhang M. A bifunctional poly(ethylene glycol) silane immobilized on metallic oxide-based nanoparticles for conjugation with cell targeting agents. J Am Chem Soc 2004; 126(23): 7206–7211.
50. Kellar KE, Fujii DK, Gunther WHH, Briley-Sabo K, Bjornerod A, Spiller M, Koenig SH. Important considerations in the design of iron oxide nanoparticles as contrast agents for T1-weighted MRI and MRA. Acad Radiol 2002; 9(suppl. 1): S34–S37.
51. Acar HYC, Garaas RS, Syud F, Bonitatebus P, Kulkarni AM. Superparamagnetic nanoparticles stabilized by polymerized PEGylated coatings. J Magn Magn Mater 2005; 293(1): 1–7.
52. Ngaboni Okassa L, Marchais H, Douziech-Eyrolles L, Cohen-Jonathan S, Soucé M, Dubois P, Chourpa I. Development and characterization of sub-micron poly(D,L-lactide-co-glycolide) particles loaded with magnetite/maghemite nanoparticles. Int J Pharm 2005; 302(1–2): 187–196.
53. Sander EA, Alb AM, Nauman EA, Reed WF, Dee KC. Solvent effects on the microstructure and properties of 75/25 poly(D,L-lactide-co-glycolide) tissue scaffolds. J Biomed Mater Res Part A 2004; 70A(3): 506–513.
54. Kopke RD, Wassel RA, Mondalek F, Grady B, Chen K, Liu J, Gibson D, Dormer KJ. Magnetic nanoparticles: inner ear targeted molecule delivery and middle ear implant. Audiol Neurotol 2005; 11(2): 123–133.
55. Mornet S, Portier J, Duguet E. A method for synthesis and functionalization of ultrasmall superparamagnetic covalent carriers based on maghemite and dextran. J Magn Magn Mater 2005; 293(1): 127–134.
56. Duguet EMS, Portier J. French patent FR2855315. Chem Abstr 2004; 141: 405023.
57. Wagner S, Schnorr J, Pilgrimm H, Hamm B, Taupitz M. Monomer-coated very small superparamagnetic iron oxide particles as contrast medium for magnetic resonance imaging: preclinical in vivo characterization. Invest Radiol 2002; 37(4): 167–177.
58. Taupitz M, Wagner S, Schnorr J, Kravec I, Pilgrimm H, Bergmann-Fritsch H, Hamm B. Phase I clinical evaluation of citrate-coated monocrystalline very small superparamagnetic iron oxide particles as a new contrast medium for magnetic resonance imaging. Invest Radiol 2004; 39(7): 394–405.
59. Fauconnier N, Pons JN, Roger J, Bee A. Thiolation of maghemite nanoparticles by dimercaptosuccinic acid. J Colloid Interface Sci 1997; 194(2): 427–433.
60. Fauconnier N, Bee A, Roger J, Pons JN. Adsorption of gluconic and citric acids on maghemite particles in aqueous medium. 1996; 100: 212–216. Q13
61. Fauconnier N, Bée A, Roger J, Pons JN. Synthesis of aqueous magnetic liquids by surface complexation of maghemite nanoparticles. J Mol Liq 1999; 83(1–3): 233–242.
62. Jung CW. Surface properties of superparamagnetic iron oxide MR contrast agents: ferumoxides, ferumoxtran, ferumoxsil. Magn Reson Imag 1995; 13(5): 675–691.
63. Cheng FY, Su CH, Yang YS, Yeh CS, Tsai CY, Wu CL, Wu MT, Shieh DB. Characterization of aqueous dispersions of Fe3O4 nanoparticles and their biomedical applications. Biomaterials 2005; 26(7): 729–738.
64. Jung CW, Jacobs P. Physical and chemical properties of superparamagnetic iron oxide MR contrast agents: ferumoxides, ferumoxtran, ferumoxsil. Magn Reson Imag 1995; 13(5): 661–674.
65. Laurent S Vander Elst L, Muller RN. Superparamagnetic iron oxide nanoparticles for MRI. Chem Contrast Agents Med Magn Reson Imag 2013; 427–447. Q14
66. Walczyk D, Bombelli FB, Monopoli MP, Lynch I, Dawson KA. What the cell 'sees' in bionanoscience. J Am Chem Soc 2010; 132(16): 5761–5768.
67. Lesniak A, Fenaroli F, Monopoli MP, Åberg C, Dawson KA, Salvati A. Effects of the presence or absence of a protein corona on silica nanoparticle uptake and impact on cells. ACS Nano 2012; 6(7): 5845–5857.
68. Monopoli MP, Walczyk D, Campbell A, Elia G, Lynch I, Baldelli Bombelli F, Dawson KA. Physical-chemical aspects of protein corona: relevance to in vitro and in vivo biological impacts of nanoparticles. J Am Chem Soc 2011; 133(8): 2525–2534.
69. Jedlovszky-Hajdú A, Bombelli FB, Monopoli MP, Tombácz E, Dawson KA. Surface coatings shape the protein corona of SPIONs with relevance to their application in vivo. Langmuir 2012; 28(42): 14983–14991.
70. Wang J, Sui M, Fan W. Nanoparticles for tumor targeted therapies and their pharmacokinetics. Curr Drug Metab 2010; 11(2): 129–141.

71. Larbanoix L, Burtea C, Laurent S, Van Leuven F, Toubeau G, Elst LV, Muller RN. Potential amyloid plaque-specific peptides for the diagnosis of Alzheimer's disease. Neurobiol Aging 2010; 31(10): 1679–1689.
72. Abdolahi M, Shahbazi-Gahrouei D, Laurent S, Sermeus C, Firozian F, Allen BJ, Boutry S, Muller RN. Synthesis and in vitro evaluation of MR molecular imaging probes using J591 mAb-conjugated SPIONs for specific detection of prostate cancer. Contrast Media Mol Imag 2013; 8(2): 175–184.
73. Salvati A, Pitek AS, Monopoli MP, Prapainop K, Bombelli FB, Hristov DR, Kelly PM, Åberg C, Mahon E, Dawson KA. Transferrin-functionalized nanoparticles lose their targeting capabilities when a biomolecule corona adsorbs on the surface. Nat Nanotechnol 2013; 8(2): 137–143.
74. Mirshafiee V, Mahmoudi M, Lou K, Cheng J, Kraft ML. Protein corona significantly reduces active targeting yield. Chem Commun 2013; 49(25): 2557–2559.
75. Amiri H, Bordonali L, Lascialfari A, Wan S, Monopoli MP, Lynch I, Laurent S, Mahmoudi M. Protein corona affects the relaxivity and MRI contrast efficiency of magnetic nanoparticles. Nanoscale 2013; 5(18): 8656–8665.
76. Ferrucci JT SD. Iron oxide-enhanced MR imaging of the liver and spleen: review of the first 5 years. Am J Roentgenol 1990; 155(5): 943–950.
77. Vogl TJ, Hammerstingl R, Schwarz W, Mack MG, Müller PK, Pegios W, Keck H, Eibl-Eibesfeldt A, Hoelzl J, Woessmer B, Bergman C, Felix R. Superparamagnetic iron oxide-enhanced versus gadolinium-enhanced MR imaging for differential diagnosis of focal liver lesions. Radiology 1996; 198(3): 881–887.
78. Namkung S, Zech CJ, Helmberger T, Reiser MF, Schoenberg SO. Superparamagnetic iron oxide (SPIO)-enhanced liver MRI with ferucarbotran: efficacy for characterization of focal liver lesions. J Magn Reson Imag 2007; 25(4): 755–765.
79. Wang YXJ, Hussain SM, Krestin GP. Superparamagnetic iron oxide contrast agents: physicochemical characteristics and applications in MR imaging. Eur Radiol 2001; 11(11): 2319–2331.
80. Gupta AK, Naregalkar RR, Vaidya VD, Gupta M. Recent advances on surface engineering of magnetic iron oxide nanoparticles and their biomedical applications. Nanomedicine 2007; 2(1): 23–39.
81. Semelka RC, Helmberger TKG. State of the art: contrast agents for MR imaging of the liver. Radiology 2001; 218(1): 27–38.
82. He Y, Song W, Lei J, Li Z, Cao J, Huang S, Meng J, Xu H, Jin Z, Xue H. Anti-CXCR4 monoclonal antibody conjugated to ultrasmall superparamagnetic iron oxide nanoparticles in an application of MR molecular imaging of pancreatic cancer cell lines. Acta Radiol 2012; 53(9): 1049–1058.
83. Adolphi NL, Butler KS, Lovato DM, Tessier TE, Trujillo JE, Hathaway HJ, Fegan DL, Monson TC, Stevens TE, Huber DL, Ramu J, Milne ML, Altobelli SA, Bryant HC, Larson RS, Flynn ER. Imaging of Her2-targeted magnetic nanoparticles for breast cancer detection: comparison of SQUID-detected magnetic relaxometry and MRI. Contrast Media Mol Imag 2012; 7(3): 308–319.
84. Wang X, Wei F, Liu A, Wang L, Wang J-C, Ren L, Liu W, Tu Q, Li L, Wang J. Cancer stem cell labeling using poly(l-lysine)-modified iron oxide nanoparticles. Biomaterials 2012; 33(14): 3719–3732.
85. Radermacher KA, Magat J, Bouzin C, Laurent S, Dresselaers T, Himmelreich U, Boutry S, Mahieu I, Vander Elst L, Feron O, Muller RN, Jordan BF, Gallez B. Multimodal assessment of early tumor response to chemotherapy: comparison between diffusion-weighted MRI, 1H-MR spectroscopy of choline and USPIO particles targeted at cell death. NMR Biomed 2012; 25(4): 514–522.
86. Rapley PL, Witiw C, Rich K, Niccoli S, Tassotto ML, Th'ng J. In vitro molecular magnetic resonance imaging detection and measurement of apoptosis using superparamagnetic iron oxide + antibody as ligands for nucleosomes. Phys Med Biol 2012; 57(21): 7015.
87. Dósa E, Tuladhar S, Muldoon LL, Hamilton BE, Rooney WD, Neuwelt EA. MRI using Ferumoxytol improves the visualization of central nervous system vascular malformations. Stroke 2011; 42(6): 1581–1588.
88. Zhu M-T, Wang B, Wang Y, Yuan L, Wang H-J, Wang M, Ouyang H, Chai Z-F, Feng W-Y, Zhao Y-L. Endothelial dysfunction and inflammation induced by iron oxide nanoparticle exposure: risk factors for early atherosclerosis. Toxicol Lett 2011; 203(2): 162–171.
89. Jacobin-Valat M-J, Deramchia K, Mornet S, Hagemeyer CE, Bonetto S, Robert R, Biran M, Massot P, Miraux S, Sanchez S, Bouzier-Sore A-K, Franconi J-M, Duguet E, Clofent-Sanchez G. MRI of inducible P-selectin expression in human activated platelets involved in the early stages of atherosclerosis. NMR Biomed 2011; 24(4): 413–424.
90. Morishige K, Kacher DF, Libby P, Josephson L, Ganz P, Weissleder R, Aikawa M. High-resolution magnetic resonance imaging enhanced with superparamagnetic nanoparticles measures macrophage burden in atherosclerosis. Circulation 2010; 122(17): 1707–1715.
91. Fayad ZA, Razzouk L, Briley-Saebo KC, Mani V. Iron oxide magnetic resonance imaging for atherosclerosis therapeutic evaluation: still 'rusty?'. J Am College Cardiol 2009; 53(22): 2051–2052.
92. Tang TY, Howarth SPS, Miller SR, Graves MJ, Patterson AJ, U-King-Im J-M, Li ZY, Walsh SR, Brown AP, Kirkpatrick PJ, Warburton EA, Hayes PD, Varty K, Boyle JR, Gaunt ME, Zalewski A, Gillard JH. The ATHEROMA (Atorvastatin Therapy: Effects on Reduction of Macrophage Activity) study: evaluation using ultrasmall superparamagnetic iron oxide-enhanced magnetic resonance imaging in carotid disease. J Am College Cardiol 2009; 53(22): 2039–2050.
93. Michalska M, Machtoub L, Manthey HD, Bauer E, Herold V, Krohne G, Lykowsky G, Hildenbrand M, Kampf T, Jakob P, Zernecke A, Bauer WR. Visualization of vascular inflammation in the atherosclerotic mouse by ultrasmall superparamagnetic iron oxide vascular cell adhesion molecule-1-specific nanoparticles. Arterioscler Thromb Vasc Biol 2012; 32(10): 2350–2357.
94. Deddens LH, Van Tilborg GAF, Mulder WJM, De Vries HE, Dijkhuizen RM. Imaging neuroinflammation after stroke: current status of cellular and molecular MRI strategies. Cerebrovasc Dis 2012; 33(4): 392–402.
95. Chen X, Wong R, Khalidov I, Wang AY, Leelawattanachai J, Wang Y, Jin MM. Inflamed leukocyte-mimetic nanoparticles for molecular imaging of inflammation. Biomaterials 2011; 32(30): 7651–7661.
96. Wong R, Chen X, Wang Y, Hu X, Jin M. Visualizing and quantifying acute inflammation using ICAM-1 specific nanoparticles and MRI quantitative susceptibility mapping. Ann Biomed Eng 2012; 40(6): 1328–1338.
97. Boutry S, Laurent S, Elst LV, Muller RN. Specific E-selectin targeting with a superparamagnetic MRI contrast agent. Contrast Media Mol Imag 2006; 1(1): 15–22.
98. Weissleder R, Lee AS, Khaw BA, Shen T, Brady TJ. Antimyosin-labeled monocrystalline iron oxide allows detection of myocardial infarct: MR antibody imaging. Radiology 1992; 182(2): 381–385.
99. Suwa T, Ozawa S, Ueda M, Ando N, Kitajima M. Magnetic resonance imaging of esophageal squamous cell carcinoma using magnetite particles coated with anti-epidermal growth factor receptor antibody. Int J Cancer 1998; 75(4): 626–634.
100. Wadghiri YZ, Sigurdsson EM, Sadowski M, Elliott JI, Li Y, Scholtzova H, Tang CY, Aguinaldo G, Pappolla M, Duff K, Wisniewski T, Turnbull DH. Detection of Alzheimer's amyloid in transgenic mice using magnetic resonance microimaging. Magn Reson Med 2003; 50(2): 293–302.
101. Reimer P, Weissleder R, Shen T, Knoefel WT, Brady TJ. Pancreatic receptors: initial feasibility studies with a targeted contrast agent for MR imaging. Radiology 1994; 193(2): 527–531.
102. Jung HI, Kettunen MI, Davletov B, Brindle KM. Detection of apoptosis using the C2A domain of synaptotagmin I. Bioconjug Chem 2004; 15(5): 983–987.
103. Artemov D, Mori N, Okollie B, Bhujwalla ZM. MR molecular imaging of the Her-2/neu receptor in breast cancer cells using targeted iron oxide nanoparticles. Magn Reson Med 2003; 49(3): 403–408.
104. Bulte JWM, Hoekstra Y, Kamman RL, Magin RL, Webb AG, Briggs RW, Go KG, Hulstaert CE, Miltenyi S, The TH, De Leij L. Specific MR imaging of human lymphocytes by monoclonal antibody-guided dextran-magnetite particles. Magn Reson Med 1992; 25(1): 148–157.
105. Go KG, Bulte JWM, De Ley L, The TH, Kamman RL, Hulstaert CE, Blaauw EH, Ma LD. Our approach towards developing a specific tumour-targeted MRI contrast agent for the brain. Eur J Radiol 1993; 16(3): 171–175.
106. Sun EY, Josephson L, Kelly KA, Weissleder R. Development of nanoparticle libraries for biosensing. Bioconjug Chem 2006; 17(1): 109–113.
107. Renshaw PF, Owen CS, Evans AE, Leigh JS Jr. Immunospecific NMR contrast agents. Magn Reson Imag 1986; 4(4): 351–357.
108. Suzuki M, Shinkai M, Kamihira M, Kobayashi T. Preparation and characteristics of magnetite-labelled antibody with the use of poly(ethylene glycol) derivatives. Biotechnol Appl Biochem 1995; 21(3): 335–345.
109. Zhou J, Leuschner C, Kumar C, Hormes JF, Soboyejo WO. Subcellular accumulation of magnetic nanoparticles in breast tumors and metastases. Biomaterials 2006; 27(9): 2001–2008.
110. Leuschner C, Kumar C, Urbina MO, Zhou J, Soboyejo W, Hansel W, Hormes F. The use of ligand conjugated superparamagnetic iron oxide nanoparticles (SPION) for early detection of mtastases. 2005; 5–6.

Q15

111. Zhang C, Jugold M, Woenne EC, Lammers T, Morgenstern B, Mueller MM, Zentgraf H, Bock M, Eisenhut M, Semmler W, Kiessling F. Specific targeting of tumor angiogenesis by RGD-conjugated ultrasmall superparamagnetic iron oxide particles using a clinical 1.5-T magnetic resonance scanner. Cancer Res 2007; 67(4): 1555–1562.
112. Peng ZG, Hidajat K, Uddin MS. Adsorption of bovine serum albumin on nanosized magnetic particles. J Colloid Interface Sci 2004; 271(2): 277–283.
113. Mehta RV, Upadhyay RV, Charles SW, Ramchand CN. Direct binding of protein to magnetic particles. Biotechnol Tech 1997; 11(7): 493–496.
114. Kresse M, Wagner S, Pfefferer D, Lawaczeck R, Elste V, Semmler W. Targeting of ultrasmall superparamagnetic iron oxide (USPIO) particles to tumor cells in vivo by using transferrin receptor pathways. Magn Reson Med 1998; 40(2): 236–242.
115. Cengelli F, Maysinger D, Tschudi-Monnet F, Montet X, Corot C, Petri-Fink A, Hofmann H, Juillerat-Jeanneret L. Interaction of functionalized superparamagnetic iron oxide nanoparticles with brain structures. J Pharmacol Exp Ther 2006; 318(1): 108–116.
116. Zhao M, Beauregard DA, Loizou L, Davletov B, Brindle KM. Non-invasive detection of apoptosis using magnetic resonance imaging and a targeted contrast agent. Nat Med 2001; 7(11): 1241–1244.
117. Weissleder R, Lee AS, Fischman AJ, Reimer P, Shen T, Wilkinson R, Callahan RJ, Brady TJ. Polyclonal human immunoglobulin G labeled with polymeric iron oxide: antibody MR imaging. Radiology 1991; 181(1): 245–249.
118. Toma A, Otsuji E, Kuriu Y, Okamoto K, Ichikawa D, Hagiwara A, Ito H, Nishimura T, Yamagishi H. Monoclonal antibody A7-superparamagnetic iron oxide as contrast agent of MR imaging of rectal carcinoma. Br J Cancer 2005; 93(1): 131–136.
119. Li M, Xu H, Zuo J, Ji A, He B, Pang Y, Huang J, Niu R. Preparation of dextran immunological magnetic nanoparticles and their application to combined targeting carrier. Sci China Ser B Chem 1996; 39(6): 577–584.
120. Remsen LG, McCormick CI, Roman-Goldstein S, Nilaver G, Weissleder R, Bogdanov A, Hellström KE, Hellström I, Kroll RA, Neuwelt EA. MR of carcinoma-specific monoclonal antibody conjugated to monocrystalline iron oxide nanoparticles: the potential for noninvasive diagnosis. Am J Neuroradiol 1996; 17(3): 411–418.
121. Funovics MA, Kapeller B, Hoeller C, Su HS, Kunstfeld R, Puig S, Macfelda K. MR imaging of the her2/neu and 9.2.27 tumor antigens using immunospecific contrast agents. Magn Reson Imag 2004; 22(6): 843–850.
122. Sonvico F, Mornet S, Vasseur S, Dubernet C, Jaillard D, Degrouard J, Hoebeke J, Duguet E, Colombo P, Couvreur P. Folate-conjugated iron oxide nanoparticles for solid tumor targeting as potential specific magnetic hyperthermia mediators: synthesis, physicochemical characterization, and in vitro experiments. Bioconjug Chem 2005; 16(5): 1181–1188.
123. Zhang Y, Zhang J. Surface modification of monodisperse magnetite nanoparticles for improved intracellular uptake to breast cancer cells. J Colloid Interface Sci 2005; 283(2): 352–357.
124. Josephson L, Tung CH, Moore A, Weissleder R. High-efficiency intracellular magnetic labeling with novel superparamagnetic-tat peptide conjugates. Bioconjug Chem 1999; 10(2): 186–191.
125. Hogemann D, Josephson L, Weissleder R, Basilion JP. Improvement of MRI probes to allow efficient detection of gene expression. Bioconjug Chem 2000; 11(6): 941–946.
126. Högemann-Savellano D, Bost E, Blondet C, Sato F, Abe T, Josephson L, Weissleder R, Gaudet J, Sgroi D, Peters PJ, Basilion JP. The transferrin receptor: a potential molecular imaging marker for human cancer. Neoplasia 2003; 5(6): 495–506.
127. Won Kang H, Josephson L, Petrovsky A, Weissleder R, Bogdanov A Jr. Magnetic resonance imaging of inducible e-selectin expression in human endothelial cell culture. Bioconjug Chem 2002; 13(1): 122–127.
128. Sun C, Sze R, Zhang M. Folic acid-PEG conjugated superparamagnetic nanoparticles for targeted cellular uptake and detection by MRI. J Biomed Mater Res Pt A 2006; 78(3): 550–557.
129. Josephson L, Kircher MF, Mahmood U, Tang Y, Weissleder R. Near-infrared fluorescent nanoparticles as combined MR/optical imaging probes. Bioconjug Chem 2002; 13(3): 554–560.
130. Dodd CH, Hsu HC, Chu WJ, Yang P, Zhang HG, Mountz JD Jr, Zinn K, Forder J, Josephson L, Weissleder R, Mountz JM, Mountz JD. Normal T-cell response and in vivo magnetic resonance imaging of T cells loaded with HIV transactivator-peptide-derived superparamagnetic nanoparticles. J Immunol Meth 2001; 256(1–2): 89–105.
131. Papisov MI, Bogdanov A Jr, Schaffer B, Nossiff N, Shen T, Weissleder R, Brady TJ. Colloidal magnetic resonance contrast agents: effect of particle surface on biodistribution. J Magn Magn Mater 1993; 122(1–3): 383–386.
132. Koch AM, Reynolds F, Merkle HP, Weissleder R, Josephson L. Transport of surface-modified nanoparticles through cell monolayers. ChemBioChem 2005; 6(2): 337–345.
133. Funovics M, Montet X, Reynolds F, Weissleder R, Josephson L. Nanoparticles for the optical imaging of tumor E-selectin. Neoplasia 2005; 7(10): 904–911.
134. Kircher MF, Josephson L, Weissleder R. Ratio imaging of enzyme activity using dual wavelength optical reporters. Mol Imag 2002; 1(2): 89–95.
135. Kircher MF, Weissleder R, Josephson L. A dual fluorochrome probe for imaging proteases. Bioconjug Chem 2004; 15(2): 242–248.
136. Moore A, Medarova Z, Potthast A, Dai G. In vivo targeting of underglycosylated muc-1 tumor antigen using a multimodal imaging probe. Cancer Res 2004; 64(5): 1821–1827.
137. Högemann D, Ntziachristos V, Josephson L, Weissleder R. High throughput magnetic resonance imaging for evaluating targeted nanoparticle probes. Bioconjug Chem 2002; 13(1): 116–121.
138. Tsourkas A, Shinde-Patil VR, Kelly KA, Patel P, Wolley A, Allport JR, Weissleder R. In vivo imaging of activated endothelium using an anti-VCAM-1 magnetooptical probe. Bioconjug Chem 2005; 16(3): 576–581.
139. Montet X, Funovics M, Montet-Abou K, Weissleder R, Josephson L. Multivalent effects of RGD peptides obtained by nanoparticle display. J Med Chem 2006; 49(20): 6087–6093.
140. Montet X, Montet-Abou K, Reynolds F, Weissleder R, Josephson L. Nanoparticle imaging of integrins on tumor cells. Neoplasia 2006; 8(3): 214–222.
141. Kelly KA, Allport JR, Tsourkas A, Shinde-Patil VR, Josephson L, Weissleder R. Detection of vascular adhesion molecule-1 expression using a novel multimodal nanoparticle. Circul Res 2005; 96(3): 327–336.
142. Weissleder R, Kelly K, Sun EY, Shtatland T, Josephson L. Cell-specific targeting of nanoparticles by multivalent attachment of small molecules. Nat Biotechnol 2005; 23(11): 1418–1423.
143. Kircher MF, Mahmood U, King RS, Weissleder R, Josephson L. A Multimodal nanoparticle for preoperative magnetic resonance imaging and intraoperative optical brain tumor delineation. Cancer Res 2003; 63(23): 8122–8125.
144. Segers J, Laumonier C, Burtea C, Laurent S, Elst LV, Muller RN. From phage display to magnetophage, a new tool for magnetic resonance molecular imaging. Bioconjug Chem 2007; 18(4): 1251–1258.
145. Burtea C, Laurent S, Roch A, Vander Elst L, Muller RN. C-MALISA (cellular magnetic-linked immunosorbent assay), a new application of cellular ELISA for MRI. J Inorg Biochem 2005; 99(5): 1135–1144.
146. Halbreich AR, Pons JN, Da Silva A, Hasmonay E, Roudier M, Boynard M, Sestier C, Amri A, Geldwerth D, Fertil B, Bacri JC, Sabolovic D. Scientific and clinical applications of magnetic carriers. 1997; 399–417.
147. Jun YW, Huh YM, Choi JS, Lee JH, Song HT, Kim S, Yoon S, Kim KS, Shin JS, Suh JS, Cheon J. Nanoscale size effect of magnetic nanocrystals and their utilisation for cancer diagnosis via magnetic resonance imaging. J Am Chem Soc 2005; 127(16): 5732–5733.
148. Huh YM, Jun YW, Song HT, Kim S, Choi JS, Lee JH, Yoon S, Kim KS, Shin JS, Suh JS, Cheon J. In vivo magnetic resonance detection of cancer by using multifunctional magnetic nanocrystals. J Am Chem Soc 2005; 127(35): 12387–12391.
149. Halbreich A, Sabolovic D, Sestier C, Amri A, Pons JN, Roger J, Geldwerth D. Annexin V binding to mouse erythrocytes following infection with Plasmodium parasites. Parasitol Today 1996; 12(7): 292–293.
150. Sestier C, Sabolovic D, Geldwerth D, Moumaris M, Roger J, Pons JN, Halbreich A. Use of annexin V-ferrofluid to enumerate erythrocytes damaged in various pathologies or during storage in vitro. Compt Rend Acad Sci Ser III 1995; 318(11): 1141–1146.
151. Roger J, Pons JN, Massart R, Halbreich A, Bacri JC. Some biomedical applications of ferrofluids. EPJ Appl Phys 1999; 5(3): 321–325.
152. Halbreich A, Roger J, Pons JN, Geldwerth D, Da Silva MF, Roudier M, Bacri JC. Biomedical applications of maghemite ferrofluid. Biochimie 1998; 80(5–6): 379–390.
153. Whitehead RAC, Groman EV, Josephson L. Magnetic particles for use in separations. US Patent 4,695,392, 1987.
154. Bridot J-L, Laurent S, Boutry S, Gossuin Y, Leclère P, Lazzaroni R, Vander Elst L, Muller RN. New carboxysilane coated iron oxide nanoparticles for non-specific cell labelling. Contrast Media Mol Imag 2013.
155. Zhang Y, Kohler N, Zhang M. Intracellular uptake of poly(ethylene glycol) and folic acid modified magnetite nanoparticles. 2001; Y9.8.1–Y9.8.5.

156. Liu X, Xing J, Guan Y, Shan G, Liu H. Synthesis of amino-silane modified superparamagnetic silica supports and their use for protein immobilization. Colloids Surf A Physicochem Eng Asp 2004; 238(1–3): 127–131.
157. Sun EY, Josephson L, Weissleder R. 'Clickable' nanoparticles for targeted imaging. Mol Imag 2006; 5(2): 122–128.
158. Müller-Schulte D FF, Lueken H, De Cuyper M. Neuer Ansatz für die AIDS-Therapie unter Verwendung superparamagnetischer Nanopartikel. Alma Mater Aquensis 1995; 31: 174–187.
159. Shinkai M, Suzuki M, Iijima S, Kobayashi T. Antibody-conjugated magnetoliposomes for targeting cancer cells and their application in hyperthermia. Biotechnol Appl Biochem 1995; 21(2): 125–137.
160. Sun EY, Josephson L, Weissleder R. 'Clickable' Nanoparticles for targeted imaging. Mol Imag 2006; 5(2): 122–128.
161. Domingo JC, Mercadal M, Petriz J, De Madariaga MA. Preparation of PEG-grafted immunomagnetoliosomes entrapping citrate stabilized magnetite particles and their application in CD34+ cell sorting. J Microencapsulation 2001; 18(1): 41–54.
162. Ito A, Kuga Y, Honda H, Kikkawa H, Horiuchi A, Watanabe Y, Kobayashi T. Magnetite nanoparticle-loaded anti-HER2 immunoliposomes for combination of antibody therapy with hyperthermia. Cancer Lett 2004; 212(2): 167–175.
163. Ito A, Ino K, Kobayashi T, Honda H. The effect of RGD peptide-conjugated magnetite cationic liposomes on cell growth and cell sheet harvesting. Biomaterials 2005; 26(31): 6185–6193.
164. Hodenius M, De Cuyper M, Desender L, Müller-Schulte D, Steigel A, Lueken H. Biotinylated Stealth® magnetoliposomes. Chem Phys Lipids 2002; 120(1–2): 75–85.
165. Nitin N, LaConte LEW, Zurkiya O, Hu X, Bao G. Functionalization and peptide-based delivery of magnetic nanoparticles as an intracellular MRI contrast agent. J Biol Inorg Chem 2004; 9(6): 706–712.
166. Nasongkla N, Bey E, Ren J, Ai H, Khemtong C, Guthi JS, Chin SF, Sherry AD, Boothman DA, Gao J. Multifunctional polymeric micelles as cancer-targeted, MRI-ultrasensitive drug delivery systems. Nano Lett 2006; 6(11): 2427–2430.
167. Brigger I, Dubernet C, Couvreur P. Nanoparticles in cancer therapy and diagnosis. Adv Drug Deliv Rev 2012; 64(suppl.): 24–36.
168. De M, Chou SS, Joshi HM, Dravid VP. Hybrid magnetic nanostructures (MNS) for magnetic resonance imaging applications. Adv Drug Deliv Rev 2011; 63(14–15): 1282–1299.
169. Kanwar RK, Chaudhary R, Tsuzuki T, Kanwar JR. Emerging engineered magnetic nanoparticulate probes for molecular MRI of atherosclerosis: how far have we come? Nanomedicine 2012; 7(6): 899–916.
170. Kanwar RK, Chaudhary R, Tsuzuki T, Kanwar JR. Emerging engineered magnetic nanoparticulate probes for targeted MRI of atherosclerotic plaque macrophages. Nanomedicine 2012; 7(5): 735–749.
171. Phinikaridou A, Botnar RM. MRI of atherosclerosis: from mouse to man. Imag Med 2012; 4(1): 41–58.
172. Torchilin VP. Multifunctional nanocarriers. Adv Drug Deliv Rev 2012; 64(suppl.): 302–315.
173. Xu C, Sun S. New forms of superparamagnetic nanoparticles for biomedical applications. Adv Drug Deliv Rev 2013; 65(5): 732–743.
174. Rennen HJ, Boerman OC, Oyen WJ, Corstens FH. Imaging infection/inflammation in the new millennium. Eur J Nucl Med 2001; 28(2): 241–252.
175. Kooi M, Cappendijk V, Cleutjens K, Kessels A, Kitslaar P, Borgers M, Frederik P, Daemen M, Van Engelshoven J. Accumulation of ultrasmall superparamagnetic particles of iron oxide in human atherosclerotic plaques can be detected by in vivo magnetic resonance imaging. Circulation 2003; 107(19): 2453–2458.
176. Beckmann N, Cannet C, Fringeli-Tanner M, Baumann D, Pally C, Bruns C, Zerwes HG, Andriambeloson E, Bigaud M. Macrophage labeling by SPIO as an early marker of allograft chronic rejection in a rat model of kidney transplantation. Magn Reson Med 2003; 49(3): 459–467.
177. Tanaka Y. The role of chemokines and adhesion molecules in the pathogenesis of rheumatoid arthritis. Drugs Today (Barc) 2001; 37(7): 477–484.
178. Khatib A-M, Kontogiannea M, Fallavollita L, Jamison B, Meterissian S, Brodt P. Rapid induction of cytokine and E-selectin expression in the liver in response to metastatic tumor cells. Cancer Res 1999; 59(6): 1356–1361.
179. Menger MD, Vollmar B. Role of microcirculation in transplantation. Microcirculation 2000; 7(5): 291–306.
180. Dousset V, Delalande C, Ballarino L, Quesson B, Seilhan D, Coussemacq M, Thiaudiére E, Brochet B, Canioni P, Caillé JM. In vivo macrophage activity imaging in the central nervous system detected by magnetic resonance. Magn Reson Med 1999; 41(2): 329–333.
181. Dousset V, Gomez C, Petry KG, Delalande C, Caille J-M. Dose and scanning delay using USPIO for central nervous system macrophage imaging. Magn Reson Mater Phys Biol Med 1999; 8(3): 185–189.
182. Fleige G, Nolte C, Synowitz M, Seeberger F, Kettenmann H, Zimmer C. Magnetic labeling of activated microglia in experimental gliomas. Neoplasia 2001; 3(6): 489.
183. Rausch M, Hiestand P, Baumann D, Cannet C, Rudin M. MRI-based monitoring of inflammation and tissue damage in acute and chronic relapsing EAE. Magn Reson Med 2003; 50(2): 309–314.
184. Ruehm SG, Corot C, Vogt P, Kolb S, Debatin JF. Magnetic resonance imaging of atherosclerotic plaque with ultrasmall superparamagnetic particles of iron oxide in hyperlipidemic rabbits. Circulation 2001; 103(3): 415–422.
185. Kang HW, Josephson L, Petrovsky A, Weissleder R, Bogdanov A. Magnetic resonance imaging of inducible E-selectin expression in human endothelial cell culture. Bioconjug Chem 2002; 13(1): 122–127.
186. Alsaid H, De Souza G, Bourdillon M-C, Chaubet F, Sulaiman A, Desbleds-Mansard C, Chaabane L, Zahir C, Lancelot E, Rousseaux O. Biomimetic MRI contrast agent for imaging of inflammation in atherosclerotic plaque of ApoE$^{-/-m}$ice: a pilot study. Invest Radiol 2009; 44(3): 151–158.
187. Winter PM, Caruthers SD, Kassner A, Harris TD, Chinen LK, Allen JS, Lacy EK, Zhang H, Robertson JD, Wickline SA. Molecular imaging of angiogenesis in nascent Vx-2 rabbit tumors using a novel $\alpha v\beta 3$-targeted nanoparticle and 1.5 tesla magnetic resonance imaging. Cancer Res 2003; 63(18): 5838–5843.
188. Albelda SM, Buck CA. Integrins and other cell adhesion molecules. FASEB J 1990; 4(11): 2868–2880.
189. Foxall C, Watson SR, Dowbenko D, Fennie C, Lasky LA, Kiso M, Hasegawa A, Asa D, Brandley BK. The three members of the selectin receptor family recognize a common carbohydrate epitope, the sialyl Lewis (x) oligosaccharide. J Cell Biol 1992; 117(4): 895–902.
190. Vestweber D, Blanks JE. Mechanisms that regulate the function of the selectins and their ligands. Physiol Rev 1999; 79(1): 181–213.
191. Boutry S, Laurent S, Elst LV, Muller RN. Specific E-selectin targeting with a superparamagnetic MRI contrast agent. Contrast Media Mol Imag 2006; 1(1): 15–22.
192. Kogan TP, Dupre B, Keller KM, Scott IL, Bui H, Market RV, Beck PJ, Voytus JA, Revelle BM, Scott D. Rational design and synthesis of small molecule, non-oligosaccharide selectin inhibitors: alpha-D-mannopyranosyloxy) biphenyl-substituted carboxylic acids. J Med Chem 1995; 38(26): 4976–4984.
193. Fu Y, Laurent S, Muller RN. Synthesis of a sialyl lewisX mimetic conjugated with DTPA, potential ligand of new contrast agents for medical imaging. Eur J Org Chem 2002; 2002(23): 3966–3973.
194. Laurent S, Vander Elst L, Fu Y, Muller RN. Synthesis and physicochemical characterization of Gd-DTPA-B (sLex) A, a new MRI contrast agent targeted to inflammation. Bioconjug Chem 2004; 15(1): 99–103.
195. Sibson NR, Blamire AM, Bernades-Silva M, Laurent S, Boutry S, Muller RN, Styles P, Anthony DC. MRI detection of early endothelial activation in brain inflammation. Magn Reson Med 2004; 51(2): 248–252.
196. Boutry S, Burtea C, Laurent S, Toubeau G, Vander Elst L, Muller RN. Magnetic resonance imaging of inflammation with a specific selectin-targeted contrast agent. Magn Reson Med 2005; 53(4): 800–807.
197. Radermacher KA, Beghein N, Boutry S, Laurent S, Vander Elst L, Muller RN, Jordan BF, Gallez B. In vivo detection of inflammation using pegylated iron oxide particles targeted at E-selectin: a multimodal approach using MR imaging and EPR spectroscopy. Invest Radiol 2009; 44(7): 398–404.
198. Veronese FM, Mero A. The impact of PEGylation on biological therapies. BioDrugs 2008; 22(5): 315–329.
199. Veronese FM, Pasut G. PEGylation, successful approach to drug delivery. Drug Discov Today 2005; 10(21): 1451–1458.
200. Funovics M, Montet X, Reynolds F, Weissleder R, Josephson L. Nanoparticles for the optical imaging of tumor E-selectin. Neoplasia – Int J Oncol Res 2005; 7(10): 904–911.
201. Serda RE, Adolphi NL, Bisoffi M, Sillerud LO. Targeting and cellular trafficking of magnetic nanoparticles for prostate cancer imaging. Mol Imag 2007; 6(4): 277–288.

202. Kou G, Wang S, Cheng C, Gao J, Li B, Wang H, Qian W, Hou S, Zhang D, Dai J, Gu H, Guo Y. Development of SM5-1-conjugated ultrasmall superparamagnetic iron oxide nanoparticles for hepatoma detection. Biochem Biophys Res Commun 2008; 374(2): 192–197.
203. Chen TJ, Cheng TH, Chen CY, Hsu SC, Cheng TL, Liu GC, Wang YM. Targeted Herceptin-dextran iron oxide nanoparticles for noninvasive imaging of HER2/neu receptors using MRI. J Biol Inorg Chem 2009; 14(2): 253–260.
204. Yang H-M, Park CW, Woo M-A, Kim MI, Jo YM, Park HG, Kim J-D. HER2/neu antibody conjugated poly(amino acid)-coated iron oxide nanoparticles for breast cancer MR imaging. Biomacromolecules 2010; 11(11): 2866–2872.
205. Remsen LG, McCormick CI, Roman-Goldstein S, Nilaver G, Weissleder R, Bogdanov A, Hellstrom I, Kroll RA, Neuwelt EA. MR of carcinoma-specific monoclonal antibody conjugated to monocrystalline iron oxide nanoparticles: the potential for noninvasive diagnosis. AJNR Am J Neuroradiol 1996; 17(3): 411–418.
206. Renshaw PF, Owen CS, Evans AE, Leigh JS Jr. Immunospecific NMR contrast agents. Magn Reson Imag 1986; 4(4): 351–357.
207. Artemov D, Mori N, Ravi R, Bhujwalla ZM. Magnetic resonance molecular imaging of the HER-2/neu receptor. Cancer Res 2003; 63(11): 2723–2727.
208. Bulte JW, Hoekstra Y, Kamman RL, Magin RL, Webb AG, Briggs RW, Go KG, Hulstaert CE, Miltenyi S, The TH, et al. Specific MR imaging of human lymphocytes by monoclonal antibody-guided dextran-magnetite particles. Magn Reson Med 1992; 25(1): 148–157.
209. Tiefenauer LX, Kuhne G, Andres RY. Antibody-magnetite nanoparticles: in vitro characterization of a potential tumor-specific contrast agent for magnetic resonance imaging. Bioconjug Chem 1993; 4(5): 347–352.
210. Tiefenauer LX, Tschirky A, Kuhne G, Andres RY. In vivo evaluation of magnetite nanoparticles for use as a tumor contrast agent in MRI. Magn Reson Imag 1996; 14(4): 391–402.
211. Yang L, Mao H, Wang YA, Cao Z, Peng X, Wang X, Duan H, Ni C, Yuan Q, Adams G, Smith MQ, Wood WC, Gao X, Nie S. Single chain epidermal growth factor receptor antibody conjugated nanoparticles for in vivo tumor targeting and imaging. Small 2009; 5(2): 235–243.
212. Yang L, Mao H, Cao Z, Wang YA, Peng X, Wang X, Sajja HK, Wang L, Duan H, Ni C, Staley CA, Wood WC, Gao X, Nie S. Molecular imaging of pancreatic cancer in an animal model using targeted multifunctional nanoparticles. Gastroenterology 2009; 136(5): 1514–1525.
213. Jain RK. Transport of molecules in the tumor interstitium: a review. Cancer Res 1987; 47(12): 3039–3051.
214. McNeil SE. Nanotechnology for the biologist. J Leukocyte Biol 2005; 78(3): 585–594.
215. Chatzistamou L, Schally AV, Nagy A, Armatis P, Szepeshazi K, Halmos G. Effective treatment of metastatic MDA-MB-435 human estrogen-independent breast carcinomas with a targeted cytotoxic analogue of luteinizing hormone-releasing hormone AN-207. Clin Cancer Res 2000; 6(10): 4158–4165.
216. Leuschner C, Kumar CS, Hansel W, Soboyejo W, Zhou J, Hormes J. LHRH-conjugated magnetic iron oxide nanoparticles for detection of breast cancer metastases. Breast Cancer Res Treat 2006; 99(2): 163–176.
217. Ichikawa T, Hogemann D, Saeki Y, Tyminski E, Terada K, Weissleder R, Chiocca EA, Basilion JP. MRI of transgene expression: correlation to therapeutic gene expression. Neoplasia 2002; 4(6): 523–530.
218. Moore A, Basilion JP, Chiocca EA, Weissleder R. Measuring transferrin receptor gene expression by NMR imaging. Biochim Biophys Acta 1998; 24(3): 239–249.
219. Weissleder R, Moore A, Mahmood U, Bhorade R, Benveniste H, Chiocca EA, Basilion JP. In vivo magnetic resonance imaging of transgene expression. Nat Med 2000; 6(3): 351–355.
220. Low PS, Henne WA, Doorneweerd DD. Discovery and development of folic-acid-based receptor targeting for imaging and therapy of cancer and inflammatory diseases. Acc Chem Res 2008; 41(1): 120–129.
221. Choi H, Choi SR, Zhou R, Kung HF, Chen IW. Iron oxide nanoparticles as magnetic resonance contrast agent for tumor imaging via folate receptor-targeted delivery. Acad Radiol 2004; 11(9): 996–1004.
222. Sun C, Sze R, Zhang M. Folic acid-PEG conjugated superparamagnetic nanoparticles for targeted cellular uptake and detection by MRI. J Biomed Mater Res A 2006; 78(3): 550–557.
223. Chen H, Gu Y, Hub Y, Qian Z. Characterization of pH- and temperature-sensitive hydrogel nanoparticles for controlled drug release. PDA J Pharm Sci Technol 2007; 61(4): 303–313.
224. Shen TT, Bogdanov A Jr, Bogdanova A, Poss K, Brady TJ, Weissleder R. Magnetically labeled secretin retains receptor affinity to pancreas acinar cells. Bioconjug Chem 1996; 7(3): 311–316.
225. Larbanoix L, Burtea C, Ansciaux E, Laurent S, Mahieu I, Vander Elst L, Muller RN. Design and evaluation of a 6-mer amyloid-beta protein derived phage display library for molecular targeting of amyloid plaques in Alzheimer's disease: comparison with two cyclic heptapeptides derived from a randomized phage display library. Peptides 2011; 32(6): 1232–1243.
226. Sunderland CJ, Steiert M, Talmadge JE, Derfus AM, Barry SE. Targeted nanoparticles for detecting and treating cancer. Drug Dev Res 2006; 67(1): 70–93.
227. Zhang C, Jugold M, Woenne EC, Lammers T, Morgenstern B, Mueller MM, Zentgraf H, Bock M, Eisenhut M, Semmler W, Kiessling F. Specific targeting of tumor angiogenesis by RGD-conjugated ultrasmall superparamagnetic iron oxide particles using a clinical 1.5-T magnetic resonance scanner. Cancer Res 2007; 67(4): 1555–1562.
228. Liu C, Liu DB, Long GX, Wang JF, Mei Q, Hu GY, Qiu H, Hu GQ. Specific targeting of angiogenesis in lung cancer with RGD-conjugated ultrasmall superparamagnetic iron oxide particles using a 4.7 T magnetic resonance scanner. Chin Med J 2013; 126(12): 2242–2247.
229. Burtea C, Laurent S, Murariu O, Rattat D, Toubeau G, Verbruggen A, Vansthertem D, Vander Elst L, Muller RN. Molecular imaging of alpha v beta3 integrin expression in atherosclerotic plaques with a mimetic of RGD peptide grafted to Gd-DTPA. Cardiovasc Res 2008; 78(1): 148–157.
230. Rerat V, Laurent S, Burtea C, Driesschaert B, Pourcelle V, Vander Elst L, Muller RN, Marchand-Brynaert J. Ultrasmall particle of iron oxide – RGD peptidomimetic conjugate: synthesis and characterisation. Bioorg Med Chem Lett 2010; 20(6): 1861–1865.
231. Xie J, Chen K, Lee HY, Xu C, Hsu AR, Peng S, Chen X, Sun S. Ultrasmall c(RGDyK)-coated Fe3O4 nanoparticles and their specific targeting to integrin alpha(v)beta3-rich tumor cells. J Am Chem Soc 2008; 130(24): 7542–7543.
232. Song E-Q, Hu J, Wen C-Y, Tian Z-Q, Yu X, Zhang Z-L, Shi Y-B, Pang D-W. Fluorescent-magnetic-biotargeting multifunctional nanobioprobes for detecting and isolating multiple types of tumor cells. ACS Nano 2011; 5(2): 761–770.
233. Bamrungsap S, Chen T, Shukoor MI, Chen Z, Sefah K, Chen Y, Tan W. Pattern recognition of cancer cells using aptamer-conjugated magnetic nanoparticles. ACS Nano 2012; 6(5): 3974–3981.
234. Medley CD, Bamrungsap S, Tan W, Smith JE. Aptamer-conjugated nanoparticles for cancer cell detection. Anal Chem 2011; 83(3): 727–734.
235. Smith JE, Medley CD, Tang Z, Shangguan D, Lofton C, Tan W. Aptamer-conjugated nanoparticles for the collection and detection of multiple cancer cells. Anal Chem 2007; 79(8): 3075–3082.
236. Yu MK, Kim D, Lee IH, So JS, Jeong YY, Jon S. Image-guided prostate cancer therapy using aptamer-functionalized thermally cross-linked superparamagnetic iron oxide nanoparticles. Small 2011; 7(15): 2241–2249.
237. Wang AZ, Bagalkot V, Vasilliou CC, Gu F, Alexis F, Zhang L, Shaikh M, Yuet K, Cima MJ, Langer R, Kantoff PW, Bander NH, Jon S, Farokhzad OC. Superparamagnetic iron oxide nanoparticle–aptamer bioconjugates for combined prostate cancer imaging and therapy. ChemMedChem 2008; 3(9): 1311–1315.
238. Yigit MV, Mazumdar D, Kim H-K, Lee JH, Odintsov B, Lu Y. Smart 'turn-on' magnetic resonance contrast agents based on aptamer-functionalized superparamagnetic iron oxide nanoparticles. ChemBioChem 2007; 8(14): 1675–1678.
239. Yigit MV, Mazumdar D, Lu Y. MRI Detection of thrombin with aptamer functionalized superparamagnetic iron oxide nanoparticles. Bioconjug Chem 2008; 19(2): 412–417.
240. Reddy LH, Couvreur P. Nanotechnology for therapy and imaging of liver diseases. J Hepatol 2011; 55(6): 1461–1466.
241. Bataller R, Brenner DA. Liver fibrosis. J Clin Invest 2005; 115(2): 209–218.
242. Faria SC, Ganesan K, Mwangi I, Shiehmorteza M, Viamonte B, Mazhar S, Peterson M, Kono Y, Santillan C, Casola G, Sirlin CB. MR imaging of liver fibrosis: current state of the art. Radiographic 2009; 29(6): 1615–1635.
243. Na HB, Song IC, Hyeon T. Inorganic nanoparticles for MRI contrast agents. Adv Mater 2009; 21(21): 2133–2148.
244. Rosen JE, Chan L, Shieh D-B, Gu FX. Iron oxide nanoparticles for targeted cancer imaging and diagnostics. Nanomed Nanotechnol Biol Med 2012; 8(3): 275–290.

245. Weissleder R, Stark DD, Engelstad BL, Bacon BR, Compton CC, White DL, Jacobs P, Lewis J. Superparamagnetic iron oxide: pharmacokinetics and toxicity. AJR Am J Roentgenol 1989; 152(1): 167–173.
246. Qiao R, Yang C, Gao M. Superparamagnetic iron oxide nanoparticles: from preparations to in vivo MRI applications. J Mater Chem 2009; 19(35): 6274–6293.
247. Gandhi SN, Brown MA, Wong JG, Aguirre DA, Sirlin CB. MR Contrast agents for liver imaging: what, when, how. Radiographics 2006; 26(6): 1621–1636.
248. Ma HL, Xu YF, Qi XR, Maitani Y, Nagai T. Superparamagnetic iron oxide nanoparticles stabilized by alginate: pharmacokinetics, tissue distribution, and applications in detecting liver cancers. Int J Pharm 2008; 354(1–2): 217–226.
249. Clement O, Frija G, Chambon C, Schouman-Clayes E, Mosnier JF, Poupon MF, Balkau B. Liver tumors in cirrhosis: experimental study with SPIO-enhanced MR imaging. Radiology 1991; 180(1): 31–36.
250. Tanimoto A, Kuribayashi S. Application of superparamagnetic iron oxide to imaging of hepatocellular carcinoma. Eur J Radiol 2006; 58(2): 200–216.
251. Aguirre DA, Behling CA, Alpert E, Hassanein TI, Sirlin CB. Liver fibrosis: noninvasive diagnosis with double contrast material–enhanced MR imaging. Radiology 2006; 239(2): 425–437.
252. Wang YX, Xuan S, Port M, Idee JM. Recent advances in superparamagnetic iron oxide nanoparticles for cellular imaging and targeted therapy research. Curr Pharm Des 2013.
253. Zhang H, Ma Y, Sun XL. Recent developments in carbohydrate-decorated targeted drug/gene delivery. Med Res Rev 2010; 30(2): 270–289.
254. Lee C-M, Jeong H-J, Kim E-M, Kim DW, Lim ST, Kim HT, Park I-K, Jeong YY, Kim JW, Sohn M-H. Superparamagnetic iron oxide nanoparticles as a dual imaging probe for targeting hepatocytes in vivo. Magn Reson Med 2009; 62(6): 1440–1446.
255. Yoo MK, Kim IY, Kim EM, Jeong HJ, Lee CM, Jeong YY, Akaike T, Cho CS. Superparamagnetic iron oxide nanoparticles coated with galactose-carrying polymer for hepatocyte targeting. J Biomed Biotechnol 2007; 2007(10): 94740.
256. Cole AJ, Yang VC, David AE. Cancer theranostics: the rise of targeted magnetic nanoparticles. Trends Biotechnol 2011; 29(7): 323–332.
257. Zhu H, Shang Y, Wang W, Zhou Y, Li P, Yan K, Wu S, Yeung KWK, Xu Z, Xu H, Chu PK. Fluorescent magnetic Fe3O4/rare earth colloidal nanoparticles for dual-modality imaging. Small 2013.
258. Zhao M, Beauregard DA, Loizou L, Davletov B, Brindle KM. Non-invasive detection of apoptosis using magnetic resonance imaging and a targeted contrast agent. Nat Med 2001; 7(11): 1241–1244.
259. Radermacher KA, Boutry S, Laurent S, Elst LV, Mahieu I, Bouzin C, Magat J, Gregoire V, Feron O, Muller RN, Jordan BF, Gallez B. Iron oxide particles covered with hexapeptides targeted at phosphatidylserine as MR biomarkers of tumor cell death. Contrast Media Mol Imag 2010; 5(5): 258–267.
260. Vu-Quang H, Muthiah M, Lee HJ, Kim Y-K, Rhee JH, Lee J-H, Cho C-S, Choi Y-J, Jeong YY, Park I-K. Immune cell-specific delivery of beta-glucan-coated iron oxide nanoparticles for diagnosing liver metastasis by MR imaging. Carbohydr Polym 2012; 87(2): 1159–1168.
261. Kolosnjaj-Tabi J, Wilhelm C, Clement O, Gazeau F. Cell labeling with magnetic nanoparticles: opportunity for magnetic cell imaging and cell manipulation. J Nanobiotechnol 2013; 11(suppl 1): S7.
262. Shapiro EM, Sharer K, Skrtic S, Koretsky AP. In vivo detection of single cells by MRI. Magn Reson Med 2006; 55(2): 242–249.
263. Puppi J, Mitry RR, Modo M, Dhawan A, Raja K, Hughes RD. Use of a clinically approved iron oxide MRI contrast agent to label human hepatocytes. Cell Transplant 2011; 20(6): 963–975.
264. Luciani A, Parouchev A, Smirnov P, Braga G, Wilhelm C, Gazeau F, Boudechiche L, L'Hermine-Coulomb A, Dagher I, Franco D, Rahmouni A, Hadchouel M, Weber A, Clement O. In vivo imaging of transplanted hepatocytes with a 1.5-T clinical MRI system – initial experience in mice. Eur Radiol 2008; 18(1): 59–69.
265. Maccioni F, Colaiacomo MC, Parlanti S. Ulcerative colitis: value of MR imaging. Abdom Imag 2005; 30(5): 584–592.
266. Wang YX, Hussain SM, Krestin GP. Superparamagnetic iron oxide contrast agents: physicochemical characteristics and applications in MR imaging. Eur Radiol 2001; 11(11): 2319–2331.
267. Hahn PF, Stark DD, Lewis JM, Saini S, Elizondo G, Weissleder R, Fretz CJ, Ferrucci JT. First clinical trial of a new superparamagnetic iron oxide for use as an oral gastrointestinal contrast agent in MR imaging. Radiology 1990; 175(3): 695–700.
268. Wang Y-XJ. Superparamagnetic iron oxide based MRI contrast agents: current status of clinical application. Quant Imag Med Surg 2011; 1(1): 35–40.
269. D'Arienzo A, Scaglione G, Vicinanza G, Manguso F, Bennato R, Belfiore G, Imbriaco M, Mazzacca G. Magnetic resonance imaging with ferumoxil, a negative superparamagnetic oral contrast agent, in the evaluation of ulcerative colitis. Am J Gastroenterol 2000; 95(3): 720–724.
270. Xiao B, Merlin D. Oral colon-specific therapeutic approaches toward treatment of inflammatory bowel disease. Expert Opin Drug Deliv 2012; 9(11): 1393–1407.
271. Frericks BB, Wacker F, Loddenkemper C, Valdeig S, Hotz B, Wolf KJ, Misselwitz B, Kuhl A, Hoffmann JC. Magnetic resonance imaging of experimental inflammatory bowel disease: quantitative and qualitative analyses with histopathologic correlation in a rat model using the ultrasmall iron oxide SHU 555 C. Invest Radiol 2009; 44(1): 23–30.
272. Jalalian SH, Taghdisi SM, Shahidi Hamedani N, Kalat SA, Lavaee P, Zandkarimi M, Ghows N, Jaafari MR, Naghibi S, Danesh NM, Ramezani M, Abnous K. Epirubicin loaded super paramagnetic iron oxide nanoparticle-aptamer bioconjugate for combined colon cancer therapy and imaging in vivo. Eur J Pharm Sci 2013; 50(2): 191–197.
273. Crater JS, Carrier RL. Barrier properties of gastrointestinal mucus to nanoparticle transport. Macromol Biosci 2010; 10(12): 1473–1483.
274. Kenzaoui BH, Vila MR, Miquel JM, Cengelli F, Juillerat-Jeanneret L. Evaluation of uptake and transport of cationic and anionic ultrasmall iron oxide nanoparticles by human colon cells. Int J Nanomed 2012; 7: 1275–1286.
275. Corem-Salkmon E, Perlstein B, Margel S. Design of near-infrared fluorescent bioactive conjugated functional iron oxide nanoparticles for optical detection of colon cancer. Int J Nanomed 2012; 7: 5517–5527.
276. Whiting JL, Sigurdsson A, Rowlands DC, Hallissey MT, Fielding JW. The long term results of endoscopic surveillance of premalignant gastric lesions. Gut 2002; 50(3): 378–381.
277. Elias A, Tsourkas A. Imaging circulating cells and lymphoid tissues with iron oxide nanoparticles. Hematology 2009; 720–726.
278. Jahan N, Narayanan P, Rockall A. Magnetic resonance lymphography in gynaecological malignancies. Cancer Imag 2010; 10: 85–96.
279. Koh DM, Cook GJ, Husband JE. New horizons in oncologic imaging. New Engl J Med 2003; 348(25): 2487–2488.
280. Benedetti-Panici P, Maneschi F, Scambia G, Greggi S, Cutillo G, D'Andrea G, Rabitti C, Coronetta F, Capelli A, Mancuso S. Lymphatic spread of cervical cancer: an anatomical and pathological study based on 225 radical hysterectomies with systematic pelvic and aortic lymphadenectomy. Gynecol Oncol 1996; 62(1): 19–24.
281. Hövels AM, Heesakkers RAM, Adang EM, Jager GJ, Strum S, Hoogeveen YL, Severens JL, Barentsz JO. The diagnostic accuracy of CT and MRI in the staging of pelvic lymph nodes in patients with prostate cancer: a meta-analysis. Clin Radiol 2008; 63(4): 387–395.
282. Islam T, Harisinghani MG. Overview of nanoparticle use in cancer imaging. Cancer Biomark 2009; 5(2): 61–67.
283. Corot C, Robert P, Idee JM, Port M. Recent advances in iron oxide nanocrystal technology for medical imaging. Adv Drug Deliv Rev 2006; 58(14): 1471–1504.
284. Weissleder R, Bogdanov A, Neuwelt EA, Papisov M. Long-circulating iron oxides for MR imaging. Adv Drug Deliv Rev 1995; 16(2–3): 321–334.
285. Bellin M-F, Beigelman C, Precetti-Morel S. Iron oxide-enhanced MR lymphography: initial experience. Eur J Radiol 2000; 34(3): 257–264.
286. Schroeder A, Heller DA, Winslow MM, Dahlman JE, Pratt GW, Langer R, Jacks T, Anderson DG. Treating metastatic cancer with nanotechnology. Nat Rev Cancer 2012; 12(1): 39–50.
287. Harisinghani MG, Barentsz J, Hahn PF, Deserno WM, Tabatabaei S, van de Kaa CH, de la Rosette J, Weissleder R. Noninvasive detection of clinically occult lymph-node metastases in prostate cancer. New Engl J Med 2003; 348(25): 2491–2499.
288. Ferrucci JT, Stark DD. Iron oxide-enhanced MR imaging of the liver and spleen: review of the first 5 years. AJR Am J Roentgenol 1990; 155(5): 943–950.
289. Daldrup-Link H, Rummeny E, Ihssen B, Kienast J, Link T. Iron-oxide-enhanced MR imaging of bone marrow in patients with non-Hodgkin's lymphoma: differentiation between tumor infiltration and hypercellular bone marrow. Eur Radiol 2002; 12(6): 1557–1566.
290. Jung CW, Rogers JM, Groman EV. Lymphatic mapping and sentinel node location with magnetite nanoparticles. J Magn Magn Mater 1999; 194(1–3): 210–216.
291. Harisinghani MG, Barentsz J, Hahn PF, Deserno WM, Tabatabaei S, van de Kaa CH, de la Rosette J, Weissleder R. Noninvasive detection

of clinically occult lymph-node metastases in prostate cancer. New Engl J Med 2003; 348(25): 2491–2499.
292. Deserno WM, Harisinghani MG, Taupitz M, Jager GJ, Witjes JA, Mulders PF, Hulsbergen van de Kaa CA, Kaufmann D, Barentsz JO. Urinary bladder cancer: preoperative nodal staging with Ferumoxtran-10-enhanced MR imaging. Radiology 2004; 233(2): 449–456.
293. Harisinghani MG, Saksena M, Ross RW, Tabatabaei S, Dahl D, McDougal S, Weissleder R. A pilot study of lymphotrophic nanoparticle-enhanced magnetic resonance imaging technique in early stage testicular cancer: a new method for noninvasive lymph node evaluation. Urology 2005; 66(5): 1066–1071.
294. Tabatabaei S, Harisinghani M, McDougal WS. Regional lymph node staging using lymphotropic nanoparticle enhanced magnetic resonance imaging with Ferumoxtran-10 in patients with penile cancer. J Urol 2005; 174(3): 923–927.
295. Nishimura H, Tanigawa N, Hiramatsu M, Tatsumi Y, Matsuki M, Narabayashi I. Preoperative esophageal cancer staging: magnetic resonance imaging of lymph node with Ferumoxtran-10, an ultrasmall superparamagnetic iron oxide. J Am College Surg 2006; 202(4): 604–611.
296. Koh D-M, Brown G, Temple L, Raja A, Toomey P, Bett N, Norman AR, Husband JE. Rectal cancer: mesorectal lymph nodes at MR imaging with USPIO versus histopathologic findings – initial observations. Radiology 2004; 231(1): 91–99.
297. Rockall AG, Sohaib SA, Harisinghani MG, Babar SA, Singh N, Jeyarajah AR, Oram DH, Jacobs IJ, Shepherd JH, Reznek RH. Diagnostic performance of nanoparticle-enhanced magnetic resonance imaging in the diagnosis of lymph node metastases in patients with endometrial and cervical cancer. J Clin Oncol 2005; 23(12): 2813–2821.
298. Shapiro EM, Medford-Davis LN, Fahmy TM, Dunbar CE, Koretsky AP. Antibody-mediated cell labeling of peripheral T cells with micron-sized iron oxide particles (MPIOs) allows single cell detection by MRI. Contrast Media Mol Imag 2007; 2(3): 147–153.
299. Yeh T-C, Zhang W, Ildstad ST, Ho C. Intracellular labeling of T-cells with superparamagnetic contrast agents. Magn Reson Med 1993; 30(5): 617–625.
300. Yeh TC, Zhang W, Ildstad ST, Ho C. In vivo dynamic MRI tracking of rat T-cells labeled with superparamagnetic iron-oxide particles. Magn Reson Med 1995; 33(2): 200–208.
301. Hu D-E, Kettunen MI, Brindle KM. Monitoring T-lymphocyte trafficking in tumors undergoing immune rejection. Magn Reson Med 2005; 54(6): 1473–1479.
302. Kircher MF, Allport JR, Graves EE, Love V, Josephson L, Lichtman AH, Weissleder R. In vivo high resolution three-dimensional imaging of antigen-specific cytotoxic T-lymphocyte trafficking to tumors. Cancer Res 2003; 63(20): 6838–6846.
303. Arbab AS, Bashaw LA, Miller BR, Jordan EK, Bulte JWM, Frank JA. Intracytoplasmic tagging of cells with ferumoxides and transfection agent for cellular magnetic resonance imaging after cell transplantation: methods and techniques. Transplantation 2003; 76(7): 1123–1130.
304. De Vries IJ, Lesterhuis WJ, Barentsz JO, Verdijk P, van Krieken JH, Boerman OC, Oyen WJ, Bonenkamp JJ, Boezeman JB, Adema GJ, Bulte JW, Scheenen TW, Punt CJ, Heerschap A, Figdor CG. Magnetic resonance tracking of dendritic cells in melanoma patients for monitoring of cellular therapy. Nat Biotechnol 2005; 23(11): 1407–1413.
305. Kobukai S, Baheza R, Cobb JG, Virostko J, Xie J, Gillman A, Koktysh D, Kerns D, Does M, Gore JC, Pham W. Magnetic nanoparticles for imaging dendritic cells. Magn Reson Med 2010; 63(5): 1383–1390.
306. Noh YW, Jang YS, Ahn KJ, Lim YT, Chung BH. Simultaneous in vivo tracking of dendritic cells and priming of an antigen-specific immune response. Biomaterials 2011; 32(26): 6254–6263.
307. Karagulle-Kendi AT, Truwit C. Neuroimaging of central nervous system infections. Handbook Clin Neurol 2010; 96: 239–255.
308. Krol S, Macrez R, Docagne F, Defer G, Laurent S, Rahman M, Hajipour MJ, Kehoe PG, Mahmoudi M. Therapeutic benefits from nanoparticles: the potential significance of nanoscience in diseases with compromise to the blood brain barrier. Chem Rev 2012; 113(3): 1877–1903.
309. Iadecola C, Alexander M. Cerebral ischemia and inflammation. Curr Opin Neurol 2001; 14(1): 89–94.
310. Vezzani A. Inflammation and epilepsy. Epilepsy Curr 2005; 5(1): 1–6.
311. Petry K, Boiziau C, Dousset V, Brochet B. Magnetic resonance imaging of human brain macrophage infiltration. Neurotherapeutics 2007; 4(3): 434–442.
312. Dousset V, Brochet B, Deloire MSA, Lagoarde L, Barroso B, Caille J-M, Petry KG. MR Imaging of relapsing multiple sclerosis patients using ultra-small-particle iron oxide and compared with gadolinium. Am J Neuroradiol 2006; 27(5): 1000–1005.
313. Heyn C, Ronald JA, Mackenzie LT, MacDonald IC, Chambers AF, Rutt BK, Foster PJ. In vivo magnetic resonance imaging of single cells in mouse brain with optical validation. Magn Reson Med 2006; 55(1): 23–29.
314. Grossman RI, Braffman BH, Brorson JR, Goldberg HI, Silberberg DH, Gonzalez-Scarano F. Multiple sclerosis: serial study of gadolinium-enhanced MR imaging. Radiology 1988; 169(1): 117–122.
315. Dousset V, Delalande C, Ballarino L, Quesson B, Seilhan D, Coussemacq M, Thiaudiere E, Brochet B, Canioni P, Caille JM. In vivo macrophage activity imaging in the central nervous system detected by magnetic resonance. Magn Reson Med 1999; 41(2): 329–333.
316. Dousset V, Gomez C, Petry K, Delalande C, Caille J-M. Dose and scanning delay using USPIO for central nervous system macrophage imaging. MAGMA 1999; 8(3): 185–189.
317. Kenzaoui BH, Bernasconi CC, Hofmann H, Juillerat-Jeanneret L. Evaluation of uptake and transport of ultrasmall superparamagnetic iron oxide nanoparticles by human brain-derived endothelial cells. Nanomedicine (Lond) 2012; 7(1): 39–53.
318. Dan M, Cochran DB, Yokel RA, Dziubla TD. Binding, transcytosis and biodistribution of anti-PECAM-1 iron oxide nanoparticles for brain-targeted delivery. PLoS One 2013; 8(11): e81051.
319. Floris S, Blezer ELA, Schreibelt G, Döpp E, van der Pol SMA, Schadee-Eestermans IL, Nicolay K, Dijkstra CD, de Vries HE. Blood–brain barrier permeability and monocyte infiltration in experimental allergic encephalomyelitis: a quantitative MRI study. Brain 2004; 127(3): 616–627.
320. Dousset V, Ballarino L, Delalande C, Coussemacq M, Canioni P, Petry KG, Caillé J-M. Comparison of ultrasmall particles of iron oxide (USPIO)-enhanced T2-weighted, conventional T2-weighted, and gadolinium-enhanced T1-weighted MR images in rats with experimental autoimmune encephalomyelitis. Am J Neuroradiol 1999; 20(2): 223–227.
321. Rausch M, Hiestand P, Foster CA, Baumann DR, Cannet C, Rudin M. Predictability of FTY720 efficacy in experimental autoimmune encephalomyelitis by in vivo macrophage tracking: clinical implications for ultrasmall superparamagnetic iron oxide-enhanced magnetic resonance imaging. J Magn Reson Imag 2004; 20(1): 16–24.
322. Bendszus M, Stoll G. Caught in the act: in vivo mapping of macrophage infiltration in nerve injury by magnetic resonance imaging. J Neurosci 2003; 23(34): 10892–10896.
323. Vellinga MM, Oude Engberink RD, Seewann A, Pouwels PJW, Wattjes MP, van der Pol SMA, Pering C, Polman CH, de Vries HE, Geurts JJG, Barkhof F. Pluriformity of inflammation in multiple sclerosis shown by ultra-small iron oxide particle enhancement. Brain 2008; 131(3): 800–807.
324. Manninger SP, Muldoon LL, Nesbit G, Murillo T, Jacobs PM, Neuwelt EA. An exploratory study of Ferumoxtran-10 nanoparticles as a blood-brain barrier imaging agent targeting phagocytic cells in CNS inflammatory lesions. Am J Neuroradiol 2005; 26(9): 2290–2300.
325. Arvin B, Neville LF, Barone FC, Feuerstein GZ. The role of inflammation and cytokines in brain injury. Neurosci Biobehav Rev 1996; 20(3): 445–452.
326. Zelivyanskaya ML, Nelson JA, Poluektova L, Uberti M, Mellon M, Gendelman HE, Boska MD. Tracking superparamagnetic iron oxide labeled monocytes in brain by high-field magnetic resonance imaging. J Neurosci Res 2003; 73(3): 284–295.
327. Rausch M, Hiestand P, Baumann D, Cannet C, Rudin M. MRI-based monitoring of inflammation and tissue damage in acute and chronic relapsing EAE. Magn Reson Med 2003; 50(2): 309–314.
328. Corot C, Petry KG, Trivedi R, Saleh A, Jonkmanns C, Le Bas J-F, Blezer E, Rausch M, Brochet B, Foster-Gareau P, Balériaux D, Gaillard S, Dousset V. Macrophage imaging in central nervous system and in carotid atherosclerotic plaque using ultrasmall superparamagnetic iron oxide in magnetic resonance imaging. Invest Radiol 2004; 39(10): 619–625.
329. Schilling M, Besselmann M, Leonhard C, Mueller M, Ringelstein EB, Kiefer R. Microglial activation precedes and predominates over macrophage infiltration in transient focal cerebral ischemia: a study in green fluorescent protein transgenic bone marrow chimeric mice. Exp Neurol 2003; 183(1): 25–33.
330. Saleh A, Schroeter M, Jonkmanns C, Hartung HP, Modder U, Jander S. In vivo MRI of brain inflammation in human ischaemic stroke. Brain 2004; 127(Pt 7): 1670–1677.

331. Deddens LH, Van Tilborg GA, Mulder WJ, De Vries HE, Dijkhuizen RM. Imaging neuroinflammation after stroke: current status of cellular and molecular MRI strategies. Cerebrovasc Dis 2012; 33(4): 392–402.
332. Oude Engberink RD, Blezer ELA, Hoff EI, van der Pol SMA, van der Toorn A, Dijkhuizen RM, de Vries HE. MRI of monocyte infiltration in an animal model of neuroinflammation using SPIO-labeled monocytes or free USPIO. J Cereb Blood Flow Metab 2007; 28(4): 841–851.
333. Henning EC, Ruetzler CA, Gaudinski MR, Hu TC, Latour LL, Hallenbeck JM, Warach S. Feridex preloading permits tracking of CNS-resident macrophages after transient middle cerebral artery occlusion. J Cereb Blood Flow 2009; 29(7): 1229–1239.
334. Sztriha LK, O'Gorman RL, Modo M, Barker GJ, Williams SCR, Kalra L. Monitoring brain repair in stroke using advanced magnetic resonance imaging. Stroke 2012; 43(11): 3124–3131.
335. Dunning MD, Lakatos A, Loizou L, Kettunen M, ffrench-Constant C, Brindle KM, Franklin RJ. Superparamagnetic iron oxide-labeled Schwann cells and olfactory ensheathing cells can be traced in vivo by magnetic resonance imaging and retain functional properties after transplantation into the CNS. J Neurosci 2004; 24(44): 9799–9810.
336. Marinescu M, Chauveau F, Durand A, Riou A, Cho TH, Dencausse A, Ballet S, Nighoghossian N, Berthezene Y, Wiart M. Monitoring therapeutic effects in experimental stroke by serial USPIO-enhanced MRI. Eur Radiol 2013; 23(1): 37–47.
337. Lorger M, Felding-Habermann B. Capturing changes in the brain microenvironment during initial steps of breast cancer brain metastasis. Am J Pathol 2010; 176(6): 2958–2971.
338. Lorger M. Tumor Microenvironment in the brain. Cancers 2012; 4(1): 218–243.
339. Enochs WS, Harsh G, Hochberg F, Weissleder R. Improved delineation of human brain tumors on MR images using a long-circulating, superparamagnetic iron oxide agent. J Magn Reson Imag 1999; 9(2): 228–232.
340. Neuwelt EA, Varallyay P, Bago AG, Muldoon LL, Nesbit G, Nixon R. Imaging of iron oxide nanoparticles by MR and light microscopy in patients with malignant brain tumours. Neuropathol Appl Neurobiol 2004; 30(5): 456–471.
341. Zimmer C, Weissleder R, Poss K, Bogdanova A, Wright SC Jr, Enochs WS. MR imaging of phagocytosis in experimental gliomas. Radiology 1995; 197(2): 533–538.
342. Varallyay P, Nesbit G, Muldoon LL, Nixon RR, Delashaw J, Cohen JI, Petrillo A, Rink D, Neuwelt EA. Comparison of two superparamagnetic viral-sized iron oxide particles ferumoxides and Ferumoxtran-10 with a gadolinium chelate in imaging intracranial tumors. Am J Neuroradiol 2002; 23(4): 510–519.
343. Fleige G, Nolte C, Synowitz M, Seeberger F, Kettenmann H, Zimmer C. Magnetic labeling of activated microglia in experimental gliomas. Neoplasia 2001; 3(6): 489–499.
344. Lorger M, Krueger JS, O'Neal M, Staflin K, Felding-Habermann B. Activation of tumor cell integrin alphavbeta3 controls angiogenesis and metastatic growth in the brain. Proc Natl Acad Sci U S A 2009; 106(26): 10666–10671.
345. Claes A, Gambarota G, Hamans B, van Tellingen O, Wesseling P, Maass C, Heerschap A, Leenders W. Magnetic resonance imaging-based detection of glial brain tumors in mice after antiangiogenic treatment. Int J Cancer 2008; 122(9): 1981–1986.
346. Hyodo F, Chandramouli GV, Matsumoto S, Matsumoto K, Mitchell JB, Krishna MC, Munasinghe JP. Estimation of tumor microvessel density by MRI using a blood pool contrast agent. Int J Oncol 2009; 35(4): 797–804.
347. Schwartz CJ, Valente AJ, Sprague EA, Kelley JL, Cayatte AJ, Mowery J. Atherosclerosis. Potential targets for stabilization and regression. Circulation 1992; 86(6 Suppl): III117–III123.
348. Corot C, Petry KG, Trivedi R, Saleh A, Jonkmanns C, Le Bas JF, Blezer E, Rausch M, Brochet B, Foster-Gareau P, Baleriaux D, Gaillard S, Dousset V. Macrophage imaging in central nervous system and in carotid atherosclerotic plaque using ultrasmall superparamagnetic iron oxide in magnetic resonance imaging. Invest Radiol 2004; 39(10): 619–625.
349. Tang TY, Muller KH, Graves MJ, Li ZY, Walsh SR, Young V, Sadat U, Howarth SP, Gillard JH. Iron oxide particles for atheroma imaging. Arterioscler Thromb Vasc Biol 2009; 29(7): 1001–1008.
350. Zhang Z, Mascheri N, Dharmakumar R, Li D. Cellular magnetic resonance imaging: potential for use in assessing aspects of cardiovascular disease. Cytotherapy 2008; 10(6): 575–586.
351. Ruehm SG, Corot C, Vogt P, Kolb S, Debatin JF. Magnetic resonance imaging of atherosclerotic plaque with ultrasmall superparamagnetic particles of iron oxide in hyperlipidemic rabbits. Circulation 2001; 103(3): 415–422.
352. Schmitz SA, Coupland SE, Gust R, Winterhalter S, Wagner S, Kresse M, Semmler W, Wolf KJ. Superparamagnetic iron oxide-enhanced MRI of atherosclerotic plaques in Watanabe hereditable hyperlipidemic rabbits. Invest Radiol 2000; 35(8): 460–471.
353. Litovsky S, Madjid M, Zarrabi A, Casscells SW, Willerson JT, Naghavi M. Superparamagnetic iron oxide-based method for quantifying recruitment of monocytes to mouse atherosclerotic lesions in vivo: enhancement by tissue necrosis factor-alpha, interleukin-1beta, and interferon-gamma. Circulation 2003; 107(11): 1545–1549.
354. Lam T, Pouliot P, Avti PK, Lesage F, Kakkar AK. Superparamagnetic iron oxide based nanoprobes for imaging and theranostics. Adv Colloid Interface Sci 2013.
355. Hyafil F, Laissy JP, Mazighi M, Tchetche D, Louedec L, Adle-Biassette H, Chillon S, Henin D, Jacob MP, Letourneur D, Feldman LJ. Ferumoxtran-10-enhanced MRI of the hypercholesterolemic rabbit aorta: relationship between signal loss and macrophage infiltration. Arterioscler Thromb Vasc Biol 2006; 26(1): 176–181.
356. Trivedi RA, U-King-Im JM, Graves MJ, Kirkpatrick PJ, Gillard JH. Non-invasive imaging of carotid plaque inflammation. Neurology 2004; 63(1): 187–188.
357. Schmitz SA, Taupitz M, Wagner S, Wolf KJ, Beyersdorff D, Hamm B. Magnetic resonance imaging of atherosclerotic plaques using superparamagnetic iron oxide particles. J Magn Reson Imag 2001; 14(4): 355–361.
358. Trivedi RA, U-King-Im JM, Graves MJ, Cross JJ, Horsley J, Goddard MJ, Skepper JN, Quartey G, Warburton E, Joubert I, Wang L, Kirkpatrick PJ, Brown J, Gillard JH. In vivo detection of macrophages in human carotid atheroma: temporal dependence of ultrasmall superparamagnetic particles of iron oxide-enhanced MRI. Stroke 2004; 35(7): 1631–1635.
359. Oude Engberink RD, van der Pol SM, Dopp EA, de Vries HE, Blezer EL. Comparison of SPIO and USPIO for in vitro labeling of human monocytes: MR detection and cell function. Radiology 2007; 243(2): 467–474.
360. Thorek DL, Tsourkas A. Size, charge and concentration dependent uptake of iron oxide particles by non-phagocytic cells. Biomaterials 2008; 29(26): 3583–3590.
361. Raynal I, Prigent P, Peyramaure S, Najid A, Rebuzzi C, Corot C. Macrophage endocytosis of superparamagnetic iron oxide nanoparticles: mechanisms and comparison of ferumoxides and Ferumoxtran-10. Invest Radiol 2004; 39(1): 56–63.
362. Herborn CU, Vogt FM, Lauenstein TC, Dirsch O, Corot C, Robert P, Ruehm SG. Magnetic resonance imaging of experimental atherosclerotic plaque: comparison of two ultrasmall superparamagnetic particles of iron oxide. J Magn Reson Imag 2006; 24(2): 388–393.
363. Tsuchiya K, Nitta N, Sonoda A, Otani H, Takahashi M, Murata K, Shiomi M, Tabata Y, Nohara S. Atherosclerotic imaging using 4 types of superparamagnetic iron oxides: new possibilities for mannan-coated particles. Eur J Radiol 2013; 31(13): 387–382. Q17
364. Truijers M, Futterer JJ, Takahashi S, Heesakkers RA, Blankensteijn JD, Barentsz JO. In vivo imaging of the aneurysm wall with MRI and a macrophage-specific contrast agent. AJR Am J Roentgenol 2009; 193(5): W437–W441.
365. Sadat U, Taviani V, Patterson AJ, Young VE, Graves MJ, Teng Z, Tang TY, Gillard JH. Ultrasmall superparamagnetic iron oxide-enhanced magnetic resonance imaging of abdominal aortic aneurysms – a feasibility study. Eur J Vasc Endovasc 2011; 41(2): 167–174.
366. Alam SR, Shah AS, Richards J, Lang NN, Barnes G, Joshi N, MacGillivray T, McKillop G, Mirsadraee S, Payne J, Fox KA, Henriksen P, Newby DE, Semple SI. Ultrasmall superparamagnetic particles of iron oxide in patients with acute myocardial infarction: early clinical experience. Circul Cardiovasc Imag 2012; 5(5): 559–565.
367. Sosnovik DE, Nahrendorf M. Cells and iron oxide nanoparticles on the move: magnetic resonance imaging of monocyte homing and myocardial inflammation in patients with ST-elevation myocardial infarction. Circul Cardiovasc Imag 2012; 5(5): 551–554.
368. Richards JM, Shaw CA, Lang NN, Williams MC, Semple SI, MacGillivray TJ, Gray C, Crawford JH, Alam SR, Atkinson AP, Forrest EK, Bienek C, Mills NL, Burdess A, Dhaliwal K, Simpson AJ, Wallace WA, Hill AT, Roddie PH, McKillop G, Connolly TA, Feuerstein GZ, Barclay GR, Turner ML, Newby DE. In vivo mononuclear cell tracking using superparamagnetic particles of iron oxide: feasibility and safety in humans. Circul Cardiovasc Imag 2012; 5(4): 509–517.

369. Kanno S, Wu YJ, Lee PC, Dodd SJ, Williams M, Griffith BP, Ho C. Macrophage accumulation associated with rat cardiac allograft rejection detected by magnetic resonance imaging with ultrasmall superparamagnetic iron oxide particles. Circulation 2001; 104(8): 934–938.
370. Jaffer FA, Libby P, Weissleder R. Molecular and cellular imaging of atherosclerosis – emerging applications. J Am College Cardiol 2006; 47(7): 1328–1338.
371. Nahrendorf M, Jaffer FA, Kelly KA, Sosnovik DE, Aikawa E, Libby P, Weissleder R. Noninvasive vascular cell adhesion molecule-1 imaging identifies inflammatory activation of cells in atherosclerosis. Circulation 2006; 114(14): 1504–1511.
372. Barreiro O, Aguilar RJ, Tejera E, Megías D, de Torres-Alba F, Evangelista A, Sánchez-Madrid F. Specific targeting of human inflamed endothelium and in situ vascular tissue transfection by the use of ultrasound contrast agents. JACC: Cardiovasc Imag 2009; 2(8): 997–1005.
373. Kaufmann BA, Carr CL, Belcik JT, Xie A, Yue Q, Chadderdon S, Caplan ES, Khangura J, Bullens S, Bunting S. Molecular imaging of the initial inflammatory response in atherosclerosis implications for early detection of disease. Arterioscler Thromb Vasc Biol 2010; 30(1): 54–59.
374. Nahrendorf M, Keliher E, Panizzi P, Zhang H, Hembrador S, Figueiredo J-L, Aikawa E, Kelly K, Libby P, Weissleder R. 18 F-4 V for PET–CT imaging of VCAM-1 expression in atherosclerosis. JACC: Cardiovasc Imag 2009; 2(10): 1213–1222.
375. Broisat A, Hernot S, Toczek J, De Vos J, Riou LM, Martin S, Ahmadi M, Thielens N, Wernery U, Caveliers V. Nanobodies targeting mouse/human VCAM1 for the nuclear imaging of atherosclerotic lesionsnovelty and significance. Circul Res 2012; 110(7): 927–937.
376. McAteer MA, Akhtar AM, von zur Muhlen C, Choudhury RP. An approach to molecular imaging of atherosclerosis, thrombosis, and vascular inflammation using microparticles of iron oxide. Atherosclerosis 2010; 209(1): 18–27.
377. McAteer MA, Mankia K, Ruparelia N, Jefferson A, Nugent HB, Stork L-A, Channon KM, Schneider JE, Choudhury RP. A leukocyte-mimetic magnetic resonance imaging contrast agent homes rapidly to activated endothelium and tracks with atherosclerotic lesion macrophage content. Arterioscler Thromb Vasc Biol 2012; 32(6): 1427–1435.
378. Briley-Saebo KC, Mani V, Hyafil F, Cornily JC, Fayad ZA. Fractionated Feridex and positive contrast: in vivo MR imaging of atherosclerosis. Magn Reson Med 2008; 59(4): 721–730.
379. Trivedi RA, Mallawarachi C, Jean-Marie U, Graves MJ, Horsley J, Goddard MJ, Brown A, Wang L, Kirkpatrick PJ, Brown J. Identifying inflamed carotid plaques using in vivo USPIO-enhanced MR imaging to label plaque macrophages. Arterioscler Thromb Vasc Biol 2006; 26(7): 1601–1606.
380. Morris JB, Olzinski AR, Bernard RE, Aravindhan K, Mirabile RC, Boyce R, Willette RN, Jucker BM. p38 MAPK inhibition reduces aortic ultrasmall superparamagnetic iron oxide uptake in a mouse model of atherosclerosis MRI assessment. Arterioscler Thromb Vasc Biol 2008; 28(2): 265–271.
381. Mulder WJ, Strijkers GJ, Vucic E, Cormode DP, Nicolay K, Fayad ZA. Magnetic resonance molecular imaging contrast agents and their application in atherosclerosis. Top Magn Reson Imag 2007; 18(5): 409–417.
382. McAteer MA, Choudhury RP. Targeted molecular imaging of vascular inflammation in cardiovascular disease using nano-and micro-sized agents. Vasc Pharmacol 2012.
383. Schellenberger E. Bioresponsive nanosensors in medical imaging. J R Soc Interface 2010; 7(suppl 1): S83–S91.
384. Chacko A-M, Hood ED, Zern BJ, Muzykantov VR. Targeted nanocarriers for imaging and therapy of vascular inflammation. Curr Opin Colloid Interface Sci 2011; 16(3): 215–227.
385. McAteer MA, Sibson NR, von zur Muhlen C, Schneider JE, Lowe AS, Warrick N, Channon KM, Anthony DC, Choudhury RP. In vivo magnetic resonance imaging of acute brain inflammation using microparticles of iron oxide. Nat Med 2007; 13(10): 1253–1258.
386. Hoyte LC, Brooks KJ, Nagel S, Akhtar A, Chen R, Mardiguian S, McAteer MA, Anthony DC, Choudhury RP, Buchan AM. Molecular magnetic resonance imaging of acute vascular cell adhesion molecule-1 expression in a mouse model of cerebral ischemia. J Cerebral Blood Flow Metab 2010; 30(6): 1178–1187.
387. Michalska M, Machtoub L, Manthey HD, Bauer E, Herold V, Krohne G, Lykowsky G, Hildenbrand M, Kampf T, Jakob P. Visualization of vascular inflammation in the atherosclerotic mouse by ultrasmall superparamagnetic iron oxide vascular cell adhesion molecule-1-specific nanoparticles. Arterioscler Thromb Vasc Biol 2012; 32(10): 2350–2357.
388. Burtea C, Ballet S, Laurent S, Rousseaux O, Dencausse A, Gonzalez W, Port M, Corot C, Vander Elst L, Muller RN. Development of a magnetic resonance imaging protocol for the characterization of atherosclerotic plaque by using vascular cell adhesion molecule-1 and apoptosis-targeted ultrasmall superparamagnetic iron oxide derivatives. Arterioscler Thromb Vasc Biol 2012; 32(6): e36–e48.
389. Subbiahdoss G, Sharifi S, Grijpma DW, Laurent S, van der Mei HC, Mahmoudi M, Busscher HJ. Magnetic targeting of surface-modified superparamagnetic iron oxide nanoparticles yields antibacterial efficacy against biofilms of gentamicin-resistant staphylococci. Acta Biomater 2012; 8(6): 2047–2055.
390. Lee SM, Lee SH, Kang HY, Baek SY, Kim SM, Shin MJ. Assessment of musculoskeletal infection in rats to determine usefulness of SPIO-enhanced MRI. AJR Am J Roentgenol 2007; 189(3): 542–548.
391. Gellissen J, Axmann C, Prescher A, Bohndorf K, Lodemann KP. Extra- and intracellular accumulation of ultrasmall superparamagnetic iron oxides (USPIO) in experimentally induced abscesses of the peripheral soft tissues and their effects on magnetic resonance imaging. Magn Reson Imag 1999; 17(4): 557–567.
392. Kaim AH, Jundt G, Wischer T, O'Reilly T, Frohlich J, von Schulthess GK, Allegrini PR. Functional-morphologic MR imaging with ultrasmall superparamagnetic particles of iron oxide in acute and chronic soft-tissue infection: study in rats. Radiology 2003; 227(1): 169–174.
393. Lee SM, Lee SH, Kang HY, Baek SY, Kim SM, Shin MJ. Assessment of musculoskeletal infection in rats to determine usefulness of SPIO-enhanced MRI. Am J Roentgenol 2007; 189(3): 542–548.
394. Baraki H, Zinne N, Wedekind D, Meier M, Bleich A, Glage S, Hedrich HJ, Kutschka I, Haverich A. Magnetic resonance imaging of soft tissue infection with iron oxide labeled granulocytes in a rat model. PLoS One 2012; 7(12): e51770.
395. Hoerr V, Tuchscherr L, Huve J, Nippe N, Loser K, Glyvuk N, Tsytsyura Y, Holtkamp M, Sunderkotter C, Karst U, Klingauf J, Peters G, Loffler B, Faber C. Bacteria tracking by in vivo magnetic resonance imaging. BMC Biol 2013; 11: 63.
396. Bierry G, Jehl F, Holl N, Sibilia J, Froelich S, Froehlig P, Dietemann JL, Kremer S. Cellular magnetic resonance imaging for the differentiation of infectious and degenerative vertebral disorders: preliminary results. J Magn Reson Imag 2009; 30(4): 901–906.
397. Ma Y, Pope RM. The role of macrophages in rheumatoid arthritis. Curr Pharm Des 2005; 11(5): 569–580.
398. Dardzinski BJ, Schmithorst VJ, Holland SK, Boivin GP, Imagawa T, Watanabe S, Lewis JM, Hirsch R. MR imaging of murine arthritis using ultrasmall superparamagnetic iron oxide particles. Magn Reson Imag 2001; 19(9): 1209–1216.
399. Simon GH, von Vopelius-Feldt J, Fu Y, Schlegel J, Pinotek G, Wendland MF, Chen MH, Daldrup-Link HE. Ultrasmall supraparamagnetic iron oxide-enhanced magnetic resonance imaging of antigen-induced arthritis: a comparative study between SHU 555 C, Ferumoxtran-10, and Ferumoxytol. Invest Radiol 2006; 41(1): 45–51.
400. Pouliquen D, Le Jeune JJ, Perdrisot R, Ermias A, Jallet P. Iron oxide nanoparticles for use as an MRI contrast agent: pharmacokinetics and metabolism. Magn Reson Imag 1991; 9(3): 275–283.
401. Arbab AS, Yocum GT, Wilson LB, Parwana A, Jordan EK, Kalish H, Frank JA. Comparison of transfection agents in forming complexes with ferumoxides, cell labeling efficiency, and cellular viability. Mol Imag 2004; 3(1): 24–32.
402. Arbab AS, Bashaw LA, Miller BR, Jordan EK, Bulte JW, Frank JA. Intracytoplasmic tagging of cells with ferumoxides and transfection agent for cellular magnetic resonance imaging after cell transplantation: methods and techniques. Transplantation 2003; 76(7): 1123–1130.
403. Frank JA, Miller BR, Arbab AS, Zywicke HA, Jordan EK, Lewis BK, Bryant LH Jr, Bulte JW. Clinically applicable labeling of mammalian and stem cells by combining superparamagnetic iron oxides and transfection agents. Radiology 2003; 228(2): 480–487.
404. Arbab AS, Bashaw LA, Miller BR, Jordan EK, Lewis BK, Kalish H, Frank JA. Characterization of biophysical and metabolic properties of cells labeled with superparamagnetic iron oxide nanoparticles and transfection agent for cellular MR imaging. Radiology 2003; 229(3): 838–846.

405. Bulte JW, Arbab AS, Douglas T, Frank JA. Preparation of magnetically labeled cells for cell tracking by magnetic resonance imaging. Meth Enzymol 2004; 386: 275–299.
406. Frank JA, Zywicke H, Jordan EK, Mitchell J, Lewis BK, Miller B, Bryant LH Jr, Bulte JW. Magnetic intracellular labeling of mammalian cells by combining (FDA-approved) superparamagnetic iron oxide MR contrast agents and commonly used transfection agents. Acad Radiol 2002; 9(2): S484–S487.
407. Suzuki Y, Zhang S, Kundu P, Yeung AC, Robbins RC, Yang PC. In vitro comparison of the biological effects of three transfection methods for magnetically labeling mouse embryonic stem cells with ferumoxides. Magn Reson Med 2007; 57(6): 1173–1179.
408. Neri M, Maderna C, Cavazzin C, Deidda-Vigoriti V, Politi LS, Scotti G, Marzola P, Sbarbati A, Vescovi AL, Gritti A. Efficient in vitro labeling of human neural precursor cells with superparamagnetic iron oxide particles: relevance for in vivo cell tracking. Stem Cells 2008; 26(2): 505–516.
409. Montet-Abou K, Montet X, Weissleder R, Josephson L. Transfection agent induced nanoparticle cell loading. Mol Imag 2005; 4(3): 165–171.
410. Reynolds F, Weissleder R, Josephson L. Protamine as an efficient membrane-translocating peptide. Bioconjug Chem 2005; 16(5): 1240–1245.
411. Wu YJ, Muldoon LL, Varallyay C, Markwardt S, Jones RE, Neuwelt EA. In vivo leukocyte labeling with intravenous ferumoxides/protamine sulfate complex and in vitro characterization for cellular magnetic resonance imaging. Am J Physiol Cell Physiol 2007; 293(5): 26.
412. Arbab AS, Rad AM, Iskander AS, Jafari-Khouzani K, Brown SL, Churchman JL, Ding G, Jiang Q, Frank JA, Soltanian-Zadeh H, Peck DJ. Magnetically-labeled sensitized splenocytes to identify glioma by MRI: a preliminary study. Magn Reson Med 2007; 58(3): 519–526.
413. Arbab AS, Frank JA. Cellular MRI and its role in stem cell therapy. Regen Med 2008; 3(2): 199–215.
414. Arbab AS, Pandit SD, Anderson SA, Yocum GT, Bur M, Frenkel V, Khuu HM, Read EJ, Frank JA. Magnetic resonance imaging and confocal microscopy studies of magnetically labeled endothelial progenitor cells trafficking to sites of tumor angiogenesis. Stem Cells 2006; 24(3): 671–678.
415. Bluemke DA, Weber TM, Rubin D, de Lange EE, Semelka R, Redvanly RD, Chezmar J, Outwater E, Carlos R, Saini S, Holland GA, Mammone JF, Brown JJ, Milestone B, Javitt MC, Jacobs P. Hepatic MR imaging with ferumoxides: multicenter study of safety and effectiveness of direct injection protocol. Radiology 2003; 228(2): 457–464.
416. Harisinghani MG, Saini S, Weissleder R, Halpern EF, Schima W, Rubin DL, Stillman AE, Sica GT, Small WC, Hahn PF. Differentiation of liver hemangiomas from metastases and hepatocellular carcinoma at MR imaging enhanced with blood-pool contrast agent Code-7227. Radiology 1997; 202(3): 687–691.
417. Harisinghani MG, Saini S, Weissleder R, Hahn PF, Yantiss RK, Tempany C, Wood BJ, Mueller PR. MR lymphangiography using ultrasmall superparamagnetic iron oxide in patients with primary abdominal and pelvic malignancies: radiographic-pathologic correlation. AJR Am J Roentgenol 1999; 172(5): 1347–1351.
418. Mack MG, Balzer JO, Straub R, Eichler K, Vogl TJ. Superparamagnetic iron oxide-enhanced MR imaging of head and neck lymph nodes. Radiology 2002; 222(1): 239–244.
419. Fleige G, Seeberger F, Laux D, Kresse M, Taupitz M, Pilgrimm H, Zimmer C. In vitro characterization of two different ultrasmall iron oxide particles for magnetic resonance cell tracking. Invest Radiol 2002; 37(9): 482–488.
420. Bulte JW, Douglas T, Witwer B, Zhang SC, Strable E, Lewis BK, Zywicke H, Miller B, van Gelderen P, Moskowitz BM, Duncan ID, Frank JA. Magnetodendrimers allow endosomal magnetic labeling and in vivo tracking of stem cells. Nat Biotechnol 2001; 19(12): 1141–1147.
421. Frank JA, Miller BR, Arbab AS, Zywicke HA, Jordan EK, Lewis BK, Bryant LH, Bulte JWM. Clinically applicable labeling of mammalian and stem cells by combining superparamagnetic iron oxides and transfection agents. Radiology 2003; 228(2): 480–487.
422. Dodd CH, Hsu HC, Chu WJ, Yang P, Zhang HG, Mountz JD Jr, Zinn K, Forder J, Josephson L, Weissleder R, Mountz JM, Mountz JD. Normal T-cell response and in vivo magnetic resonance imaging of T cells loaded with HIV transactivator-peptide-derived superparamagnetic nanoparticles. J Immunol Meth 2001; 256(1–2): 89–105.
423. Moore A, Sun PZ, Cory D, Hogemann D, Weissleder R, Lipes MA. MRI of insulitis in autoimmune diabetes. Magn Reson Med 2002; 47(4): 751–758.
424. Moore A, Grimm J, Han B, Santamaria P. Tracking the recruitment of diabetogenic CD8+ T-cells to the pancreas in real time. Diabetes 2004; 53(6): 1459–1466.
425. Bulte JWM, Zhang S-C, van Gelderen P, Herynek V, Jordan EK, Duncan ID, Frank JA. Neurotransplantation of magnetically labeled oligodendrocyte progenitors: magnetic resonance tracking of cell migration and myelination. Proc Natl Acad Sci U S A 1999; 96(26): 15256–15261.
426. Ahrens ET, Feili-Hariri M, Xu H, Genove G, Morel PA. Receptor-mediated endocytosis of iron-oxide particles provides efficient labeling of dendritic cells for in vivo MR imaging. Magn Reson Med 2003; 49(6): 1006–1013.
427. Walczak P, Zhang J, Gilad AA, Kedziorek DA, Ruiz-Cabello J, Young RG, Pittenger MF, van Zijl PC, Huang J, Bulte JW. Dual-modality monitoring of targeted intraarterial delivery of mesenchymal stem cells after transient ischemia. Stroke 2008; 39(5): 1569–1574.
428. Heyn C, Ronald JA, Ramadan SS, Snir JA, Barry AM, MacKenzie LT, Mikulis DJ, Palmieri D, Bronder JL, Steeg PS, Yoneda T, MacDonald IC, Chambers AF, Rutt BK, Foster PJ. In vivo MRI of cancer cell fate at the single-cell level in a mouse model of breast cancer metastasis to the brain. Magn Reson Med 2006; 56(5): 1001–1010.
429. Himmelreich U, Hoehn M. Stem cell labeling for magnetic resonance imaging. Min Invasive Ther Allied Technol 2008; 17(2): 132–142.
430. Bulte JW, Kraitchman DL. Iron oxide MR contrast agents for molecular and cellular imaging. NMR Biomed 2004; 17(7): 484–499.
431. Lewin M, Carlesso N, Tung CH, Tang XW, Cory D, Scadden DT, Weissleder R. Tat peptide-derivatized magnetic nanoparticles allow in vivo tracking and recovery of progenitor cells. Nat Biotechnol 2000; 18(4): 410–414.
432. Modo M, Cash D, Mellodew K, Williams SC, Fraser SE, Meade TJ, Price J, Hodges H. Tracking transplanted stem cell migration using bifunctional, contrast agent-enhanced, magnetic resonance imaging. Neuroimage 2002; 17(2): 803–811.
433. Kim D, Hong KS, Song J. The present status of cell tracking methods in animal models using magnetic resonance imaging technology. Mol Cells 2007; 23(2): 132–137.
434. Kustermann E, Himmelreich U, Kandal K, Geelen T, Ketkar A, Wiedermann D, Strecker C, Esser J, Arnhold S, Hoehn M. Efficient stem cell labeling for MRI studies. Contrast Media Mol Imag 2008; 3(1): 27–37.
435. Guzman R, Uchida N, Bliss TM, He D, Christopherson KK, Stellwagen D, Capela A, Greve J, Malenka RC, Moseley ME, Palmer TD, Steinberg GK. Long-term monitoring of transplanted human neural stem cells in developmental and pathological contexts with MRI. Proc Natl Acad Sci U S A 2007; 104(24): 10211–10216.
436. Walter GA, Cahill KS, Huard J, Feng H, Douglas T, Sweeney HL, Bulte JW. Noninvasive monitoring of stem cell transfer for muscle disorders. Magn Reson Med 2004; 51(2): 273–277.
437. Arai T, Kofidis T, Bulte JW, de Bruin J, Venook RD, Berry GJ, McConnell MV, Quertermous T, Robbins RC, Yang PC. Dual in vivo magnetic resonance evaluation of magnetically labeled mouse embryonic stem cells and cardiac function at 1.5 T. Magn Reson Med 2006; 55(1): 203–209.
438. Kraitchman DL, Tatsumi M, Gilson WD, Ishimori T, Kedziorek D, Walczak P, Segars WP, Chen HH, Fritzges D, Izbudak I, Young RG, Marcelino M, Pittenger MF, Solaiyappan M, Boston RC, Tsui BM, Wahl RL, Bulte JW. Dynamic imaging of allogeneic mesenchymal stem cells trafficking to myocardial infarction. Circulation 2005; 112(10): 1451–1461.
439. Kustermann E, Roell W, Breitbach M, Wecker S, Wiedermann D, Buehrle C, Welz A, Hescheler J, Fleischmann BK, Hoehn M. Stem cell implantation in ischemic mouse heart: a high-resolution magnetic resonance imaging investigation. NMR Biomed 2005; 18(6): 362–370.
440. Arbab AS, Liu W, Frank JA. Cellular magnetic resonance imaging: current status and future prospects. Expert Rev Med Devices 2006; 3(4): 427–439.
441. Lewin JS, Nour SG, Duerk JL. Magnetic resonance image-guided biopsy and aspiration. Top Magn Reson Imag 2000; 11(3): 173–183.
442. Zhu J, Zhou L, XingWu F. Tracking neural stem cells in patients with brain trauma. New Engl J Med 2006; 355(22): 2376–2378.
443. Mahmoudi M, Hosseinkhani H, Hosseinkhani M, Boutry S, Simchi A, Shane Journeay W, Subramani K, Laurent S. Magnetic resonance imaging tracking of stem cells in vivo using iron oxide nanoparticles as a tool for the advancement of clinical regenerative medicine. Chem Rev 2011; 111(2): 253–280.

444. Mizuno H, Tobita M, Uysal AC. Concise review: adipose-derived stem cells as a novel tool for future regenerative medicine. Stem Cells 2012; 30(5): 804–810.
445. Takahashi K, Tanabe K, Ohnuki M, Narita M, Ichisaka T, Tomoda K, Yamanaka S. Induction of pluripotent stem cells from adult human fibroblasts by defined factors. Cell 2007; 131(5): 861–872.
446. Caplan AI. Adult mesenchymal stem cells for tissue engineering versus regenerative medicine. J Cell Physiol 2007; 213(2): 341–347.
447. Saldanha KJ, Doan RP, Ainslie KM, Desai TA, Majumdar S. Micrometer-sized iron oxide particle labeling of mesenchymal stem cells for magnetic resonance imaging-based monitoring of cartilage tissue engineering. Magn Reson Imag 2011; 29(1): 40–49.
448. Chen CL, Zhang H, Ye Q, Hsieh WY, Hitchens TK, Shen HH, Liu L, Wu YJ, Foley LM, Wang SJ, Ho C. A new nano-sized iron oxide particle with high sensitivity for cellular magnetic resonance imaging. Mol Imag Biol 2011; 13(5): 825–839.
449. Wimpenny I, Markides H, El Haj AJ. Orthopaedic applications of nanoparticle-based stem cell therapies. Stem Cell Res Ther 2012; 3(2).
450. Jing Xh, Yang L, Duan Xj, Xie B, Chen W, Li Z, Tan Hb. In vivo MR imaging tracking of magnetic iron oxide nanoparticle labeled, engineered, autologous bone marrow mesenchymal stem cells following intraarticular injection. Joint Bone Spine 2008; 75(4): 432–438.
451. van Buul GM, Kotek G, Wielopolski PA, Farrell E, Bos PK, Weinans H, Grohnert AU, Jahr H, Verhaar JAN, Krestin GP, van Osch GJVM, Bernsen MR. Clinically translatable cell tracking and quantification by MRI in cartilage repair using superparamagnetic iron oxides. PLoS One 2011; 6(2).
452. Mahmoudi M, Bonakdar S, Shokrgozar MA, Aghaverdi H, Hartmann R, Pick A, Witte G, Parak WJ. Cell-imprinted substrates direct the fate of stem cells. ACS Nano 2013; 7(10): 8379–8384.
453. Chen J, Wang F, Zhang Y, Jin X, Zhang L, Feng Y, Yang L. In vivo MRI tracking of polyethylenimine-wrapped superparamagnetic iron oxide nanoparticle-labeled BMSCs for cartilage repair: a minipig model. Cartilage 2013; 4(1): 75–82.
454. Chan SC, Gantenbein-Ritter B. Intervertebral disc regeneration or repair with biomaterials and stem cell therapy – feasible or fiction? Swiss Med Wkly 2012; 31(142): 13598.
455. Jiang Xh, Chen Jy, Cai Zx, Ya Z, Liu Zz, Xie Cm, Wu Yp, Wu Ph. In vivo tracking superparamagnetic iron oxide labeled adipose derived stem cells to repair rabbit degenerated intervertebral disc. J Clin Rehab Tissue Eng Res 2011; 15(40): 7515–7519.
456. Lalande C, Miraux S, Derkaoui SM, Mornet S, Bareille R, Fricain JC, Franconi JM, Le Visage C, Letourneur D, Amédée J, Bouzier-Sore AK. Magnetic resonance imaging tracking of human adipose derived stromal cells within three-dimensional scaffolds for bone tissue engineering. Eur Cells Mater 2011; 21: 341–354.
457. Serpooshan V, Zhao M, Metzler SA, Wei K, Shah PB, Wang A, Mahmoudi M, Malkovskiy AV, Rajadas J, Butte MJ. The effect of bioengineered acellular collagen patch on cardiac remodeling and ventricular function post myocardial infarction. Biomaterials 2013; 34(36): 9048–9055.
458. Mathiasen AB, Haack-Sørensen M, Kastrup J. Mesenchymal stromal cells for cardiovascular repair: current status and future challenges. Fut Cardiol 2009; 5(6): 605–617.
459. Tallheden T, Nannmark U, Lorentzon M, Rakotonirainy O, Soussi B, Waagstein F, Jeppsson A, Sjögren-Jansson E, Lindahl A, Omerovic E. In vivo MR imaging of magnetically labeled human embryonic stem cells. Life Sci 2006; 79(10): 999–1006.
460. Au KW, Liao SY, Lee YK, Lai WH, Ng KM, Chan YC, Yip MC, Ho CY, Wu EX, Li RA, Siu CW, Tse HF. Effects of iron oxide nanoparticles on cardiac differentiation of embryonic stem cells. Biochem Biophys Res Commun 2009; 379(4): 898–903.
461. Carr CA, Stuckey DJ, Tatton L, Tyler DJ, Hale SJM, Sweeney D, Schneider JE, Martin-Rendon E, Radda GK, Harding SE, Watt SM, Clarke K. Bone marrow-derived stromal cells home to and remain in the infarcted rat heart but fail to improve function: an in vivo cine-MRI study. Am J Physiol Heart Circul Physiol 2008; 295(2): H533–H542.
462. Delo DM, Olson J, Baptista PM, D'Agostino RB Jr, Atala A, Zhu JM, Soker S. Non-invasive longitudinal tracking of human amniotic fluid stem cells in the mouse heart. Stem Cells Devl 2008; 17(6): 1185–1193.
463. Wang L, Deng J, Wang J, Xiang B, Yang T, Gruwel M, Kashour T, Tomanek B, Summer R, Freed D, Jassal DS, Dai G, Glogowski M, Deslauriers R, Arora RC, Tian G. Superparamagnetic iron oxide does not affect the viability and function of adipose-derived stem cells, and superparamagnetic iron oxide-enhanced magnetic resonance imaging identifies viable cells. Magn Reson Imag 2009; 27(1): 108–119.
464. Vallée JP, Hauwel M, Lepetit-Coiffée M, Bei W, Montet-Abou K, Meda P, Gardier S, Zammaretti P, Kraehenbuehl TP, Herrmann F, Hubbell JA, Jaconi ME. Embryonic stem cell-based cardiopatches improve cardiac function in infarcted rats. Stem Cells Translat Med 2012; 1(3): 248–260.
465. Emmert MY, Weber B, Wolint P, Frauenfelder T, Zeisberger SM, Behr L, Sammut S, Scherman J, Brokopp CE, Schwartländer R, Vogel V, Vogt P, Grünenfelder J, Alkadhi H, Falk V, Boss A, Hoerstrup SP. Intramyocardial transplantation and tracking of human mesenchymal stem cells in a novel intra-uterine pre-immune fetal sheep myocardial infarction model: a proof of concept study. PLoS One 2013; 8(3).
466. Willenbrock S, Knippenberg S, Meier M, Hass R, Wefstaedt P, Nolte I, Murua Escobar H, Petri S. In vivo MRI of intraspinally injected SPIO-labelled human CD34+ cells in a transgenic mouse model of ALS. In Vivo 2012; 26(1): 31–38.
467. Hu SL, Lu PG, Zhang LJ, Li F, Chen Z, Wu N, Meng H, Lin JK, Feng H. In Vivo magnetic resonance imaging tracking of SPIO-labeled human umbilical cord mesenchymal stem cells. J Cell Biochem 2012; 113(3): 1005–1012.
468. Gonzalez-Lara LE, Xu X, Hofstetrova K, Pniak A, Chen Y, McFadden CD, Martinez-Santiesteban FM, Rutt BK, Brown A, Foster PJ. The use of cellular magnetic resonance imaging to track the fate of iron-labeled multipotent stromal cells after direct transplantation in a mouse model of spinal cord injury. Mol Imag Biol 2011; 13(4): 702–711.
469. Walczak P, Zhang J, Gilad AA, Kedziorek DA, Ruiz-Cabello J, Young RG, Pittenger MF, Van Zijl PCM, Huang J, Bulte JWM. Dual-modality monitoring of targeted intraarterial delivery of mesenchymal stem cells after transient ischemia. Stroke 2008; 39(5): 1569–1574.
470. Jackson JS, Golding JP, Chapon C, Jones WA, Bhakoo KK. Homing of stem cells to sites of inflammatory brain injury after intracerebral and intravenous administration: a longitudinal imaging study. Stem Cell Res Ther 2010; 1(2).
471. Canzi L, Castellaneta V, Navone S, Nava S, Dossena M, Zucca I, Mennini T, Bigini P, Parati EA. Human skeletal muscle stem cell antiinflammatory activity ameliorates clinical outcome in amyotrophic lateral sclerosis models. Mol Med (Camb, Mass) 2012; 18(1): 401–411.
472. Lu SS, Liu S, Zu QQ, Xu XQ, Yu J, Wang JW, Zhang Y, Shi HB. In vivo MR imaging of intraarterially delivered magnetically labeled mesenchymal stem cells in a canine stroke model. PLoS One 2013; 8(2).
473. Kallur T, Farr TD, Böhm-Sturm P, Kokaia Z, Hoehn M. Spatiotemporal dynamics, differentiation and viability of human neural stem cells after implantation into neonatal rat brain. Eur J Neurosci 2011; 34(3): 382–393.
474. Gu L, Fang RH, Sailor MJ, Park JH. In vivo clearance and toxicity of monodisperse iron oxide nanocrystals. ACS Nano 2012; 6(6): 4947–4954.
475. Levy M, Luciani N, Alloyeau D, Elgrabli D, Deveaux V, Pechoux C, Chat S, Wang G, Vats N, Gendron F, Factor C, Lotersztajn S, Luciani A, Wilhelm C, Gazeau F. Long term in vivo biotransformation of iron oxide nanoparticles. Biomaterials 2011; 32(16): 3988–3999.
476. Schulze E, Ferrucci JT Jr, Poss K, Lapointe L, Bogdanova A, Weissleder R. Cellular uptake and trafficking of a prototypical magnetic iron oxide label in vitro. Invest Radiol 1995; 30(10): 604–610.
477. Mahmoudi M, Lohse SE, Murphy CJ, Fathizadeh A, Montazeri A, Suslick KS. Variation of protein corona composition of gold nanoparticles following plasmonic heating. Nano Lett 2014; 14(1): 6–12.
478. Mahmoudi M, Saeedi-Eslami SN, Shokrgozar MA, Azadmanesh K, Hassanlou M, Kalhor HR, Burtea C, Rothen-Rutishauser B, Laurent S, Sheibani S, Vali H. Cell 'vision': complementary factor of protein corona in nanotoxicology. Nanoscale 2012; 4(17): 5461–5468.
479. Rauch J, Kolch W, Mahmoudi M. Cell type-specific activation of AKT and ERK signaling pathways by small negatively-charged magnetic nanoparticles. Sci Rep 2012; 2.
480. Laurent S, Burtea C, Thirifays C, Häfeli UO, Mahmoudi M. Crucial ignored parameters on nanotoxicology: the importance of toxicity assay modifications and 'cell vision'. PLoS One 2012; 7(1): e29997.
481. Hajipour MJ, Laurent S, Aghaie A, Rezaee F, Mahmoudi M. Personalized protein coronas: a 'key' factor at the nanobiointerface. Biomater Sci 2014. doi: 10.1039/c4bm00131a

Review

Superparamagnetic iron oxide nanoparticle for *in vivo* molecular and cellular imaging

Shahriar Sharifi, Hajar Seyednejad, Sophie Laurent, Fatemeh Atyabi and Morteza Mahmoudi

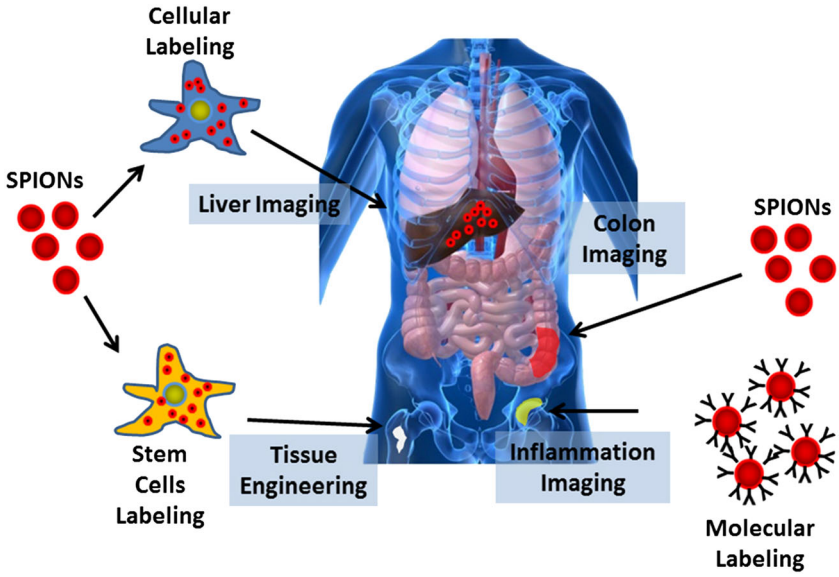

Owing to their unique magnetic properties, biocompatibility and controllable physicochemical properties, superparamagnetic iron oxide nanoparticles have significant potential for various biomedical applications such as molecule detection, cell tracking, early detection of diseases, biosensing, magnetic resonance imaging, targeted drug delivery and tissue engineering.

Author Query Form

Journal: Contrast Media & Molecular Imaging

Article: cmmi_1614

Dear Author,

During the copyediting of your paper, the following queries arose. Please respond to these by annotating your proofs with the necessary changes/additions.

- If you intend to annotate your proof electronically, please refer to the E-annotation guidelines.
- If you intend to annotate your proof by means of hard-copy mark-up, please refer to the proof mark-up symbols guidelines. If manually writing corrections on your proof and returning it by fax, do not write too close to the edge of the paper. Please remember that illegible mark-ups may delay publication.

Whether you opt for hard-copy or electronic annotation of your proofs, we recommend that you provide additional clarification of answers to queries by entering your answers on the query sheet, in addition to the text mark-up.

Query No.	Query	Remark
Q1	AUTHOR: 157b changed to 157, OK? Also, Ref. 157 is not by Thorek, please check.	
Q2	AUTHOR: References 205-210 are not mentioned in the text? Please insert citation.	
Q3	AUTHOR: Resupplied figures 1 and 2 still contain poor quality text. Please check and resupply if necessary.	
Q4	AUTHOR: 235b changed to 235, OK?	
Q5	AUTHOR: Ref. 278 is not by Chen? Please check.	
Q6	AUTHOR: Ref. 343 is not by Fleigie? Please check.	
Q7	AUTHOR: Please define G.	
Q8	AUTHOR: MSC has been defined differently earlier, please use different abbreviation.	
Q9	AUTHOR: References 29 and 283, 79 and 266, 93 and 387, 94 and 331, 97 and 191, 104 and 208, 107 and 206, 111 and 227, 116 and 258, 130 and 422, 157 and 160, 180 and 315, 182 and 343, 184 and 351, 287 and 291, 303 and 402, 328 and 348, 403 and 421, 427 and 469 shares the same name of authors and year-of-publication details. Please provide an alternative reference to avoid duplication or delete the duplicate reference in the list.	
Q10	AUTHOR: Please provide the page number for References 7, 279, 449, 451, 465, 470, 472, and 479.	
Q11	AUTHOR: Please provide the initial(s) of Rinck in Reference 8.	
Q12	AUTHOR: Please provide the volume and page number for References 16, 154, 252, 257, 354, and 382, 481.	
Q13	AUTHOR: Please provide the journal title for References 60 and 155.	
Q14	AUTHOR: Please provide the volume number for References 65 and 277.	
Q15	AUTHOR: Please provide the journal title and volume number for References 110, 146, and 155.	
Q16	AUTHOR: Please provide all authors name for Reference 208.	
Q17	AUTHOR: The page range of Reference 363 seems incorrect. Please check.	

WILEY

Online Proofing System

1. Corrections should be marked with the Adobe Annotation & Comment Tools below:

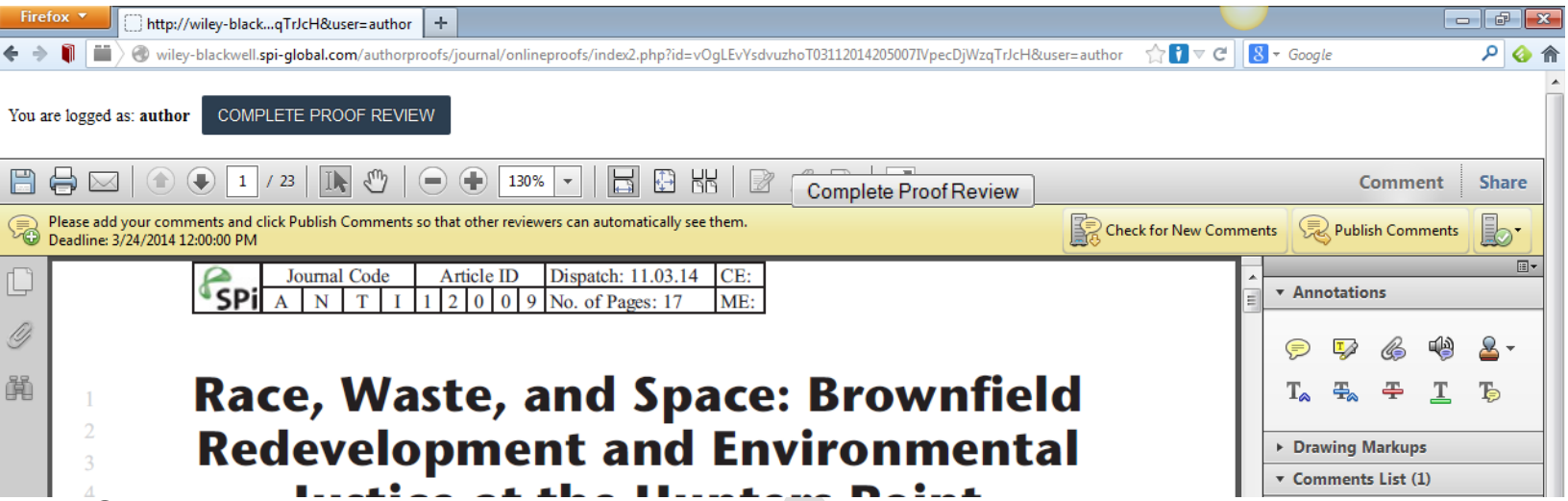

2. To save your proof corrections, click the 'Publish Comments' button. Publishing your comments saves the marked up version of your proof to a centralized location in Wiley's Online Proofing System. Corrections don't have to be marked in one sitting – you can publish corrections and log back in at a later time to add more.

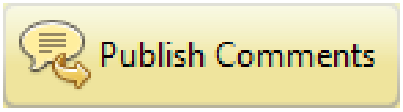

3. When your proof review is complete we recommend you download a copy of your annotated proof for reference in any future correspondence concerning the article before publication. You can do this by clicking on the icon to the right of the 'Publish Comments' button and selecting 'Save as Archive Copy…'.

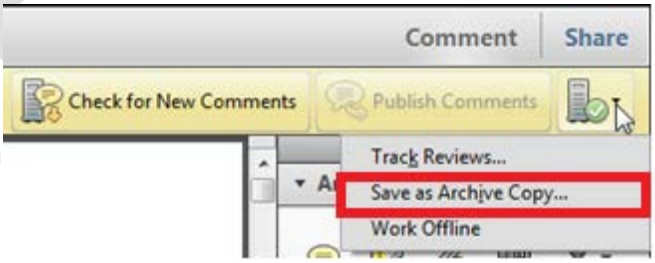

4. When your proof review is complete and you are ready to send corrections to the publisher click the 'Complete Proof Review' button that appears above the proof in your web browser window. Do not click the 'Complete Proof Review' button without replying to any author queries found on the last page of your proof. Incomplete proof reviews will cause a delay in publication. **Note: Once you click 'Complete Proof Review' you will not be able to mark any further comments or corrections**.

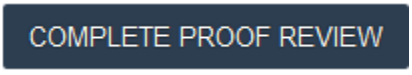

Firefox, Chrome, Safari Users

If your PDF article proof opens in any PDF viewer other than Adobe Reader or Adobe Acrobat, you will not be able to mark corrections and query responses, nor save them. To mark and save corrections, please follow these instructions to disable the built-in browser PDF viewers in Firefox, Chrome, and Safari so the PDF article proof opens in Adobe within a Firefox, Chrome, or Safari browser window.